UNIVERSIDADE DE SÃO PAULO

INSTITUTO DE QUÍMICA

Pâmela Aiako Hypólito Brito Kakimoto

Bioenergetic and redox signaling in hepatic steatosis models: Integrative analysis of nutritional, hormonal, and inflammatory stimuli

Bioenergética e sinalização redox em modelos de esteatose hepática: análise integrativa de estímulos nutricionais, hormonais e inflamatórios

São Paulo

Data do depósito na SPG:

05/11/2020

PÂMELA AIAKO HYPÓLITO BRITO KAKIMOTO

Bioenergetic and redox signaling in hepatic steatosis models: Integrative analysis of nutritional, hormonal, and inflammatory stimuli

Bioenergética e sinalização redox hepática em modelo de esteatose hepática: análise integrativa de estímulos nutricionais, hormonais e inflamatórios

Versão Corrigida da Tese Defendida

Tese apresentada ao Instituto de Química da Universidade de São Paulo para obtenção do título de Doutora em Ciências Biológicas (Bioquímica).

Orientadora: Alicia J. Kowaltowski

São Paulo

2020

Ficha Catalográfica elaborada eletronicamente pelo autor, utilizando o programa desenvolvido pela Seção Técnica de Informática do ICMC/USP e adaptado para a Divisão de Biblioteca e Documentação do Conjunto das Químicas da USP

Bibliotecária responsável pela orientação de catalogação da publicação:
Marlene Aparecida Vieira - CRB - 8/5562

K11b

Kakimoto, Pâmela Aiako Hypólito Brito
Bioenergética e sinalização redox em modelos de esteatose hepática: análise integrativa de estímulos nutricionais, hormonais e inflamatórios / Pâmela Aiako Hypólito Brito Kakimoto. - São Paulo, 2020.
100 p.

Tese (doutorado) - Instituto de Química da Universidade de São Paulo. Departamento de Bioquímica.
Orientador: Kowaltowski, Alicia Juliana

1. Mitocôndrias. 2. Fígado. 3. Esteatose. 4. Ácidos Graxos. 5. Óxido nítrico. I. T. II. Kowaltowski, Alicia Juliana, orientador.

FOLHA DE APROVAÇÃO

Com amor, para
Aledir, Carlos, Danielle,
Josefina, Sachiko,
Valdete (*in memorian*), Setsuya
e Gustavo,
que permitiram que tudo fosse possível.

AGRADECIMENTOS

À Fundação de Amparo à Pesquisa de São Paulo pelo financiamento durante todo o doutorado e iniciação científica.

À Coordenação de Aperfeiçoamento de Pessoal de Nível Superior pelo financiamento durante o período sanduíche.

À Professora Dra. Alicia Kowaltowski, por ser o melhor exemplo de cientista que uma aluna poderia querer. Foram quase 9 anos de apoio irrestrito e inabalável, desde a iniciação científica, e sei que nunca poderei agradecer o suficiente. Obrigada pela confiança, paciência e apoio.

À Camille Caldeira, pelo inestimável apoio e amizade, eficiência imbatível sempre sorridente e amável. Obrigada por tornar tudo sempre mais fácil.

Ao Bruno Chausse, pela irmandade científica capaz de produzir grandiosas ceias de Natal. Obrigada pela mentoria 24/7 independente do fuso.

Ao Ariel Cardoso que me guiou durante os primeiros passos e me ensinou os fundamentos do fazer e do pensar em ciência.

Aos companheiros de doutorado: João Victor Cabral-Costa (grande *tovarishch* farmacêutico, supergêmeo, e vizinho de mesa), Marcel Vieira-Lara (paixão pela gordura e por memes peculiares, vocês não entenderiam), Sérgio de Menezes (controle de qualidade de memes, pai do Paquito), Felipe Macedo (o domador do Oroboros), Julian David Serna (cultura brasileira e otimização musical de protocolos), e Vitor Ramos (sempre *good vibes*, porto-seguro do Western Blot e das linhagens de hepatócitos), obrigada pela companhia, pelas discussões, pelo café (e a cerveja e o hamburguer) e pelo *happy hour* no espetinho da Elisângela (restrição calórica pra quem?). Sem deixar de mencionar, é claro, o agradecimento especial por também compartilharem o estranho amor por mapas metabólicos, consumo de oxigênio, e medidas de acoplamento.

À minha querida amiga Cíntia Reis Ballard por estar sempre disponível para me ensinar e discutir doenças metabólicas e formulação dietas.

Aos companheiros Fernanda Marques da Cunha, Luis Alberto Luévano-Martinez, e Maria Fernanda Forni, pela disposição e paciência infinitas de sempre me ajudar, especialmente em momentos de elucubrações experimentais.

Aos colegas de IQ e USP, sempre fazendo a diferença pela conversa do dia, seja de ideias de experimentos, me salvando com reagentes prontamente disponíveis, conversas mitocondriais e metabólicas, ou desabafo gerais da pós-graduação: Tiago Eugênio Oliveira, Gabriel Arini, Júlio César Gomes (*in memorian)*, Douglas Moraes, Maíra Nagai, Marcos Yoshinaga, Adriano de Britto Chaves, Luciana Machado, Denise Yamamoto, Érique Castro, e tantos outros companheiros ao longo da jornada que a memória não me permitiu mencionar.

Aos tantos e sempre queridos membros do MitoLab, cada um à sua maneira: Bruno Queliconi, Fernanda Cerqueira, Wilson Garcia-Neto, Nicole Torelli, Ignacio Amigo, Talita Romanatto, Julia Peloggia, Carla Santana Santos, Chen Minzhen, Phablo Abreu, Osvaldo Pereira, Natália Branco e Ana Bonassa, obrigada pela companhia, pela ciência e por me acompanharem pela sempre excelente cozinha Kowaltowski dos brownies, empanadas, hommus, e bolo de abobrinha, quase sempre antes das 8 AM.

Especial obrigada aos amigos do *Journal Club overseas* metabólico-mitocondrial Bruno Chausse, João Victor Cabral-Costa, José Carlos Lima Junior, Nathalia Dragano e Marcel Vieira-Lara, pelos encontros semanais e pela discussão científica quase diária.

Aos sempre amáveis Dóris Dias Araújo, Edson Alves Gomes e Sirlei Mendes de Oliveira pelo apoio absoluto e fundamental.

Às Silvania Peris Neves, Renata Spalutto, Flavia Ong, Edlaine Linares, José Galeote e Wagner Botelho pelo suporte irrestrito, sempre me ajudando a entender melhor meus experimentos.

Ao professor Sandro Marana, com o qual tive a grande oportunidade de trabalhar por perto desde a iniciação científica, obrigada pela confiança e apoio, sempre tão paciente. Agradeço também aos incríveis Daniela Beton, Fábio Tamaki e Vitor Medeiros por toda ajuda pelo mundo da clonagem e das bactérias.

Aos membros do Redoxoma, obrigada pela ciência e pelo ambiente incrivelmente colaborativo.

Aos meus queridos companheiros de Farma-USP 010N, um grande abraço e obrigada pela companhia durante a jornada fantástica de carregar o Lehninger pela Lineu. Em especial, pela amizade, a Henrique Fernandes, Gabriela Braz, Mariane Pereira, Marianne Baptista, Miriam Kasai, Nataly Wasicovichi, e Thayane Moreira.

Ao José Geraldo Vieira pelo suporte e confiança em momentos cruciais, desde sempre.

Aos meus pais, Aledir e Carlos, pelo suporte, estrutura e compreensão que sempre garantiram que eu pudesse ter o privilégio de nunca parar de estudar.

Ao meu parceiro de vida, Gustavo Grenfell, obrigada por ser esse cientista incrível, meu companheiro complementar, paciente, amável, gentil, e de inesgotável capacidade de me colocar para cima e para frente. Com você, *já não tenho medo do mundo* e sei que podemos continuar a crescer juntos.

Lastly, I want to thank Professor Antonio Zorzano for the amazing opportunity to work in your lab and learn so much more about mitochondrial dynamics. Your thoughtful mentorship was especially important to me during the year abroad. It was an outstanding experience to be close to your group. I cannot thank enough Dr Maribel Hernández-Alvarez, Dr Juan Pablo Muñoz, and Dr Nikolaos Giakoumakis for the openness and good humor to mentor me and

discuss science. Also, *muchas gracias/ moltes gràcies* to the all amazing women scientists that I met during my Spanish-Catalan journey: Susana Barros (Pelas infinitas discussões e reflexões sobre ciência, vida, telenovelas, muito axé, obrigada especial para minha tuga preferida), Andrea Irazoki, Isabel Gordaliza, Paloma Escudero, Petra Frager, Alba Sabate, Saska Ivanova, Sara Cano, Manuela Sánchez, Montserrat Romero, and all the lab members from de Zorzano's and Manuel Palacin's lab. Many thanks for the kindness and the science.

“Hey!
So don't you forget your youth
Who you are and where you stand in the
struggle”

Bob Marley

RESUMO EM PORTUGUÊS

Kakimoto, P. A. **Bioenergética e sinalização redox em modelos de esteatose hepática: análise integrativa de estímulos nutricionais, hormonais e inflamatórios.** 2020. 100p. Tese de Doutorado - Programa de Pós-Graduação em Ciências Biológicas (Bioquímica). Instituto de Química, Universidade de São Paulo, São Paulo.

A doença hepática gordurosa não alcoólica (DHGNA) é um termo que compreende um espectro de doenças hepáticas nas quais os lipídios se acumulam no citoplasma dos hepatócitos, variando de esteatose simples à esteatohepatite e à fibrose. Comumente encontrada em indivíduos obesos e em pacientes diabéticos tipo 2, a prevalência de DHGNA está crescendo globalmente e, atualmente, não há tratamentos aprovados para prevenir sua progressão. No centro do metabolismo lipídico hepático estão as mitocôndrias, e a compreensão de sua resposta funcional à sobrecarga de nutrientes é vital para mapear o desenvolvimento da doença. Além disso, a produção de oxidantes é alterada na obesidade e estimulada pela sobrecarga lipídica e ativação de vias pró-inflamatórias. Sabendo que o estado redox celular é fundamental no controle da função mitocondrial e que a atividade de muitas enzimas metabólicas e sinalizadoras é suscetível a modificações oxidativas, entender o escopo da ação dos oxidantes é uma etapa crítica para acompanhar o mecanismo fisiopatológico de doenças associadas à dieta. Nesta tese, propomos avaliar se a sinalização redox participa das alterações metabólicas promovidas pela sobrecarga lipídica usando abordagens *in vivo* e *in vitro*. Na primeira parte, caracterizamos que a função mitocondrial hepática é sustentada durante o tempo em camundongos C57BL/6NTac selvagem e nocaute para a enzima óxido nítrico sintase induzível (iNOS) submetidos a 2, 4 e 8 semanas de dieta rica em gordura, independentemente da dieta, do estado de iNOS, da adiposidade e da sensibilidade sistêmica à insulina. Na segunda parte, caracterizamos em linhagens de hepatócitos como as fontes de ATP são afetadas pela sobrecarga de palmitato, um ácido graxo saturado. Identificamos que a produção de ATP glicolítico é ativada de forma aguda

pelo palmitato e modulada pela produção de oxidantes. Além disso, a produção de ATP mitocondrial é sustentada sob extenso estresse oxidativo e fragmentação mitocondrial. Usando inibidores seletivos, descobrimos que a produção de superóxido e / ou peróxido de hidrogênio no sítio I_Q do complexo mitocondrial respiratório I está associada ao remodelamento metabólico promovido pelo palmitato. Demonstramos que o aumento do fluxo glicolítico ligado ao desequilíbrio redox gerado pela mitocôndria é um resultado lipotóxico agudo da sobrecarga de palmitato. Em conclusão, identificamos em dois modelos diferentes de esteatose que a função mitocondrial pode resistir a muitos insultos e ainda sustentar a produção de ATP. Sua notória disfunção no fígado gorduroso provavelmente não é causadora, mas sim um alvo a jusante da toxicidade.

Palavras-chave: Mitocôndria, Fígado, Esteatose, Ácidos Graxos, Óxido Nítrico, Espécies Reativas de Oxigênio

ABSTRACT IN ENGLISH

Kakimoto, P. A. **Bioenergetic and redox signaling in hepatic steatosis models: Integrative analysis of nutritional, hormonal, and inflammatory stimuli.** 2020. 100p. PhD Thesis - Graduate Program in Biochemistry. Instituto de Química, Universidade de São Paulo, São Paulo.

Non-alcoholic fatty liver disease (NAFLD) is a term comprising a spectrum of liver diseases in which lipids accumulate in the hepatocyte cytoplasm, ranging from simple steatosis to steatohepatitis, and fibrosis. Commonly found in obese individuals and type 2 diabetic patients, NAFLD prevalence is growing globally, and currently there are no approved treatments to prevent its progression. In the center of hepatic lipid metabolism are mitochondria, and the comprehension of their functional response to nutrient overload is vital to map disease development. Moreover, oxidant production is altered in obesity and stimulated by lipidic overload and the activation of pro-inflammatory pathways. Since cellular redox state is fundamental in the control of mitochondrial function and that the activity of many metabolic and signaling enzymes susceptible to oxidative modifications, understanding the action of oxidants is a critical step to uncover the pathophysiological mechanisms of diet-associated metabolic diseases . In this thesis, we propose to evaluate whether redox signaling participates in metabolic changes promoted by lipidic overload using *in vivo* and *in vitro* approaches. In the first part, we characterized, in C57BL/6NTac wild type mice and knockout for the enzyme inducible nitric oxide synthase (iNOS) submitted to 2, 4, and 8 weeks of high-fat feeding, that hepatic mitochondrial function is sustained over the time, independently of the diet, iNOS status, adiposity, and systemic insulin sensitivity. In the second part, we characterized, in hepatocyte cell lines, how ATP sources are affected by overload of palmitate, a saturated fatty acid. We identified that glycolytic ATP production is acutely activated by palmitate and modulated by oxidant production. Furthermore, mitochondrial ATP production is sustained

under extensive oxidative stress and mitochondrial fragmentation. Using selective inhibitors, we found that the production of superoxide and/or hydrogen peroxide at the I_Q site of respiratory mitochondrial complex I is associated with the metabolic rewiring promoted by palmitate. We demonstrate that increased glycolytic flux linked to mitochondrially-generated redox imbalance is an early bioenergetic result of palmitate overload and lipotoxicity. In conclusion, we identified, in two different steatosis models, that mitochondrial function can resist many insults and still sustain ATP production. Its notorious dysfunction in the fatty liver is probably not causative, but rather a downstream target of toxicity.

Keywords: Mitochondria, Liver, Steatosis, Fatty Acids, Nitric Oxide, Reactive Oxygen Species

LISTS OF ABBREVIATIONS AND ACRONYMS

DNP	2,4-dinitrophenol
2-DG	2-deoxyglucose
ACAD	Acyl-CoA dehydrogenase
AMP	Adenine monophosphate
AMPK	Adenine monophosphate kinase
ADP	Adenosine diphosphate
ATP	Adenosine triphosphate
ANOVA	Analysis of variance
BMI	Body mass index
BSA	Bovine serum albumin
CCCP	Carbonyl cyanide 3-chlorophenylhydrazone
CPT1	Carnitine-palmitoyltransferase 1
CoA	Coenzyme A
DAMP	Damage-associated molecular pattern
DNA	Deoxyribonucleic acid
DAG	Diacylglycerol
DGAT1	Diacylglycerol acyltransferase 1
DGAT2	Diacylglycerol acyltransferase 2
DMSO	Dimethyl sulfoxide
DMEM	Dulbecco's Modified Eagle's medium
DRP1	Dynamin-related protein 1
ETF	Electron transferring flavoprotein
ETC	Electron transport chain
ER	Endoplasmic reticulum
eNOS	Endothelial nitric oxide synthase
ECAR	Extracellular acidification rate
FA	Fatty acid
FBS	Fetal bovine serum
FGF21	Fibroblast growth factor 21
FAD/FADH2	Flavin adenine dinucleotide
FFA	Free fatty acid
Glc	Glucose
Gln	Glutamine
GPAT4	Glycerol-3-phosphate acyltransferase 4
GAN	Gubra-Amylin NASH
HGP	Hepatic glucose production
HSC	Hepatic stellate cells
HFD	High-fat diet
iNOS	Inducible nitric oxide synthase
IRS1/2	Insulin receptor substrate 1 and 2
KD	Knockdown
KO	Knockout
LD	Lipid droplet
LCAD	Long-chain acyl-CoA dehydrogenase
LCFA	Long-chain fatty acid

LPA	Lysophosphatidic acid
MCAD	Medium-chain acyl-CoA dehydrogenase
MetS	Metabolic syndrome
MCD	Methionine-choline deficient
MAMP	Microbial-associated molecular patterns
Mdivi-1	Mitochondrial division inhibitor 1
Mfn1	Mitofusin 1
Mfn2	Mitofusin 2
MitoQ	Mitoquinone
MUFA	Monounsaturated fatty acid
NAD/NADH	Nicotinamide adenine dinucleotide
NADP/NADPH	Nicotinamide adenine dinucleotide phosphate
NNT	Nicotinamide nucleotide transhydrogenase
NAFL	Non-alcoholic fatty liver
NAFLD	Non-alcoholic fatty liver disease
NASH	Non-alcoholic steatohepatitis
NEFA	Non-esterified fatty acids
Opa1	Optic atrophy 1
OCR	Oxygen consumption rate
PNPLA3	Patatin-like phospholipase domain-containing 3
PAMP	Pathogen-associated molecular patterns
P/O	Phosphate to oxygen ratio
PUFA	Polyunsaturated fatty acid
PVDF	Polyvinylidene difluoride
PKC	Protein kinase C
PER	Proton efflux rate
SFA	Saturated fatty acid
GSNO	S-nitrosoglutathione
S1QEL	Suppressors of complex I site Q electron leak
S3QEL	Suppressors of complex III site Q electron leak
TMRM	Tetramethylrhodamine ester
TAG	Triacylglycerol
TCA	Tricarboxylic acid cycle
T2D	Type 2 diabetes
VLCAD	Very-long-chain acyl-CoA dehydrogenase
WAT	White adipose tissue
WT	Wild type
WHO	World Health Organization

SUMMARY

1. Introduction

In this Thesis, we aim to present and discuss the data collected during my Ph.D. studies, from 2016 to 2020. I worked with hepatic steatosis models, *in vivo* and *in vitro*, and focused on the effects of lipid overload on mitochondrial form and function, considering the scope of redox signaling. This introductory section highlights information regarding the epidemiology, pathophysiology, and the molecular players of hepatic steatosis described up to now.

1.1. Metabolic diseases and liver steatosis

The global pandemic of obesity has wide repercussions on public health. Beyond the social and psychological impacts on individuals, obesity is a risk factor for many non-communicable diseases that are prominent as causes of deaths worldwide: heart diseases, stroke, Alzheimer's disease, and type 2 diabetes mellitus (T2D) (Blüher, 2019; Parto and Lavie, 2017; Silva et al., 2019; Soto-Cámara et al., 2020; Tomiyama, 2019). The World Health Organization (WHO) defines overweight and obesity based on body mass index (BMI = body mass/height^2); for adults, 25 and 30 kg/m^2 are the respective cutoffs (World Health Organization, 2020). In Brazil, data from 2019 shows the prevalence of overweight of about 55%, and, for obesity, 20% (Brasil, Ministério da Saúde, 2020).

Obesity is a heterogeneous condition and is clinically relevant when associated with comorbidities (Godoy-Matos et al., 2020; Tchernof and Després, 2013). A critical scenario to be considered for an obese individual is the occurrence of the Metabolic Syndrome (MetS). Although there is no consensus of the definition MetS, most Associations defining it agree that in addition to high waist circumference ("central obesity"), dyslipidemia, high insulin or high fasting glucose and hypertension must be present to be diagnosed with MetS (Godoy-Matos et al., 2020; O'Neill and O'Driscoll, 2015). The molecular players of MetS are complex and not yet fully understood, although clearly associated with overeating and sedentarism. Pharmacological and behavioral interventions may lead to decreased body mass and the rescue

of glucose homeostasis, but are insufficient in the long term, making the main molecular culprits tricky to pursue.

One of the targets of increased adiposity is the liver. Non-alcoholic fatty liver disease (NAFLD) is a term that comprises a spectrum of liver diseases that has lipid accumulation in the hepatocyte cytoplasm, i.e., steatosis. It does not include steatosis caused by heavy alcohol drinking (Majumdar and Tsochatzis, 2020). NAFLD ranges from simple steatosis (non-alcoholic fatty liver, NAFL) to a more severe condition with inflammation and cell damage (non-alcoholic steatohepatitis, NASH). The progression of NAFL entails inflammation, liver fibrosis at the pericentral zone, and can evolve irreversibly to cirrhosis and hepatocellular carcinoma. While the clinical evolution is widely variable, up to 30% of NAFL patients will reversibly develop NASH, while up to 20% of NASH patients can develop cirrhosis (Loomba and Adams, 2019; Younossi et al., 2016).

MetS is the highest risk associated with the development of NAFLD, although steatosis may also exacerbate MetS outcomes such as cardiovascular diseases (Godoy-Matos et al., 2020). Other notable epidemiological data are that obese individuals have at least a 5-fold higher risk of being diagnosed with steatosis (Loomis et al., 2016), and about 75% of T2D patients have steatosis. Importantly, NAFLD is the leading cause of liver disease and has increased as an indication for liver transplantation (Majumdar and Tsochatzis, 2020). Its growing global prevalence is currently 25%, higher in men than in premenopausal women (Majumdar and Tsochatzis, 2020; Younossi et al., 2016). Currently, there are no approved treatments for NAFLD, but interventions to curb obesity, MetS, and T2D are usually employed to reduce lipid accumulation, inflammation, and fibrosis (Friedman et al., 2018; Godoy-Matos et al., 2020).

1.2. Hepatic signaling and inter-organ crosstalk

The liver is a highly vascularized organ regulating circulatory glucose and lipid levels in response to the metabolic state (i.e., fed vs. fasted). It is under the close influence of many factors coming from diet, the pancreas, white adipose tissue (WAT), gut, skeletal muscle, etc. Insulin and glucagon, coming from the pancreas, are canonical textbook examples of hormonal influence on liver metabolism and, hence, physiological regulation of whole-body nutrient availability. Upon fasting-fed cycles, the liver controls glucose levels "on demand" to adjust the availability of glucose to cells and tissues that require this nutrient, such as erythrocytes and neurons. Notably, hepatic glucose production (HGP) is responsible for 90% of endogenous glucose production, and 50% of that is derived from gluconeogenesis (Petersen et al., 2017).

The concept of "metaflammation" in obesity is centered on the development of chronic, systemic, low-grade inflammation in response to nutrient excess (Hotamisligil, 2017; Kuryłowicz and Koźniewski, 2020). WAT hypertrophy and increasing pro-inflammatory signaling in this tissue are important and possibly primary steps during metaflammation and MetS development. Insulin resistance and inflammation are promoted by nutrient oversupply, and described to increase the circulation of non-esterified fatty acids (NEFAs) and cytokines, promote ectopic accumulation of fat (not only in the liver, but skeletal muscle and heart), and disturb the production of adiponectin and leptin (Tchernof and Després, 2013). Both hormones have been suggested as biomarkers of NAFLD progression, since hyperleptinemia and hypoadiponectinemia are common findings in NASH patients (Boutari and Mantzoros, 2020).

T2D is characterized by high fasting glycemia, mostly due to uncontrolled HGP. The gold standard test for liver insulin sensitivity is its ability to suppress HGP, even though insulin inhibition of lipolysis in WAT (and, thus, reducing the circulatory levels of glycerol and NEFAs) also plays a significant role in non-hepatocyte autonomous restrain of HGP. An intriguing aspect of liver insulin resistance in obesity is its dichotomous signaling. While unable

to reduce HGP, insulin still stimulates the *de novo* synthesis of fatty acids (Kubota et al., 2016; Santoleri and Titchenell, 2019). The crosstalk is evident: NASH development is facilitated by insulin resistance (Hodson and Gunn, 2019), and steatosis is a better predictor of liver insulin resistance than higher BMI (Petersen et al., 2017).

Furthermore, the gut-liver axis is connected through the hepatic secretions into the bile duct (containing bile acids, immunoglobulins), the portal vein (containing metabolites from the diet and the microbiome, and pathogen- and microbial-associated molecular patterns – PAMPs and MAMPs), and the systemic circulation (Di Ciaula et al., 2020), and is emerging as an important player in MetS and NAFLD. The intestinal barrier's increased permeability allows MAMPs to reach the circulation, compromising systemic insulin sensitivity, and promoting inflammation (Anhê et al., 2015). Changes in the gut microbiome equilibrium, e.g., gut dysbiosis, are frequently found in obesity and have been associated with the initiation and/or aggravation of liver damage in NAFLD and relate to disease severity (Anhê et al., 2015; Boursier et al., 2016; Di Ciaula et al., 2020).

Besides balancing the availability of nutrients, the liver additionally adjusts systemic metabolism by the secretion of hormones (i.e., hepatokines and bile acids) that direct- or indirectly regulate food intake, body mass gain, energy expenditure, insulin sensitivity, etc. Steatosis may change the levels of many hepatokines (Meex and Watt, 2017; Priest and Tontonoz, 2019). For instance, fetuins are increased NAFLD patients' circulation and may contribute to adipose tissue inflammation and glucose intolerance (Meex et al., 2015; Pal et al., 2012). On the other hand, adropin is decreased in steatosis. The rescue of its effects is associated with improved insulin sensitivity and glucose clearance in response to feeding (Ganesh-Kumar et al., 2012). Particularly, fibroblast growth factor 21 (FGF21), usually produced by the liver in response to exercise and fasting, is paradoxically increased in obese humans (Priest and Tontonoz, 2019). Its actions on adipose tissue and central nervous system were described to

increase glucose clearance and energy expenditure. FGF21 agonists and mimetics are currently promising pharmacological strategies under study to treat obesity-related metabolic diseases (Geng et al., 2020a).

1.3. NAFLD physiopathology

The pathogenesis of NAFLD was defined some time ago based on the "two-hits" hypothesis. The first hit is the accumulation of fat in the hepatocyte cytoplasm, and the second hit is the establishment of another insult, e.g., inflammation or oxidative stress, that would lead to NASH. However, since NAFL is benign and nonprogressive for most patients there is currently more agreement about NASH having distinct pathogenesis, not always preceded by steatosis. In one scenario, steatosis results from imbalanced lipid handling (i.e., increased import and synthesis combined to decreased export and catabolism) that results in lipotoxicity and is followed by inflammation. In another, it might be caused by inflammation *per se*. Tilg and Moschen proposed the "multiple-hits" hypothesis that considers factors coming from the diet, WAT, and gut sustaining disease complexity and heterogeneity (Tilg and Moschen, 2010; Tilg et al., 2020). The two scenarios converge to activating liver pathways associated with ER stress and inflammation to promote and exacerbate NASH. Moreover, a genomic-wide association study of NAFLD confirmed a single nucleotide substitution in the patatin-like phospholipase domain-containing 3 (PNPLA3) gene, that changes isoleucine to methionine in the position 148, as the main genetic risk factor for the full spectrum of NAFLD (Anstee et al., 2020), but also found HSD17B13, TM6SF2, and GCKR as steatosis genetic modifiers.

Both innate and adaptative immunity are important to liver inflammation in NAFLD (Parthasarathy et al., 2020; Sutti and Albano, 2020). Kupffer cells, i.e. liver-resident macrophages, can be activated by damage-associated molecular patterns (DAMPs) released by steatotic and/or injured hepatocytes, and NEFAs, cytokines, chemokines, hormones, and PAMPs coming from the WAT- and/or gut-liver axis (Sutti and Albano, 2020). The pro-

inflammatory cytokines and chemokines recruit monocytes, neutrophils, and lymphocytes to the liver, that sustain NASH progression. Many of these pro-inflammatory factors activate hepatic stellate cells (HSCs) that are responsible for collagen and extracellular matrix formation, the required step for fibrosis establishment (Tsuchida and Friedman, 2017).

Rodent models of NAFLD are centered on *ad libitum* high-fat diets (HFD) and sedentarism, but the lipidic composition of the diets in rodent models is often overlooked and can be a confounding factor in the metabolic outcomes. For example, in a study comparing fat sources using isocaloric diets, Enos et al. observed that from 6 to 12% energy from saturated fatty acid (SFA) in substitution to monounsaturated fatty acid (MUFA) increased adiposity, WAT inflammation, glycemia, and insulinemia, but a further increase to 24% had milder effects compared 12% (Enos et al., 2013, 2014). Interestingly, 24% has proportionally more medium-chain saturated fatty acids compared to the other two, which can be more easily oxidized than long- and very-long- chains, and have different protein acylation capacities (Enos et al., 2014; Resh, 2016). Furthermore, mice usually develop NAFL upon HFD, but NASH is more difficult to achieve (Friedman et al., 2018). Some protocols take advantage of the methionine-choline deficient (MCD) diet that can promote NASH in only 4 weeks. However, these animals do not resemble human MetS since they lose weight and are not insulin resistant. A promising diet-induced model is the Gubra-Amylin NASH diet (GAN diet), similar to the so-called “Western diet”, that combines around 40% of energy from fat (46% of that from SFA), but high concentrations of sucrose and fructose as carbohydrate sources, and added cholesterol. These mice develop metabolic syndrome and histological characteristics of human NASH over time: steatosis, inflammation, ballooning, and fibrosis (Boland et al., 2019; Hansen et al., 2020).

1.4. Hepatic lipotoxicity

Fatty acids can be esterified into diacylglycerols (DAG) and triacylglycerols (TAG) and stored in specialized organelles named lipid droplets (LDs). LDs originate from the

endoplasmic reticulum (ER) and consist of a hydrophobic core containing TAG and cholesterol esters surrounded by a monolayer of phospholipids and harbor their own proteome (Olzmann and Carvalho, 2018). NAFL is established when more than 5% of hepatocytes present LDs (Kleiner et al., 2005). The segregation of lipids in specialized organelles has an energetic function, as a reservoir of readily available substrates, but it is also critical to prevent toxicity at some level. For example, overexpression of diacylglycerol acyltransferase 2 (DGAT2) in mice increased steatosis, but prevented glucose and insulin intolerance (Monetti et al., 2007), while its inhibition exacerbated diet-induced liver damage (Yamaguchi et al., 2007).

Over a threshold, the accumulation of LDs disrupts cellular homeostasis and tissue function. LDs can interact virtually with all the organelles and are prone to sequester proteins on their surface, challenging organellar dynamics and signaling pathways when increased in quantity (Olzmann and Carvalho, 2018; Seebacher et al., 2020). Diet-induced liver steatosis was described to promote protein relocation to the LDs and increase mitochondria-LD contacts (Arruda et al., 2014; Krahmer et al., 2018). The functional implications of these findings are still unclear and controversial but may be relevant for NAFLD progression (Mason et al., 2014; Wang et al., 2015). The liver-specific deletion of perilipin 5, the main protein coating LDs, reduced the contact between mitochondria and LDs and promoted glucose intolerance in both chow- and high fat-fed mice, without changing plasmatic NEFAs and triglycerides (Keenan et al., 2019). Under HFDs, the perilipin 5 KO has exacerbated steatosis and accumulated different acyl-chain DAG, suggesting that the hepatic rearrangement of lipidic species can impact on systemic glucose homeostasis.

The increased concentration of harmful lipids and their molecular deployment is collectively called lipotoxicity (Ertunc and Hotamisligil, 2016). The major outcomes associated with lipotoxicity are ER stress, oxidative stress, lysosomal dysfunction, DNA damage, and insulin resistance. Notably, in *in vitro* models of steatosis, lipid overload is promoted by

exposing the cells to fatty acids conjugated to bovine serum albumin (Alsabeeh et al., 2018). Palmitate, the main circulating fatty acid in human serum, promotes ER stress, oxidative stress, insulin resistance, mitochondrial fragmentation and dysfunction, and cell death in many models. Remarkably, all these effects can be counterbalanced by oleate, stearate, or polyunsaturated fatty acids (PUFAs).

Piccolis et al. recently mapped the effects of palmitate overload on the proteome and lipidome of K562 cells (Piccolis et al., 2019). Interestingly, they describe the synthesis of lysophosphatidic acid (LPA) by glycerol-3-phosphate acyltransferase 4 (GPAT4) as one of the nodal points of lipotoxicity. LPA is a precursor of glycerolipids synthesis, i.e., DAG and TAG, and the partial blockage of DAG synthesis by GPAT4 KD prevented lipotoxicity. In addition, palmitate increases the saturation of acyl-chains, making DAG a poor substrate for TAG synthesis by DGAT1. Increasing the cells' abilities to desaturate fatty acids reduced ER stress and cell death (Masuda et al., 2015; Piccolis et al., 2019).

The accumulation of DAG has been widely described as the main player of hepatic insulin resistance. DAG is enriched in the plasma membrane and stimulates a novel isoform of protein kinase C, PKCε, that phosphorylates the insulin receptor at the Thr1160 residue and inactivates it (Lyu et al., 2020; Petersen et al., 2016). Interestingly, this inhibition is liver specific.

1.5. Mitochondrial form

Mitochondria are dynamic organelles regarding function and form and can quickly adapt to profound changes in their surroundings (Chan, 2020; Gordaliza-Alaguero et al., 2019; Spinelli and Haigis, 2018). In addition to their roles related to ATP production and cell death, mitochondria act as important cell hubs regulating calcium signaling, supplying intermediates for lipid synthesis, and modulating oxidant production and removal. Concomitantly, they cooperate with pathways regulating metabolism, such as the insulin cascade, providing flexibility for nutrient usage (Betz et al., 2013; Cheng et al., 2010).

Mitochondria are continuously alternating between tubular to circular shapes due to fusion and fission events (Liesa and Shirihai, 2013). These processes enable the retention of healthy organelles and the degradation of damaged mitochondria, and the cell adaptation to external stimuli (Chan, 2020). For instance, nutrient oversupply typically promotes a more interrupted network, with small, oval- or circular-shaped mitochondria, while starvation increases the size and the connectivity of mitochondria (Molina et al., 2009; Rambold et al., 2011). The ability to fuse is associated with more homogeneous distribution and oxidation of fatty acids by the mitochondrial network, and higher calcium uptake and retention capacity (Kowaltowski et al., 2019; Rambold et al., 2015). It is unclear, though, if mitochondrial shape *per se* compromises bioenergetic efficiency.

The fusion machinery is composed of the proteins mitofusin 1 and 2 (Mfn1 and Mfn2) and optic atrophy 1 (Opa1), and fission is mediated by adaptor proteins that recruit dynamin-related protein 1 (DRP1) to execute it (Chan, 2020; Wai and Langer, 2016). Liver-specific deletion of Mfn1 leads to fragmented mitochondrial networks and protects mice from insulin resistance induced by a high-fat diet. It does not disturb lipid accumulation, but increases LD mean size (Kulkarni et al., 2016). The deletion of liver Mfn2 also promotes mitochondrial fragmentation. However, even on a normal diet, these mice present impaired insulin signaling and glucose homeostasis (Sebastián et al., 2012). Interestingly, both mitofusins can mediate outer membrane fusion, but they are not functionally redundant (Li et al., 2019b). Mfn2 has roles beyond mitochondrial fusion (Filadi et al., 2018). For instance, Mfn2 is involved in mitochondria-ER tethering and changes in these contacts are described to disrupt cellular calcium signaling and mitochondrial function in mice obesity models (Arruda et al., 2014). More recently, Hernández-Alvarez et al. described that NASH patients and NAFLD mouse models have lower Mfn2 protein levels, and the pathogenesis is related to a deficient shuttling

of lipidic intermediates between mitochondria and ER, that compromises phospholipid synthesis (Hernández-Alvarez et al., 2019).

In *in vitro* studies, saturated myristic and palmitic fatty acids (SFAs), but not stearic nor unsaturated fatty acids such as oleic and docosahexaenoic acids, promote mitochondrial fission in C2C12 cells. Palmitic acid treatment reduced insulin sensitivity, and this effect was abrogated by both Drp1 silencing and pharmacological inhibition by Mdivi-1 (Jheng et al., 2012). Similar observations were made by Zhang et al. (2011) in HepG2 hepatocytes, where docosahexaenoic acid reversed fatty acid-induced fission by promoting fusion (Zhang et al., 2011). In Huh7 cells, palmitate decreased insulin sensitivity in a Mfn2-dependent manner (Tubbs et al., 2014). Remarkably, the SFA stearic acid promotes mitochondrial elongation by decreasing Mfn2 turnover (Senyilmaz et al., 2015), an effect not reproduced by palmitate (Senyilmaz-Tiebe et al., 2018).

1.6. Mitochondrial function

The liver is a highly flexible organ that can oxidize and synthesize carbohydrates, fatty acids, and amino acids, and promptly detoxify xenobiotics. The center of its metabolism are mitochondria playing many roles in providing ATP, regulating calcium dynamics and redox signaling, lipid and amino acid synthesis and catabolism, synthesis of ketone bodies, and many other functions to sustain basal metabolism. Unsurprisingly, "mitochondrial function" is of vital importance when studying liver diseases. The broad term usually refers to the organelle's abilities to produce ATP efficiently, and can be assessed by monitoring oxygen consumption in isolated organelles or intact cells (Brand and Nicholls, 2011).

1.6.1. Isolated systems

For isolated organelles, the rationale is to provide substrates that fuel the electron transport chain complexes directly or indirectly (**Fig 1.1**) and allow the phosphorylation of ADP to occur. The oxygen consumption rate (OCR) is a readout of the system's capacity to work

within the chosen experimental setup. Briefly, mitochondria, resuspended in an adequate buffer containing phosphate and osmotic support, are challenged by the sequential addition of i) saturating concentrations of a substrate, ii) ADP (state 3) and iii) the ATP synthase inhibitor oligomycin (state 4o) (**Fig 1.2**).

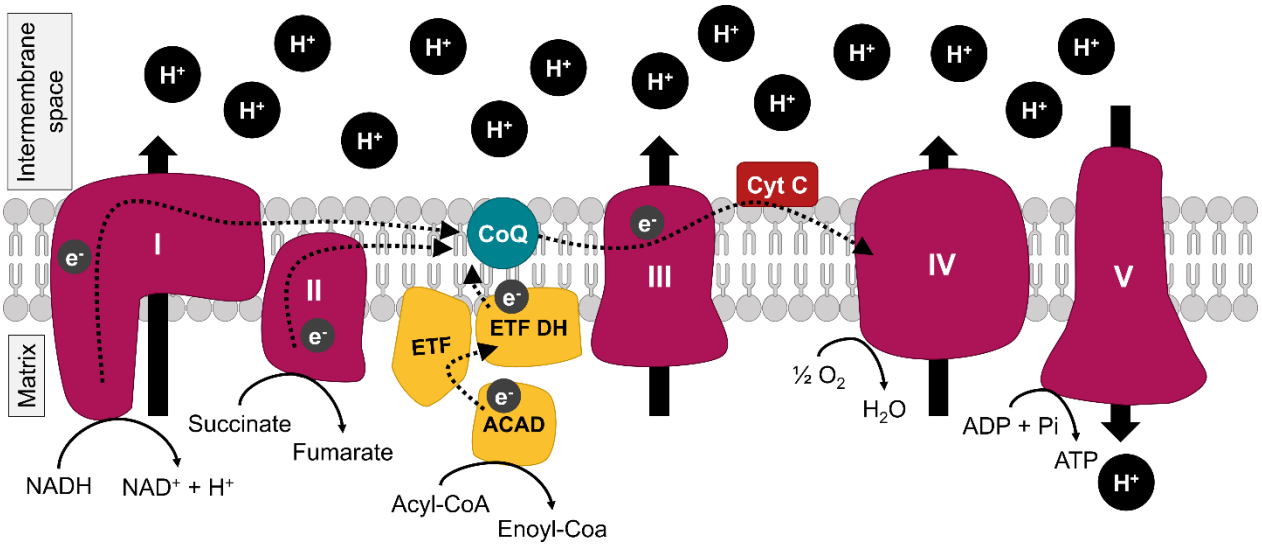

Figure 1.1: Scheme of the mitochondrial electron transport chain.

The varying oxygen concentration is measured real-time in a sealed chamber containing an oxygen electrode, e.g., an Oroboros O2k-Respirometer (Austria). The OCR in state 3 is associated with maximal respiration that mitochondria can perform, relying on functional respiratory complexes and ATP synthase, and efficient transportation and oxidation of the chosen substrate. State 4 is the system's residual proton leak, i.e., reentry of protons to the matrix independently of ATP synthase. The respiratory control ratio (RCR) is defined as the ratio of state 3/state 4. If the isolation process did not damage the mitochondrial membranes, higher values of RCR would imply relatively functional mitochondria, i.e., more "coupled", while lower, dysfunctional, or less coupled. Another strategy of oxygen consumption manipulation is to use uncouplers, e.g., 2,4-dinitrophenol (DNP) or carbonyl cyanide 3-chlorophenylhydrazone (CCCP). Those are highly lipophilic compounds that dissipate the mitochondrial membrane potential by promoting the reentry of protons to the matrix and

accelerating the respiration to the maximal capacity of transport and oxidation of a given substrate, independently of the ATP synthase.

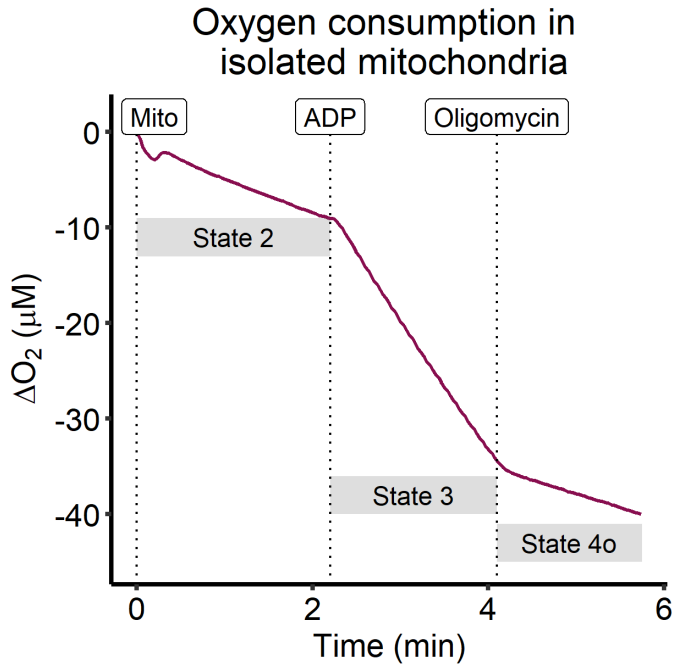

Figure 1.2: Representative plot of an oxygen consumption experiment in a high-resolution oxygraph.

Of particular interest for steatosis development, the catabolism of fatty acids can take place in mitochondria and peroxisomes, by β-oxidation, or through ω-oxidation in the ER. Mitochondrial β-oxidation degrades short- to very-long- chain fatty acids (4-20 carbons), while the peroxisomes are effective with long- to very-long-chain- fatty acids (above 10 carbons) (Eaton, 2002; Reddy and Hashimoto, 2001). The fatty acids are conjugated to a coenzyme A (CoA) in the cytoplasm and access the mitochondrial matrix through the carnitine shuttle. Mitochondrial β-oxidation is a cyclic path, and one cycle generates a two-carbon shorter acyl-CoA for the next round, and an acetyl-CoA, a $FADH_2$ and a NADH that connects FA oxidation directly to the Krebs cycle and electron transport chain (ETC). The first step is a dehydrogenation of the acyl-CoA by the acyl-CoA dehydrogenase (ACADs) family of enzymes. Each isoform is specific for a range of acyl-chain size and yields one $FADH_2$ and one trans-Δ^2-Enoyl-CoA per cycle (Ghisla and Thorpe, 2004). $FADH_2$-bound ACADs are oxidized by the electron transferring flavoprotein (ETF). These electrons are then transferred to the ETF-

dehydrogenase and subsequently to the coenzyme Q, which contributes to the mitochondrial membrane potential when oxidized by Complex III. The other product of the first dehydrogenation, trans-Δ^2-Enoyl-CoA, is further hydrated to 3-L-hydroxyacyl-CoA, dehydrogenated to β-ketoacyl-CoA, and cleaved to a two-carbon shorter acyl-CoA and an acetyl-CoA by a three-set of enzymes, or by the mitochondrial trifunctional protein (Adeva-Andany et al., 2019). The second dehydrogenation step yields one NADH that can be oxidized in Complex I. Therefore, the fatty acid oxidation capacity through mitochondrial β-oxidation can be assessed in isolated organelles by oxygen consumption experiments.

In Kakimoto and Kowaltowski, 2016, we reviewed the literature regarding liver mitochondrial bioenergetics and oxidative stress in diet-induced obesity rodent models. We summarized the effects of high-fat diets on mitochondrial respiration and production of oxidants, i.e., hydrogen peroxide and superoxide. Most of the studies found increased production of hydrogen peroxide and of oxidative stress markers in HF-fed animals. Interestingly, oxygen consumption with energized complex I or II was unchanged or decreased, while palmitoylcarnitine-supported respiration could be found to increase or decrease. Some authors suggest a dynamic process ongoing in which the fluxes adapt while coping with the nutrient availability and energetic demand. However, it is still unclear when and how mitochondrial dysfunction occurs in diet-inducing models of hepatic steatosis.

On the other hand, human liver mitochondria are more consensually described to have higher FA oxidation rates in NAFL. In a cohort of obese individuals, mitochondria were found to be uncoupled independently of the steatosis grading, having higher overall respiration in all states and substrates tested (Koliaki et al., 2015). However, when comparing obese NAFL versus NASH, authors found decreased state 3 and maximal respiration in NASH patients while still building up the markers of inflammation and oxidative stress. This suggests a lower mitochondrial oxidative capacity in NASH, appearing after the other stress signaling pathways

were already active. Furthermore, in an interesting approach, Fletcher & Deja et al. recently described the reduced capacity of NAFL subjects to produce ketone bodies when under prolonged fasting. Curiously, the rates of acetyl-CoA production by β-oxidation were unchanged. However, the metabolite was re-routed to the TCA, followed by increased oxygen consumption rates, pyruvate carboxylase flux, and endogenous glucose production that may account for hyperglycemia observed in the subjects (Fletcher et al., 2019). In another cohort of humans, Peng et al. described an accumulation of acyl-carnitines in NASH patients, but not in NAFL. This accumulation may result from the impaired mitochondrial oxidative capacity described previously and corroborates with the hypothesis of ongoing metabolic changes supporting nutrient flexibility upon the advance of NAFL to NASH (Peng et al., 2018).

1.6.2. Intact cells

In intact cells, the OCR can be measured by oxygraphy as well. However, this may be costly for some models since the cells need to be suspended and in high numbers (~1 million per replicate). An alternative is to use the Seahorse equipment (Agilent, USA) that measures real-time oxygen concentration and pH by fluorescence in a small volume of media (~10 μL). In this setup, the cells are adhered to plates (~twenty thousand per replicate) during all processes and the fluorescent probe is approached to the cells using mobile pistons only during the measurements, providing both OCR and the media pH variation (ECAR, extracellular acidification rate) for a given time. Analogously, the OCR is measured under basal conditions and modulated by oligomycin and uncouplers (**Fig 1.3**). Non-mitochondrial respiration is assessed by blocking respiratory complexes I and III with rotenone and antimycin A, respectively. This experiment can provide many parameters, e.g., ATP-linked respiration, proton-leak, maximal respiration capacity, and reserve respiration, useful to assess mitochondrial function (Brand and Nicholls, 2011; Hill et al., 2012).

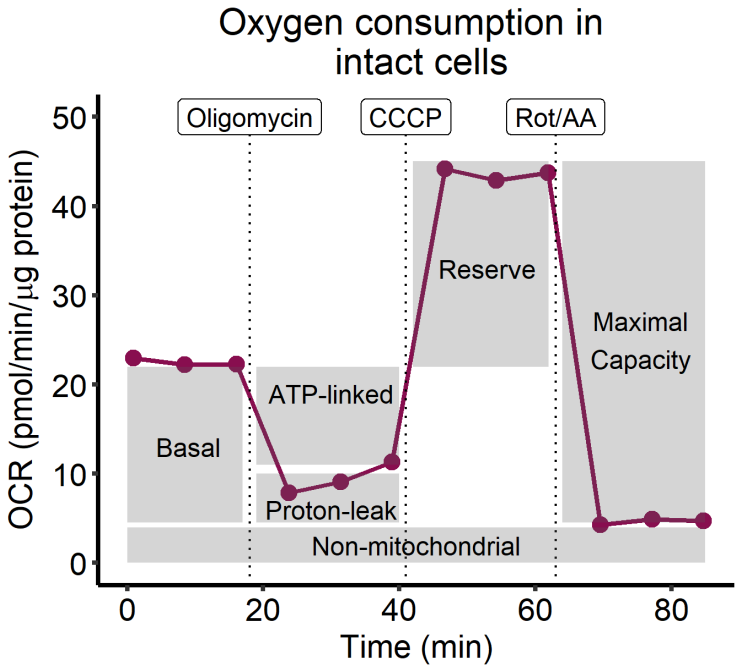

Figure 1.3: Representative plot of an oxygen consumption experiment in a Seahorse (Agilent) equipment.

Interestingly, primary hepatocytes from ob/ob mice (that lack leptin) and high-fat-fed WT animals show decreased basal, ATP-linked, and maximal OCR compared to lean counterparts, which suggests an overall decrease in the ETC capacity (Arruda et al., 2014; Liu et al., 2015). In an *in vitro* model, Egnatchik et al. demonstrated that palmitate, but not oleate, after 3 and 6 hours, increased basal oxygen consumption in rat H4IIEC3 hepatoma cells (Egnatchik et al., 2014a, 2019). They suggested that increased calcium flux from the ER is stimulated by palmitate, therefore increasing TCA flux through anaplerotic contribution of glutamine. Inhibition of aspartate aminotransferase reduced the lipotoxic effects of palmitate in both H4IIEC3 and primary rat hepatocytes (Egnatchik et al., 2014b).

1.6.1. Indirect quantification of ATP production rate

Another strategy takes advantage of the ECAR and OCR to calculate ATP production and to ascribe, indirectly, its source: i.e., if mitochondrial or glycolytic. The main assumptions are described in detail in Mookerjee et al., 2017, and the experiment is conducted as standardized by Seahorse (Agilent). Briefly, glucose catabolism decreases the pH by two pathways: 1)

production of lactate, and 2) production of CO_2 in the TCA. Each ATP produced from glycolysis yields 1 lactate and 1 proton in the extracellular media and each ATP produced from the ETC consumes 0.18 O_2 (considering the P/O as 2.75, the mean for a mixture of substrates). Some parameters are already standardized by the manufacturer: the CO_2 contribution factor to the pH variation and the chamber volume for each equipment. The buffer capacity is defined for each culture media and is used to correct the ECAR to the real proton efflux rate (PER). The glycolytic PER is defined as the subtraction of mitochondrial PER (calculated by the conversion of mitochondrial respiration to protons, by the CO_2 contribution factor) from total PER **(Fig 1.3)**. Using this stoichiometry, every glycolytic proton comes from 1 lactate secreted, and, thus, 1 ATP. Mitochondrial ATP is calculated by the ATP-linked OCR corrected by the P/O*2. The ATP production rate is obtained in the pmol/min unit, useful to compare the contribution of each pathway in cellular metabolism.

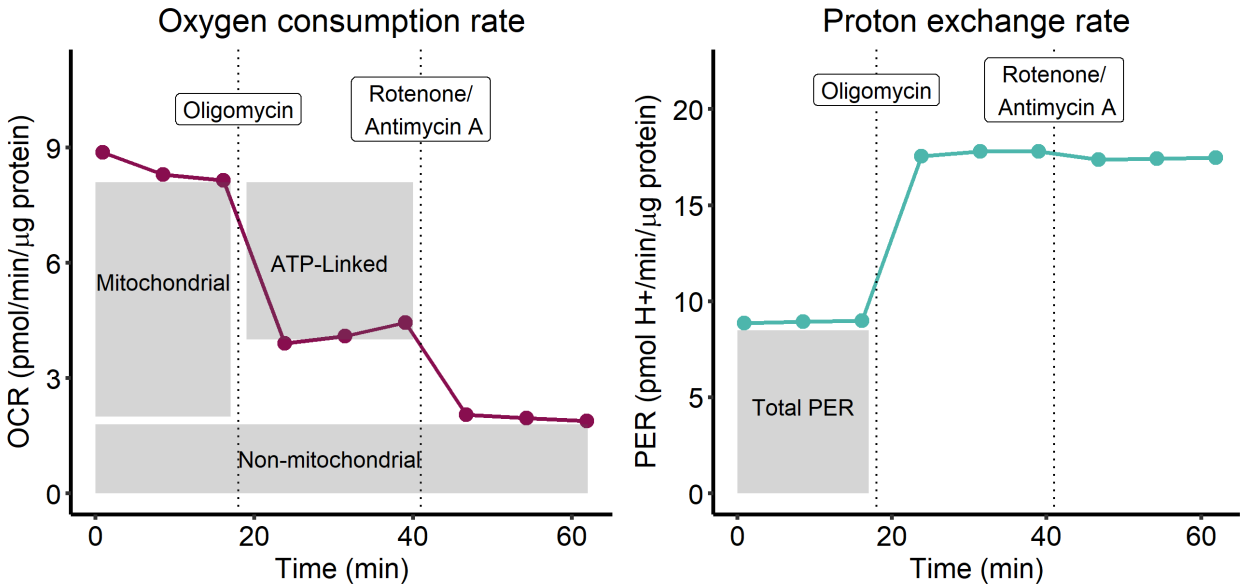

Figure 1.4: Representative plot of an experiment in a Seahorse (Agilent) equipment for ATP production rate calculations. Both traces are obtained simultaneously.

1.7. Redox signaling

Mitochondria are one of the main sites of oxidant production inside the cell (Figueira et al., 2013). Complexes I, II, and III can transfer 1 or 2 electrons directly to molecular oxygen,

forming superoxide or hydrogen peroxide, respectively. There are more than 12 sites of electron leakage in the ETC and in the dehydrogenases that feed electrons to it (Brand, 2016). For example, mitochondrial β-oxidation enzymes inherently produce superoxide or hydrogen peroxide at the level of MCAD, LCAD, VLCAD, and ETF, as a by-product of their reactions (Kakimoto et al., 2015; Rodrigues and Gomes, 2012; Zhang et al., 2019). Short-term high-fat feeding to mice increased hydrogen peroxide generation by liver mitochondria in a VLCAD-dependent manner (Cardoso et al., 2013). Nonetheless, in unstressed conditions, mitochondria have effective antioxidant systems that counteract superoxide and hydrogen peroxide production at physiological levels and prevent unrestrained modification of biomolecules (Figueira et al., 2013).

The relevance of both production and removal of mitochondrial oxidants in steatosis is evidenced when studied under the light of the nicotinamide nucleotide transhydrogenase (NNT) function. NNT is a proton-translocating enzyme, located in the inner mitochondrial membrane, that catalyzes the transfer of a hydride from NADH to $NADP^+$ while consuming mitochondrial inner membrane potential (Rydström, 2006). NADPH is used by the antioxidant systems to restore glutathione and thioredoxin to the reduced forms, that are oxidized during the removal of hydrogen peroxide. Consequently, NNT activity couples the detoxification of oxidants to the electron transport chain since the forward reaction is stimulated by high mitochondrial membrane potentials and by the antioxidant machinery. In 2005, C57BL/6J mice from Jackson Laboratories were found to carry a mutation developed spontaneously sometime in the 1970s, that yields a non-functional, truncated NNT (Toye et al., 2005). Ronchi et al. characterized the poor peroxide removal capacity by liver mitochondria in these animals compared to C57BL/6JUnib mice, which do not harbor the mutation (Ronchi et al., 2013, 2016). Remarkably, animals lacking NNT challenged by HFD are more prone to gain body mass, develop steatosis, and have disturbed glucose homeostasis, while their liver mitochondria

produce more hydrogen peroxide and have higher susceptibly to open the permeability transition pore, a consequence of mitochondrial redox imbalance (Navarro et al., 2017; Nicholson et al., 2010).

Furthermore, nitric oxide signaling may also be relevant for mitochondrial function and steatosis development. $NO^{\bullet}$ is a second messenger with distinctive characteristics: it is a gaseous, diatomic, and uncharged free radical that is water-soluble but also membrane-permeant (Toledo and Augusto, 2012). The types of modifications promoted by $NO^{\bullet}$ to propagate signals vary widely and depend on its concentration and the target's environment. For example, $NO^{\bullet}$ interacts with mitochondrial respiratory complex IV through a ferrous heme site, promoting competitive respiration inhibition, since this is the same site for O_2 binding. The classic activation of soluble guanylate cyclases is fast and reversible and also involves $NO^{\bullet}$ binding to the ferrous heme. Interestingly, the interaction of $NO^{\bullet}$ with non-heme ferrous iron and peptide/protein thiols has been gaining attention due to the formation of dinitrosyl iron complexes, ascribed to be the most abundant $NO^{\bullet}$ adducts in both physiological and pathological ranges (Hickok et al., 2011). Moreover, $NO^{\bullet}$ ability to scavenge superoxide is not negligible when $NO^{\bullet}$ is in high concentration; the reaction produces peroxynitrite, that can react with thiol and hemes of proteins, carbon dioxide, and decompose forming the even more reactive hydroxyl radical (Toledo and Augusto, 2012).

S-nitrosation of cysteines is an important modification arising from $NO^{\bullet}$ and peroxynitrite. Doulias et al. 2013 characterized the S-nitrosocysteine proteome of many organs and identified that many glycolytic and TCA enzymes are modified. Interestingly, at least 20% of mitochondrial proteins were modified. They further described that VLCAD activity is regulated through a S-nitrosation of the cysteine 238, in an eNOS-dependent manner. Authors found that ob/ob mice had lower liver palmitate oxidation and higher VLCAD Km, both effects abrogated by the NO-donor S-nitrosoglutathione (GSNO). Curiously, GSNO decreased

triglyceride accumulation in these mice. Likewise, tyrosine nitration, another post-translational modification resulting from peroxynitrite reaction, is described to modify insulin signaling proteins (IRS1/2 and AKT) upon lipid challenge. Interestingly, AKT nitration was shown to compromise insulin-induced phosphorylation at the residue serine 473, but not threonine 308 (Charbonneau and Marette, 2010).

However, $NO^{\bullet}$ signaling in the obese liver is still under investigation and has some intricate interactions. The inducible nitric oxide synthase (iNOS) is expressed through pro-inflammatory pathway activation and produces nitric oxide in an unrestrained manner in the micromolar range. Endothelial nitric oxide synthase (eNOS), on the other hand, is regulated by calcium, and the $NO^{\bullet}$ output is in the nanomolar range. Both are expressed in hepatocytes and Kupffer and endothelial cells (Cunningham et al., 2020; McNaughton et al., 2002). Interestingly, while the iNOS knockout (KO) has been associated with protection from insulin resistance induced by diet (Charbonneau and Marette, 2010; Fujimoto et al., 2005; Nozaki et al., 2015a; Perreault and Marette, 2001; Shinozaki et al., 2011), eNOS KO increased liver inflammation and fibrosis induced by a Western diet (i.e., high fat, high sucrose, and high cholesterol) (Nozaki et al., 2015b; Sheldon et al., 2019). Oral supplementation of $NO^{\bullet}$ donors also improved steatosis and glucose tolerance (Maslak et al., 2015). Conversely, Qian et al. described that the KO of GSNO reductase, an enzyme that reduces S-nitrosothiols of cysteines in proteins and GSNO back to thiols (Barnett and Buxton, 2017), *per se* increases steatosis and reduces liver insulin sensitivity depending on lysosomal function and autophagy activation (Qian et al., 2018). Recently, the same group found iNOS in close proximity to the lysosomal surface of HF-fed mice, contributing to nitrosative stress and lysosomal dysfunction (Qian et al., 2019).

These studies suggest that the control of metabolism by nitric oxide is well-adjusted and affects the signaling and metabolic pathways differently. The opposite effects of iNOS versus

eNOS are probably related to the range of output (physiological vs. pathophysiological), the timely production, and the intracellular production location (Toledo and Augusto, 2012).

2. Objectives

The main objective of this Thesis is to determine whether redox signaling participates in metabolic changes promoted by diets rich in lipids. To verify this possibility, we characterized the modulation of mitochondrial bioenergetics upon nutritional stimuli related to lipid overload through two approaches:

1. Evaluation of changes in hepatic energy metabolism that accompany the decrease in systemic insulin sensitivity in C57BL/6NTac wild-type mice and knockout animals for iNOS submitted to high-fat diet, discussed in “Results - Part 1”.

2. Identification and characterization, in hepatocyte cell lines, of the metabolic and signaling pathways related to fatty acid toxicity, discussed in “Results - Part 2”.

3. Results – Part 1: Resilient hepatic mitochondrial function and lack of iNOS dependence in diet-induced insulin resistance

In this Section, we aimed to evaluate the combinatory effects of diet-induced obesity and inflammatory nitric oxide on liver mitochondrial function. Part of the work was conduct in collaboration with Professor José Donato Junior from *Instituto de Ciências Biomédicas da Universidade de São Paulo.* These results were published as an original article in PLoS One on February 4th, 2019, (Kakimoto et al., 2019) and it is attached to this thesis.

PLOS ONE

RESEARCH ARTICLE

Resilient hepatic mitochondrial function and lack of iNOS dependence in diet-induced insulin resistance

Pamela A. Kakimoto[1]*, Bruno Chausse[1¤], Camille C. Caldeira da Silva[1], José Donato Júnior[2], Alicia J. Kowaltowski[1]

1 Departamento de Bioquímica, Instituto de Química, Universidade de São Paulo, São Paulo, Brazil, **2** Departamento de Fisiologia e Biofísica, Instituto de Ciência Biomédicas, Universidade de São Paulo, São Paulo, Brazil

¤ Current address: Institute of Physiology and Pathophysiology, University of Heidelberg, Heidelberg, Germany
* pamela.kakimoto@gmail.com

OPEN ACCESS

Citation: Kakimoto PA, Chausse B, Caldeira da Silva CC, Donato Júnior J, Kowaltowski AJ (2019) Resilient hepatic mitochondrial function and lack of iNOS dependence in diet-induced insulin resistance. PLoS ONE 14(2): e0211733. https://doi.org/10.1371/journal.pone.0211733

Editor: Vanessa Souza-Mello, State University of Rio de Janeiro, BRAZIL

Received: September 21, 2018

Accepted: January 18, 2019

Published: February 4, 2019

Data Availability Statement: All relevant data are within the manuscript and its Supporting Information files.

Funding: This work was funded by CEPID 2013/07937-8, FAPESP DD 2015/25862-0, FAPESP PD 2015/07670-7, FAPESP 2017/18972-0, CAPES and CNPq. The funders had no role in study design, data collection and analysis, decision to publish, or preparation of the manuscript.

Competing interests: The authors have declared that no competing interests exist.

Abstract

Obesity-derived inflammation and metabolic dysfunction has been related to the activity of the inducible nitric oxide synthase (iNOS). To understand the interrelation between metabolism, obesity and $NO^{\cdot}$, we evaluated the effects of obesity-induced $NO^{\cdot}$ signaling on liver mitochondrial function. We used mouse strains containing mitochondrial nicotinamide transhydrogenase activity, while prior studies involved a spontaneous mutant of this enzyme, and are, therefore, more prone to oxidative imbalance. Wild-type and iNOS knockout mice were fed a high fat diet for 2, 4 or 8 weeks. iNOS knockout did not protect against diet-induced metabolic changes. However, the diet decreased fatty-acid oxidation capacity in liver mitochondria at 4 weeks in both wild-type and knockout groups; this was recovered at 8 weeks. Interestingly, other mitochondrial functional parameters were unchanged, despite significant modifications in insulin resistance in wild type and iNOS knockout animals. Overall, we found two surprising features of obesity-induced metabolic dysfunction: (i) iNOS does not have an essential role in obesity-induced insulin resistance under all experimental conditions and (ii) liver mitochondria are resilient to functional changes in obesity-induced metabolic dysfunction.

Introduction

Nitric oxide ($NO^{\cdot}$) is a gaseous membrane-permeable free radical that acts as a cellular signaling molecule through many mechanisms including activating soluble guanylyl cyclases, covalent modification of amino acids residues and lipids, scavenging of superoxide (forming peroxynitrite), and competing with molecular oxygen within mitochondrial Complex IV [1,2]. $NO^{\cdot}$ is synthesized mainly by nitric oxide synthase (NOS) family enzymes, which includes three isoforms that catalyze the reaction of arginine, NADPH and O_2 to citrulline, $NADP^+$ and $NO^{\cdot}$ [3]. NOS2 is the inducible nitric oxide synthase (iNOS) isoform, expressed under pro-inflammatory

stimuli that activate the transcriptional factor NF-κB [4]. Conversely, calcium-dependent NOS1 and NOS3 are constitutively expressed. Upon induction of expression, iNOS has a much higher $NO^{\cdot}$ output than other NOSs, and is not controlled by Ca^{2+} [3,5].

Because of its high output and inducible characteristic, iNOS has been suggested to participate in inflammatory mechanisms associated with obesity [6], acting both within the physiopathology of the disorder and in the development of comorbidities [5,7]. In obese mouse livers, iNOS is found in hepatocytes as well as in macrophages/Kupffer cells [8]. Interestingly, insulin resistance induced by high fat diets (HFD) has been shown to be prevented by iNOS KO in mice [9], while its overexpression promotes liver steatosis and insulin resistance [10]. In a lipid infusion model, Charbonneau et al. demonstrated that fatty acids acutely promoted liver insulin resistance, increased hepatic glucose production and the nitration of important insulin downstream effectors (e.g. IRS1, IRS2 and AKT). All effects were prevented by iNOS KO [11]. Indeed, nitration and nitros(yl)ation of amino acids residues are important post-translational modifications that modulate metabolic pathways such as insulin signaling [12,13]. HFDs were shown to increase nitrotyrosine content in the liver [14], while a S-nitrosocysteine proteome analysis identified metabolic enzymes that are be S-nitros(yl)ated. The very long chain acyl-CoA dehydrogenase (VLCAD), an important β-oxidation enzyme, is one of the enzymes that can be S-nitros(yl)ated and, surprisingly, is activated by this modification at Cys238 [15]. Overall, these results consist of a strong set of evidence indicating that $NO^{\cdot}$ has significant roles in metabolic control resulting from HFDs.

$NO^{\cdot}$ may act in metabolic diseases by affecting mitochondria, central hubs for both the regulation of metabolism and oxidant production. As reviewed by Shiva et al., 2017, mitochondria and $NO^{\cdot}$ can interact at many different levels, since nitric oxide permeates membranes and may react directly with electron transport chain complexes, matrix enzymes, and superoxide radicals [16]. As such, disease-related $NO^{\cdot}$ and nutrient oversupply may compromise mitochondrial metabolic function.

In a recent review covering the effects of HFDs on liver mitochondria, we found that (i) many studies show prominent oxidative imbalance, (ii) some studies find NADH-linked or succinate-supported respiration to be decreased (while others do not), (iii) oxygen consumption was more susceptible to $NO^{\cdot}$ inhibition in one study [14], and (iv) some studies also find changes in fatty acid oxidation (reviewed in [17]). The discrepancies in prior studies are probably due to different protocols including in dietary composition and time on the HFD.

Notably, most HFD protocols do not compare their animals to those reared on synthetic diets with controlled content, using instead grain-based diets which may have variable nutritional composition, and differ from HFD in more than just the fat content [16]. It is also important to note that most studies in mice were conducted using the C57BL/6J mouse from Jackson Laboratories, a strain with a spontaneous mutation in the mitochondrial nicotinamide nucleotide transferase (NNT), which hampers the production of mitochondrial NADPH and thus impacts significantly on mitochondrial redox state [18]. This strain has been shown to be prone to the development of metabolic diseases [18–21].

Here, we aimed to evaluate the time-dependent roles of obesity-derived $NO^{\cdot}$ on hepatic mitochondrial function, by monitoring the effect of deletion of the iNOS enzyme in C57BL/6 mice, which contain normal NNT activity. Surprisingly, after 2, 4 and 8 weeks of high fat feeding to induce obesity, we did not observe any protection against loss of insulin sensitivity by iNOS absence, nor did we observe an overt, sustained, decline in liver mitochondrial function. We believe these findings, while negative and unexpected, are important to re-evaluate the suggested protagonist role of liver mitochondrial dysfunction and inflammatory $NO^{\cdot}$ signaling in the development of diet-induced insulin resistance.

Materials and methods

1. Animal use and ethics

Experiments were conducted in agreement with the NIH Guidelines for the humane treatment of animals and were approved by the local Animal Care and Use Committee (*Comissão de Ética em Cuidado e Uso Animal*, *Instituto de Química*, *USP*; Permit number: 17/2013). Male, C57BL/6 wild type mice (WT, N = 64) and C57BL/6 iNOS knockout mice (KO, N = 65) were obtained from the *Biotério do Conjunto das Químicas* (University of São Paulo/SP) and genotyped by PCR for both iNOS KO and NNT presence (not shown). Animals were kept in air-filtered cages containing 3–4 animals with 12-hours light/dark cycles. Food and water were given *ad libitum*.

2. Diets

Known-component low and high fat diets (LFD and HFD, respectively) were manufactured by Pragsoluções Biociências (Brazil) based on AIN 93-M diets with some modifications [22–24], as shown in Table 1. At 8 weeks of age, regular chow was replaced by the LFD. After 2 weeks of acclimation, half of the animals were randomly kept on the LFD and half started the HFD. Body mass and food intake were monitored weekly. Food intake was converted to energy content as described in Table 1. Energy efficiency was estimated per animal as (mean body mass gain)/(food intake). After 2, 4 and 8 weeks on the HFD, mice were euthanized by cervical dislocation after overnight fasting and used for the experiments.

3. Indirect calorimetry and spontaneous physical activity

Eight-week LFD and HFD-fed mice were individualized in Columbus Instruments Comprehensive Lab Animal Monitoring System (CLAMS) cages for 24 hours for acclimation plus 24 hours for measurements. Oxygen consumption, CO_2 production and locomotion were recorded for each animal every 4 minutes. Respiratory exchange ratios (RER) and energy expenditure (or "Heat") were acquired by the equipment, respectively, as VCO_2/VO_2 and

Table 1. Diet composition (adapted from [18–20]).

	Low Fat Diet (LFD)		High Fat Diet (HFD)	
	g/kg	g/1000 kcal	g/kg	g/1000 kcal
Casein	147.5	38.8	204.3	38.7
L-Cistin	1.9	0.5	2.6	0.5
Corn starch	435.1	114.6	0.0	0.0
Dextrinized corn starch	170.1	44.8	138.9	26.3
Sucrose	93.6	24.7	130.4	24.7
Cellulose	57.5	15.1	79.7	15.1
Soy oil	4.5	1.2	37.5	7.1
Lard	40.4	10.6	337.6	63.9
Mineral mix	36.9	9.7	51.5	9.8
Vitamin mix	10.5	2.8	14.7	2.8
Choline bitartrate	2.0	0.5	2.8	0.5
BHT	0.008	0.002	0.009	0.002
Calculated energy content	(kcal/kg)	3796.7		5280.7
Protein	(% Energy)	15.7		15.8
Carbohydrates		73.6		20.4
Fat		10.6		63.9

https://doi.org/10.1371/journal.pone.0211733.t001

$(3.815+1.232^{*}RER)^{*}VO_2$, as described in the manufacturer's manual. Spontaneous physical activity (SPA) was calculated as the sum of the total XYZ axis infrared beam breaks.

4. Body composition

Eight-week LFD and HFD-fed mouse body composition was assessed by nuclear magnetic resonance in a Bruker's Minispec LF50 Body Composition Analyzer (WT N = 12, KO N = 9).

5. Insulin tolerance test

After 6 hours of morning fasting, insulin (0.6 units/kg body mass) was injected into the peritoneal cavity. Glucose concentrations were determined at 0, 10, 15, 30 and 60 minutes after insulin injection using a digital glucose meter (Roche). The analysis involved integrating the values obtained as a function of time. Measurements were done a few days prior to tissue isolations from the same animals, hence the slightly earlier time points.

6. Glucose tolerance test

After 6 hours of morning fasting, glucose (1 g/kg body mass) was administrated by gavage. Glucose concentrations were determined at 0, 15, 30, 60, 90 and 120 minutes after gavage using a digital glucose meter (Roche). The analysis involved integrating the values obtained as a function of time. Measurements were done a few days after ITT.

7. Mitochondrial isolation

Livers were finely minced immediately after dissection, washed in isolation buffer (250 mM Sucrose, 10 mM Hepes, 1 mM EGTA, pH 7.2) at 4˚C and homogenized in a tissue grinder. The suspension was centrifuged at 800 g for 5 minutes and the resulting supernatant centrifuged at 12000 g for 10 min. The pellet was washed and resuspended in minimal volume of isolation buffer [25]. Outer mitochondrial membrane integrity was evaluated by quantifying cytochrome c using SDS-PAGE followed by Western Blotting (S1 Fig) and was equal in all samples.

8. Oxygen consumption

Freshly isolated mitochondria were incubated in respiratory buffer containing 120 mM sucrose, 65 mM KCl, 2 mM $MgCl_2$, 1 mM KH_2PO_4, 1 mM EGTA, 10 mM Hepes, 0.1% fatty acid free BSA, pH 7.4, at 37˚C, in an Oroboros O2K High Resolution Respirometer (Innsbruck, Austria). Oxygen consumption was monitored by sequential additions of ADP (1 mM) and the ATP synthase inhibitor oligomycin (1 $\mu g.mL^{-1}$) to mitochondrial suspensions energized by respiratory substrates malate (2 mM), glutamate (2 mM) and succinate (2 mM) or malate (2 mM) and palmitoyl carnitine (12.5 μM). Oxygen consumption was normalized to total mitochondrial protein content (125 $\mu g.mL^{-1}$) [25].

9. Complex I, II and glutamate dehydrogenase activities

Complex I and II activities were assessed in liver isolated mitochondria as described in Spinazzi et al., 2012, [26] with some modifications. Briefly, for complex I, 10 μg of mitochondrial protein were incubated in phosphate buffer (50 mM, pH 7.5) containing fatty acid free bovine serum albumin (3 $mg.mL^{-1}$), antimycin A (1 $\mu g.mL^{-1}$) and NADH (10 mM). The activity was monitored as the decrease in NADH absorbance after ubiquinone (10 mM) addition at 340 nm ($\varepsilon = 6.2\ mmol^{-1}.cm^{-1}$). Complex II activity was obtained by incubating 4 μg of mitochondrial protein in phosphate buffer (25 mM, pH 7.5) containing fatty acid free bovine serum

albumin (3 $mg.mL^{-1}$), antimycin A (1 $\mu g.mL^{-1}$), succinate (20 μM) and 2,6-dichlorophenolindolphenol (80 μM). The activity was followed as the decrease in 2,6-dichlorophenolindolphenol absorbance after decylubiquinone (50 μM) addition at 600 nm ($\varepsilon = 19.1\ mmol^{-1}.cm^{-1}$). Glutamate dehydrogenase activity was assessed by incubating 10 μg of mitochondrial protein in Tris-HCl buffer (100 mM, pH 7.5) containing NH_4Cl (50 mM) and NADH (0.2 mM). The activity was monitored as the decrease in NADH absorbance after α-ketoglutarate (2.5 mM) addition, as described in Herrero-Yraola et al., 2001 [27].

10. SDS-PAGEs and western blots

Isolated liver mitochondria were diluted in Laemli buffer and proteins were separated using a 10% polyacrylamide denaturating gel. Proteins were transferred to nitrocellulose membranes and incubated with 1:2000 anti-VLCAD, 1:1000 anti-CPT1, or 1:1000 anti-Cyt C. Anti-COX IV (1:1000) or Ponceau S staining were used as a loading controls. Fluorescent secondary antibodies (IRDye anti-mouse and anti-Rabbit, 1:20000) were added to the membranes and bands were obtained using a near-infrared Odissey System. Bands were semi-quantified using ImageJ densitometric analysis.

11. Serum measurements

Blood was harvested, kept room temperature for 30 minutes, and centrifuged 20 minutes for serum separation. Commercial kits were used, following the manufacturer's instructions. Triglycerides and cholesterol were measured using LabTest (Brazil) kits. The ketone bodies kit was from Sigma-Merck, and the non-esterified fatty acid kit was from Wako Chemicals.

12. Materials

All reagents were obtained from Sigma-Merck, except for oligomycin (cat. sc-201551), CCCP (cat. sc-202984) and palmitoyl-L-carnitine (cat. sc-203176), from Santa Cruz, and insulin (Humulin R), from Eli Lilly. VLCAD (cat. ab155138), CPT-1 (cat. ab128568) antibodies from Abcam; COX IV (cat. 4844) antibodies from Cell Signaling: cytochrome c (cat. 612504) from Biolegend, and anti-mouse (cat. 926–68070) and anti-rabbit IRDye (cat. 926–68071) were from LI-COR Biotechnology. Triglycerides (cat. 87) and cholesterol (cat. 76) kits were from Labtest. The NEFA kit (cat. 434.71795) was from Wako Chemicals.

13. Statistics

Data are shown as means + SEM. Outliers were identified by the ROUT method (Q = 1%). Two-way analysis of variance (ANOVA), and Sidak's post-test were used to compare differences between means. Differences were considered significant when $p < 0.05$. Repetitions (N) are indicated in the methods section.

Results

1. iNOS KO mice present lower spontaneous activity and are more susceptible to body mass gain induced by HFD

We promoted obesity in mice using a HFD composed of 64% energy from fat, mainly derived from pork lard (90%, Table 1) and a corresponding known-component low fat diet (LFD). The HFD promoted body mass gains at all feeding periods tested in iNOS KO animals (Fig 1A), while in WT animals the gain was only significant after 8 weeks. The HFD also increased body fat mass in both groups (Fig 1B). Curiously, iNOS KO mice tended to eat less (genotype effect, P value = 0.041, Figs 1C and S2). The higher body mass gains they achieved combined

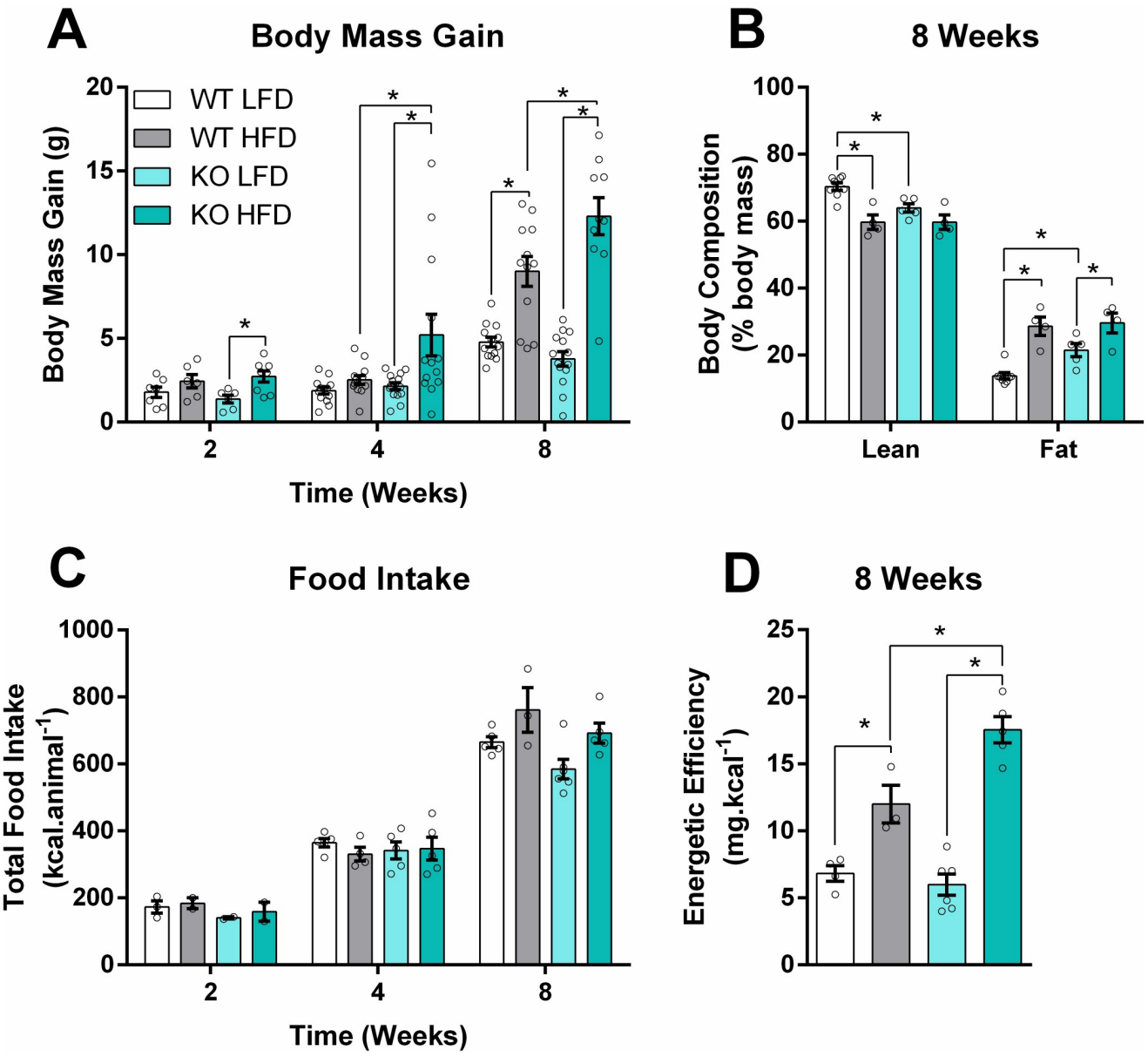

Fig 1. iNOS KO mice are more susceptible to body mass gain under HFDs. Body mass and food intake were monitored weekly. (A) Body mass gain 2, 4 or 8 weeks after the HFD started (n = 6–14). (B) Body composition assessed by nuclear magnetic resonance after 8 weeks of high fat feeding (n = 4–8). (C) Total food intake (n = 2–6 cages containing 3–4 mice) estimated as described in Material and Methods. (D) Energy conversion efficiency calculated as the ratio of body mass gain (in A) to food intake (in C) after 8 weeks. Data are mean + SEM. Unfilled circles represent biological replicates. Differences among means were evaluated by two-way ANOVA. * = $p < 0.05$ in Sidak's posttest analysis.

https://doi.org/10.1371/journal.pone.0211733.g001

with lower food intake indicate a high energy efficiency of iNOS KO mice compared to WT when fed the HFD, but not on the LFD (Fig 1D).

Interestingly, KO mice showed the same energy expenditure compared to WT counterparts (Fig 2A). However, HFD-feeding promoted a shift in fuel utilization, increasing the use of fat, as indicated by lower respiratory exchange ratios (RER, Fig 2B), while reducing spontaneous physical activity in WT animals (SPA, Fig 2C). iNOS KO mice tended to move less during the

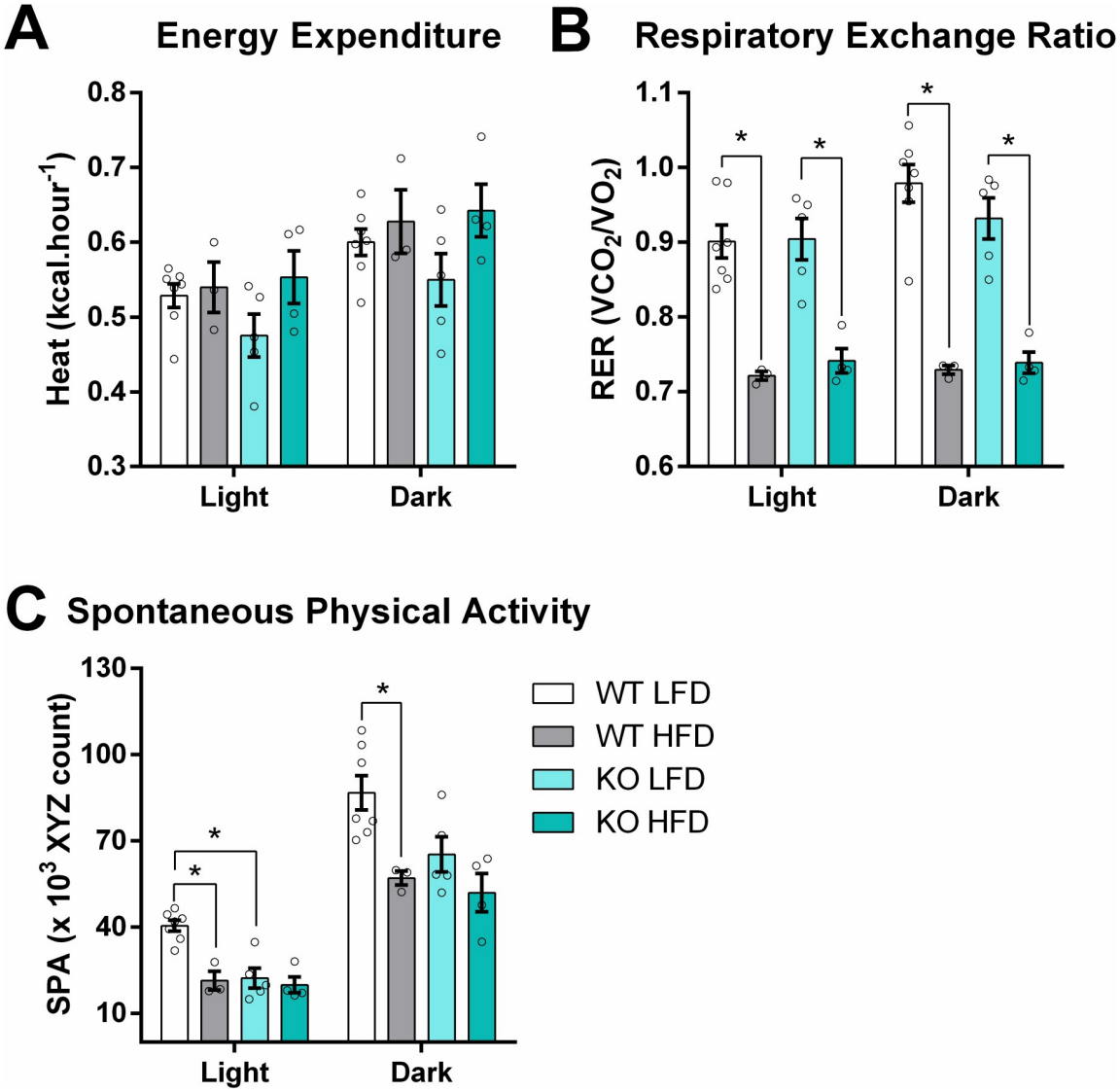

Fig 2. HFDs increase energy expenditure while decreasing spontaneous activity. Indirect calorimetry and SPA measurements were performed after 8 weeks of HFD feeding. Light and dark cycles represent means of uninterrupted 12 h periods (7 AM—7 PM and 7 PM– 7 AM, respectively). Heat (A) and RER (B) were quantified automatically while SPA (spontaneous physical activity; C) represents XYZ axes infrared beams breaks, as described in Material and Methods. Data are mean + SEM, n = 3–8. Unfilled circles represent biological replicates. Differences among means were evaluated by two-way ANOVA. * = $p < 0.05$ in Sidak's posttest analysis.

https://doi.org/10.1371/journal.pone.0211733.g002

light and dark periods (genotype effect, P value = 0.004 and 0.062, respectively), which corroborates the higher energy efficiency and mass gain observed.

2. iNOS absence protects from insulin resistance only on the LFD

Systemic insulin sensitivity was evaluated using insulin and oral glucose tolerance tests at different time points (ITT and oGTT, respectively, Fig 3). As expected, the HFD decreased insulin sensitivity after 1.5 weeks in WT animals, as measured by the glycemic response at 15 min (Fig 3E) and the ITT area under the curve (AUC, Fig 3F). Fasting glycemia was higher in the iNOS KO HFD group at 1.5 weeks (Fig 3D), despite no significant changes in the ITT 15 min glycemia (Fig 3E) nor the ITT AUC (Fig 3F). Insulin sensitivity is significantly reduced in both

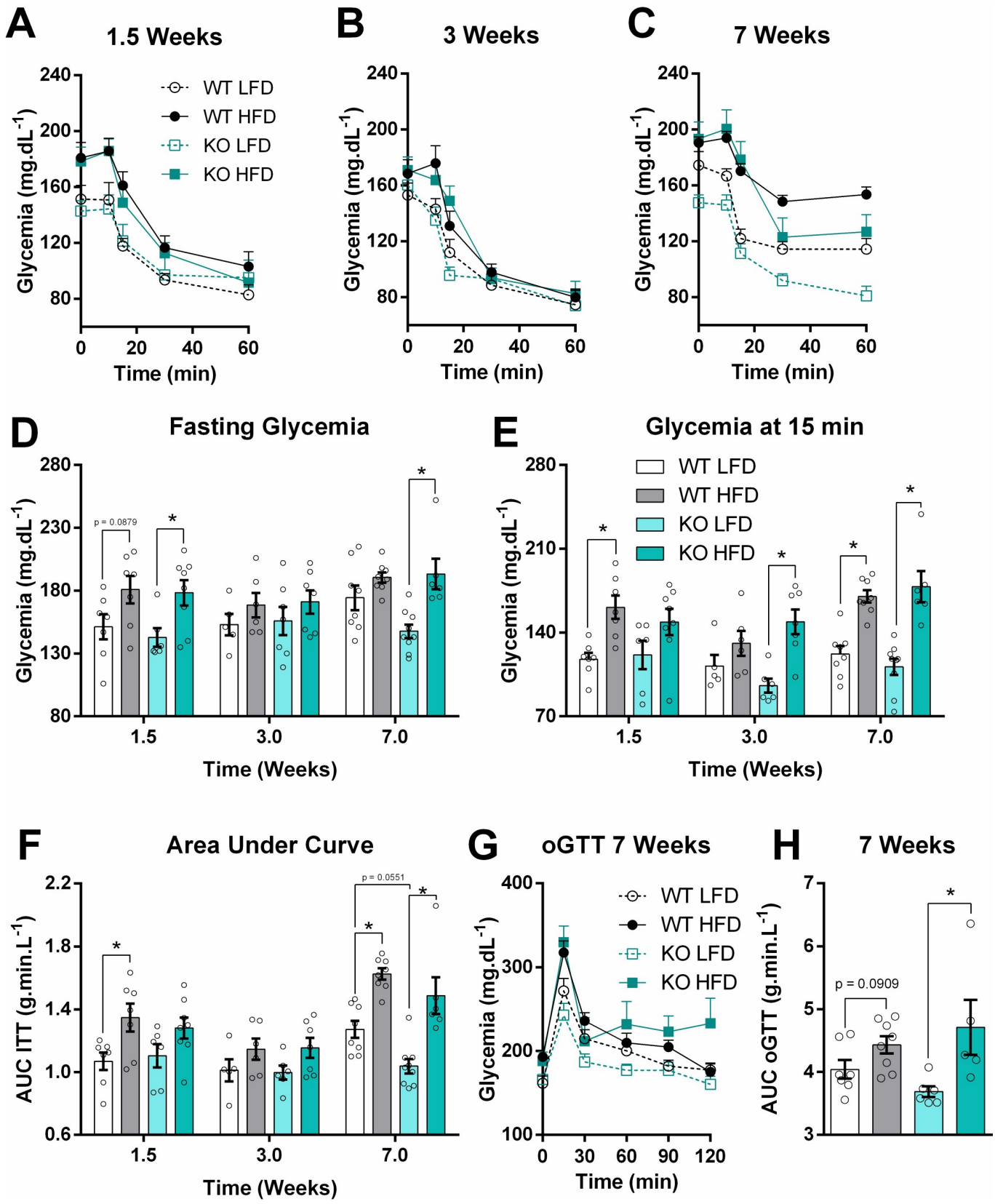
A
1.5 Weeks
B
3 Weeks
C
7 Weeks
WT LFD
WT HFD
KO LFD
KO HFD
Glycemia (mg.dL-1)
Time (min)
D
Fasting Glycemia
E
Glycemia at 15 min
Time (Weeks)
p = 0.0879
F
Area Under Curve
AUC ITT (g.min.L-1)
p = 0.0551
G
oGTT 7 Weeks
H
7 Weeks
AUC oGTT (g.min.L-1)
p = 0.0909

Fig 3. HF-feeding promotes insulin resistance despite iNOS absence. Insulin sensitivity was evaluated through insulin and glucose tolerance tests. (A-C) Time course glycemia after insulin injection in animals fed the HFD for 2, 4 or 8 weeks. (D) Glycemia after 6 hours of morning fasting. (E) Glycemia after 15 minutes of insulin injection. (F) Area under the curve for graphs A-C. (G) Time course glycemia after oral administration of glucose. (H) Area under the curve for graph F. Data are means + SEM, n = 5–9. Unfilled circles represent biological replicates. Differences among means were evaluated by two-way ANOVA. * = $p < 0.05$ in Sidak's posttest analysis.

https://doi.org/10.1371/journal.pone.0211733.g003

WT and KO groups at 7 weeks, a time point in which the oGTT also showed changes promoted by the HFD (Fig 3G and 3H). Interestingly, even LFD WT animals tended to be less sensitive to insulin at 7 weeks, suggesting that diets with only 10% energy from fat can already promote metabolic disturbances when ingested *ad libitum*. These effects were not observed in LFD iNOS KO mice. Conversely, iNOS KO mice have increased circulation of NEFA and ketone bodies after overnight fasting, both on high- and low-fat diets (S1 Table)

3. Glutamate, succinate, and palmitoyl-L-carnitine-supported oxygen consumption are decreased by HFDs, but recover over time

Mitochondrial function was assessed by oxygen consumption measurements under different functional states (Fig 4). Liver mitochondria were isolated and energized by complex I and II substrates glutamate and succinate, respectively, and respiration was measured in the presence (state 3) and absence (state 4) of ATP production, promoted by the addition of ADP and ATP-synthase inhibitor oligomycin, respectively (S3 Fig). The HFD slightly decreased state 3 and 4 respiration at 4 weeks in WT mitochondria (Fig 4A versus Fig 4B), although this was recovered at 8 weeks (Fig 4C). No changes were promoted by the diets on respiratory control ratios (RCR, Fig 4G), a measure of mitochondrial oxidative phosphorylation efficiency. In line with these findings, no changes in Complex I, II, and glutamate dehydrogenase enzymatic activities were observed (Table 2).

A similar trend in lower respiration at 4, but not 8 weeks, was observed with respiration supported by palmitoyl-L-carnitine, a long chain fatty acid (LCFA) activated with L-carnitine that readily enters the mitochondrial matrix (Fig 4D–4F), albeit independently of iNOS absence. Again, no changes were promoted by the diets on fatty acid-supported respiratory control ratios (Fig 4H). Carnitine palmitoyl transferase 1A (CPT1-A) protein levels tended to be increased in the KO HFD group at 8 weeks of feeding (Fig 5A and 5B). No changes were observed in the protein levels of very long chain acyl-CoA dehydrogenase (VLCAD, Fig 5A and 5C), a result compatible with the lack of change in fatty acid-supported respiration.

Discussion

High fat diets are a widely used model to induce obesity that mirrors, in rodents, many of the effects of human overnutrition and lack of physical activity. Indeed, we identified that after 1.5 weeks on a HFD, mice already exhibited increased body mass and adiposity. iNOS KO mice were more susceptible to body mass gain and had an increased content of fat mass even on the LFD (Fig 1). Interestingly, iNOS KO animals were found to be spontaneously hypercholesterolemic [28], a finding that we also observed at 4 weeks in both LFD and HFD groups (S1 Table). In addition, iNOS KO mice have increased circulation of NEFA and ketone bodies after overnight fasting (S1 Table). These findings corroborates with the already described susceptibility to increased fat mass [9] and higher energetic efficiency of these animals (Fig 1D), suggesting differential lipid handling in iNOS KO animals that may be exacerbated under HFDs.

Unexpectedly, iNOS KO did not protect from HFD-induced insulin resistance even at 1.5 weeks (Fig 3), although the deleterious effects of iNOS on insulin sensitivity have been widely described in mice [9–11,29,30]. Part of the discrepancies between our results and those from

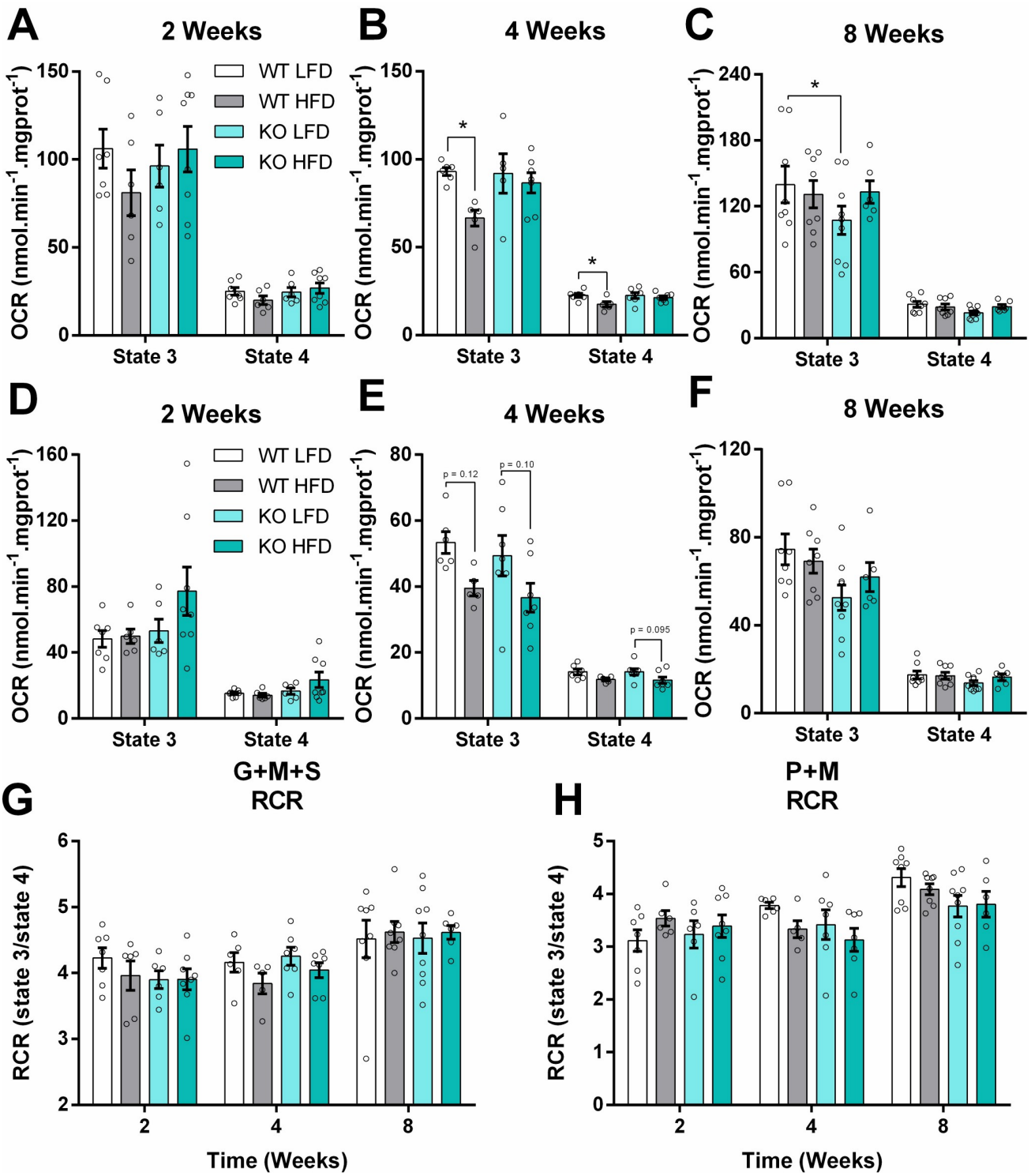

Fig 4. Glutamate, succinate, and palmitoyl-L-carnitine-supported oxygen consumption decreased mildly with HFD, but recovered over time. Oxygen consumption rates (OCR) of isolated mitochondria from livers after 2, 4 and 8 weeks of high-fat feeding. (A, B and G) Glutamate, malate and succinate were used as substrates. (D, F and H) Palmitoyl-carnitine and malate as substrates. "State 3" is the oxygen consumption rate in presence of ADP; "state 4" represents oxygen consumption measured in the presence of ATP synthase inhibitor oligomycin. Data are means + SEM, n = 5–9. Unfilled circles represent a biological replicate. Differences among means were evaluated by two-way ANOVA. * = $p < 0.05$ in Sidak's posttest analysis.

https://doi.org/10.1371/journal.pone.0211733.g004

Table 2. Complex I, II and glutamate dehydrogenase activities.

	WT LFD			WT HFD			KO LFD			KO HFD		
	Activity (μM.min^{-1}.μg protein)											
	Mean	SEM	N	Mean	SEM	N	Mean	SEM	N	Mean	SEM	N
	2 Weeks											
Complex I	0.35	0.02	4	0.29	0.04	5	0.41	0.03	5	0.35	0.04	5
Complex II	1.83	0.26	6	1.86	0.28	6	2.00	0.18	6	1.94	0.15	6
GDH	1.14	0.06	5	1.18	0.08	5	1.24	0.03	5	1.28	0.04	5
	4 Weeks											
Complex I	0.35	0.02	5	0.32	0.01	5	0.32	0.03	5	0.31	0.02	5
Complex II	1.95	0.07	6	1.85	0.02	6	2.02	0.24	6	1.94	0.16	6
GDH	1.15	0.11	5	1.24	0.05	5	1.12	0.12	4	1.19	0.06	5
	8 Weeks											
Complex I	0.41	0.04	5	0.40	0.06	5	0.35	0.02	5	0.34	0.01	5
Complex II	1.93	0.03	6	1.87	0.11	6	1.88	0.11	6	1.87	0.08	6
GDH	1.11	0.07	5	1.31	0.05	5	1.23	0.17	4	1.36	0.11	4

Data are: Mean, Standard error of the mean (SEM), and the Number of biological replicated (N). The means at the same animal age are not statistically different ($p < 0.05$). Two-way ANOVA.

https://doi.org/10.1371/journal.pone.0211733.t002

other laboratories may be due to at least two important differences when rodent obesity models are considered [31,32]: 1) *the genetic background*—our WT and KO animals are Nnt +/+ backgrounds while some of the other groups used the spontaneously mutated Nnt-/- mice from Jackson Laboratories [9,29]. The NNT (nicotinamide nucleotide translocase) enzyme promotes re-reduction of NADPH required for the removal of mitochondrial oxidants, and its absence may promote changes in redox signaling in the presence/absence of nitric oxide [20,33,34]; 2) *the formulation and timing of the HFD provided*—both diets (HFD and LFD) we used are composed mainly of lard and soybean oil (9:1) as lipid sources, and the HFD was able to reduce insulin sensitivity in only 1.5 weeks. Using a similar approach, Nozaki and colleagues observed protection of iNOS absence after 10 and 48 weeks of a HFD containing 57.5% of energy from fat derived from beef tallow and safflower oil (~3:4). Pork lard contains a higher proportion of monounsaturated fatty acids than saturated fatty acids, contrary to beef tallow, and different types of triacylglycerols [35]. Safflower oil can be rich in linoleic acid or in oleic acid, depending on the crop used for oil extraction [36,37], while soybean oil is consistently linoleic acid-enriched. The different HFD composition due to the source of fats and also the slightly higher content of sucrose (~10% in our diets versus ~5% in theirs) could explain the disparities seen, since some authors already described differences in insulin sensitivity and adipose tissue inflammation modulating just fatty acid types, but not total quantities [38–40]. Overall, the fact that iNOS is not necessary for metabolic responses under all conditions described to date suggests that its role as a protagonist in the pathology of obesity should be reconsidered.

Of note, we see signs of decreased insulin sensitivity in WT LFD animals after 7 weeks, an effect probably related to the fact that, despite being low in fat, the diet is offered *ad libitum* and animals are not exercised, resulting in mild obesity [38]. In contrast, iNOS KO LFD animals have lower spontaneous physical activity, while showing higher fat mass and insulin sensitivity. Thus, some of the beneficial effects of iNOS absence seen by other authors were in partially mirrored in our model using the LFD. A recent paper by Kanuri and co-authors observed, in the spontaneously-mutated NNT-deficient background, that iNOS KO animals on a LFD (10%

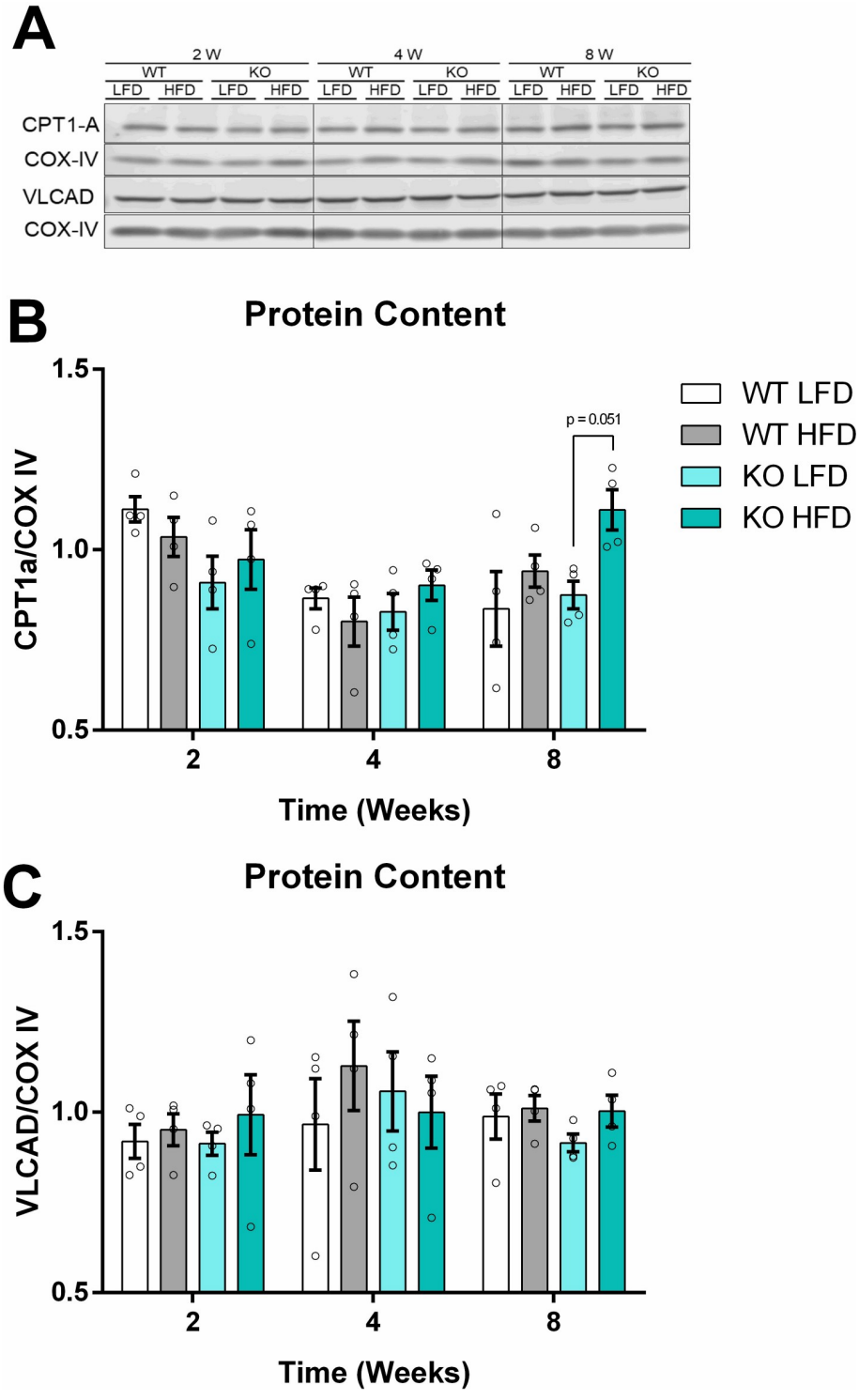

Fig 5. HFD increases CPT1-A content. SDS-PAGE Western blots of liver mitochondria from animals fed the HFD for 2, 4 or 8 weeks. Representative bands in (A) and quantification by densitometry in (B) and (C). Data are means + SEM, n = 4. Unfilled circles represent a biological replicate. Differences among means were evaluated by two-way ANOVA and Sidak's posttest analysis.

https://doi.org/10.1371/journal.pone.0211733.g005

energy from fat, mainly soybean oil) had reduced energy expenditure and RER compared to WT animals after 5 weeks of feeding [41]. They propose that there are optimal iNOS/eNOS/nNOS relations that maintain glucose and lipid homeostasis and that iNOS KO could compromise basal homeostatic levels of $NO^{\cdot}$, a hypothesis that finds resonance with our data.

One of the roles of the liver in type 2 diabetes is unregulated glucose production [42], contributing toward hyperglycemia. Some authors hypothesize that liver mitochondria have a central role coordinating fuel substrate use under these conditions [43–45]. We evaluated the relationship between systemic insulin resistance and liver mitochondrial function, and found a non-significant trend toward lower state 3 oxygen consumption with a fatty acid as substrate at 4 weeks (Fig 4E), which is parallel to a discrete decrease in the ITT area under the curve at 3 weeks on the HFD (Fig 3B). Shulman's group proposed a mechanism in which hepatic glucose production is indirectly controlled by lipolysis in the white adipose tissue, increasing fatty acid flow to the liver and culminating in a surplus of acetyl-CoA through β-oxidation and subsequent allosteric activation of pyruvate carboxylase, the first step of hepatic gluconeogenesis [46]. In line with the idea that mitochondrial integrity is preserved, with enhanced β-oxidation activity, we observed that mitochondrial function is fully recovered and more coupled after 8 weeks on the HFD using complex I and II substrates, as well as fatty acids (Fig 4), while insulin sensitivity is even more compromised (Fig 3C). Similar findings were obtained by Franko and co-authors (2014) using three different models of insulin resistance, agreeing with the resilient function of liver mitochondria that we observed [47]. Additionally, although palmitoyl-L-carnitine oxidation may be independent of CPT1-mediated transport, the increased content of this protein (Fig 5A and 5B) suggests a higher lipid oxidation capacity *in situ*. Overall, literature data and our findings strongly support the idea that liver mitochondrial integrity is largely maintained in obesity-mediated insulin resistance, with enhanced lipid oxidation capacity but no functional damage.

In conclusion, we observed that our HFD can induce metabolic disturbances over a short period of time, while the LFD control is also not innocuous, decreasing insulin sensitivity at 7 weeks. We believe that this LFD effect should always be expected and considered in time-point assessments of metabolic effects of high fat diets, since animals on *ad libitum* feeding tend to be obese even with chow diets [48]. Furthermore, we replicated the tendency of iNOS KO animals to gain more body mass under HFDs, but failed to show any protection against insulin sensitivity, suggesting iNOS is not essential for insulin resistance development under all conditions. In parallel with systemic insulin resistance, we uncovered that hepatic mitochondrial function is sustained over time. We thus believe that the observation of mitochondrial dysfunction by some authors may be a consequence of systemic decline and not its cause. Together, these results demonstrate that neither iNOS nor hepatic mitochondrial damage are indispensable players in all forms of HFD-mediated insulin resistance.

Supporting information

S1 Fig. Mitochondrial outer membrane integrity. Cytochrome c content was evaluated by SDS-PAGE Western Blotting isolated liver mitochondria from 8-week old HF-fed animals. Densitometric semiquantitative analysis was performed in ImageJ. Data are mean + SEM, n = 4. Unfilled circles represent biological replicates. Differences among means were evaluated by two-way ANOVA and are not significant for $p < 0.05$.
(TIF)

S2 Fig. Total food intake over time. Food intake was monitored weekly. Total food intake (N = 2–6 cages containing 3–4 mice) was estimated as described in Material and Methods. Data are mean + SEM. Unfilled circles represent biological replicates. Differences among

means were evaluated by two-way ANOVA. * = $p < 0.05$ in Sidak's posttest analysis.
(TIF)

S3 Fig. Representative oxygen consumption assay. Isolated liver mitochondrial oxygen consumption after 4 weeks of high-fat feeding. (A) Glutamate, malate and succinate were used as substrates. (B) Palmitoyl-carnitine and malate were used as substrates. "State 3" is the oxygen consumption rate in presence of ADP; "state 4" represents oxygen consumption measured in the presence of ATP synthase inhibitor oligomycin.
(TIF)

S1 Table. iNOS KO mice are hypertriglyceridemic and hypercholesterolemic.
(DOCX)

Acknowledgments

The authors thank Edson Alves Gomes, Renata Spalutto, Dr. Maira Nagai, Flavia Ong, Silvania Peris Neves, Ana Maria Peracoli Campos, Dr. Angela Castoldi and Chen Minzhen for excellent technical support and experimental help. We would like to thank Profs. William Festuccia and Cristoforo Scavone for material donations.

Author Contributions

Conceptualization: Pamela A. Kakimoto, Bruno Chausse, José Donato Júnior, Alicia J. Kowaltowski.

Data curation: Pamela A. Kakimoto, Bruno Chausse, Camille C. Caldeira da Silva, José Donato Júnior.

Formal analysis: Pamela A. Kakimoto, Bruno Chausse, José Donato Júnior, Alicia J. Kowaltowski.

Funding acquisition: Camille C. Caldeira da Silva, José Donato Júnior, Alicia J. Kowaltowski.

Investigation: Pamela A. Kakimoto, Bruno Chausse, Camille C. Caldeira da Silva, José Donato Júnior.

Methodology: Pamela A. Kakimoto, Bruno Chausse, Camille C. Caldeira da Silva, José Donato Júnior, Alicia J. Kowaltowski.

Project administration: Camille C. Caldeira da Silva, Alicia J. Kowaltowski.

Resources: Alicia J. Kowaltowski.

Supervision: Alicia J. Kowaltowski.

Writing – original draft: Pamela A. Kakimoto, Bruno Chausse, José Donato Júnior, Alicia J. Kowaltowski.

Writing – review & editing: Pamela A. Kakimoto, Bruno Chausse, Camille C. Caldeira da Silva, José Donato Júnior, Alicia J. Kowaltowski.

References

1. Martínez-Ruiz A, Cadenas S, Lamas S. Nitric oxide signaling: Classical, less classical, and nonclassical mechanisms. Free Radic Biol Med. 2011; 51: 17–29. https://doi.org/10.1016/j.freeradbiomed.2011.04.010 PMID: 21549190
2. Toledo JC, Augusto O. Connecting the chemical and biological properties of nitric oxide. Chem Res Toxicol. 2012; 25: 975–89. https://doi.org/10.1021/tx300042g PMID: 22449080

3. Förstermann U, Sessa WC. Nitric oxide synthases: regulation and function. Eur Heart J. 2012; 33: 829–837. https://doi.org/10.1093/eurheartj/ehr304 PMID: 21890489
4. Kleinert H, Pautz A, Linker K, Schwarz PM. Regulation of the expression of inducible nitric oxide synthase. Eur J Pharmacol. 2004; 500: 255–66. https://doi.org/10.1016/j.ejphar.2004.07.030 PMID: 15464038
5. Iwakiri Y, Kim MY. Nitric oxide in liver diseases. Trends Pharmacol Sci. 2015; 36: 524–536. https://doi.org/10.1016/j.tips.2015.05.001 PMID: 26027855
6. Gregor MF, Hotamisligil GS. Inflammatory mechanisms in obesity. Annu Rev Immunol. 2011; 29: 415–445. https://doi.org/10.1146/annurev-immunol-031210-101322 PMID: 21219177
7. Sansbury BE, Hill BG. Regulation of obesity and insulin resistance by nitric oxide. Free Radic Biol Med. 2014; 73: 383–99. https://doi.org/10.1016/j.freeradbiomed.2014.05.016 PMID: 24878261
8. Ha S-K, Chae C. Inducible nitric oxide distribution in the fatty liver of a mouse with high fat diet-induced obesity. Exp Anim. 2010; 59: 595–604. https://doi.org/10.1538/expanim.59.595 PMID: 21030787
9. Perreault M, Marette A. Targeted disruption of inducible nitric oxide synthase protects against obesity-linked insulin resistance in muscle. Nat Med. 2001; 7: 1138–1143. https://doi.org/10.1038/nm1001-1138 PMID: 11590438
10. Shinozaki S, Choi CS, Shimizu N, Yamada M, Kim M, Zhang T, et al. Liver-specific inducible nitric-oxide synthase expression is sufficient to cause hepatic insulin resistance and mild hyperglycemia in mice. J Biol Chem. 2011; 286: 34959–34975. https://doi.org/10.1074/jbc.M110.187666 PMID: 21846719
11. Charbonneau A, Marette A. Inducible nitric oxide synthase induction underlies lipid-induced hepatic insulin resistance in mice: potential role of tyrosine nitration of insulin signaling proteins. Diabetes. 2010; 59: 861–71. https://doi.org/10.2337/db09-1238 PMID: 20103705
12. White PJ, Charbonneau A, Cooney GJ, Marette A. Nitrosative modifications of protein and lipid signaling molecules by reactive nitrogen species. Am J Physiol Endocrinol Metab. 2010; 299: E868–78. https://doi.org/10.1152/ajpendo.00510.2010 PMID: 20876760
13. Patel RP, Yuan S, Kevil CG. S-Nitrosothiols and nitric oxide biology. Third Edit. Nitric Oxide. 2017. https://doi.org/10.1016/B978-0-12-804273-1/00004-1
14. Mantena SK, Vaughn DP, Andringa KK, Eccleston HB, King AL, Abrams GA, et al. High fat diet induces dysregulation of hepatic oxygen gradients and mitochondrial function in vivo. Biochem J. 2009; 417: 183–193. https://doi.org/10.1042/BJ20080868 PMID: 18752470
15. Doulias PT, Tenopoulou M, Greene JL, Raju K, Ischiropoulos H. Nitric oxide regulates mitochondrial fatty acid metabolism through reversible protein S-nitrosylation. Sci Signal. 2013; 6: 1–7. https://doi.org/10.1126/scisignal.2003252 PMID: 23281369
16. Shiva S, Castro L, Brookes PS. Mitochondria and Nitric Oxide. Third Edit. Nitric Oxide: Biology and Pathobiology: Third Edition. 2017. https://doi.org/10.1016/B978-0-12-804273-1.00011–9
17. Kakimoto PA, Kowaltowski AJ. Effects of high fat diets on rodent liver bioenergetics and oxidative imbalance. Redox Biol. 2016; 8: 216–225. https://doi.org/10.1016/j.redox.2016.01.009 PMID: 26826574
18. Ronchi JA, Figueira TR, Ravagnani FG, Oliveira HCF, Vercesi AE, Castilho RF. A spontaneous mutation in the nicotinamide nucleotide transhydrogenase gene of C57BL/6J mice results in mitochondrial redox abnormalities. Free Radic Biol Med. 2013; 63: 446–456. https://doi.org/10.1016/j.freeradbiomed.2013.05.049 PMID: 23747984
19. Figueira TR. A word of caution concerning the use of Nnt-mutated C57BL/6 mice substrains as experimental models to study metabolism and mitochondrial pathophysiology. Exp Physiol. 2013; 98: 1643–1643. https://doi.org/10.1113/expphysiol.2013.074682 PMID: 24058187
20. Navarro CDC, Figueira TR, Francisco A, Dal 'bó GA, Ronchi JA, Rovani JC, et al. Redox imbalance due to the loss of mitochondrial NAD(P)-transhydrogenase markedly aggravates high fat diet-induced fatty liver disease in mice. Free Radic Biol Med. 2017; 113: 190–202. https://doi.org/10.1016/j.freeradbiomed.2017.09.026 PMID: 28964917
21. Nicholson A, Reifsnyder PC, Malcolm RD, Lucas CA, MacGregor GR, Zhang W, et al. Diet-induced obesity in two C57BL/6 substrains with intact or mutant nicotinamide nucleotide transhydrogenase (Nnt) gene. Obesity. 2010; 18: 1902–1905. https://doi.org/10.1038/oby.2009.477 PMID: 20057372
22. Reeves PG, Nielsen FH, Fahey GC. AIN-93 purified diets for laboratory rodents: final report of the American Institute of Nutrition ad hoc writing committee on the reformulation of the AIN-76A rodent diet. J Nutr. 1993; 123: 1939–1951. https://doi.org/10.1093/jn/123.11.1939 PMID: 8229312
23. Fiamoncini J, Turner N, Hirabara SM, Salgado TML, Marçal AC, Leslie S, et al. Enhanced peroxisomal β-oxidation is associated with prevention of obesity and glucose intolerance by fish oil-enriched diets. Obesity. 2013; 21: 1200–1207. https://doi.org/10.1002/oby.20132 PMID: 23666909
24. Belchior T, Paschoal VA, Magdalon J, Chimin P, Farias TM, Chaves-Filho AB, et al. Omega-3 fatty acids protect from diet-induced obesity, glucose intolerance, and adipose tissue inflammation through

PPARγ-dependent and PPARγ-independent actions. Mol Nutr Food Res. 2015; 59: 957–967. https://doi.org/10.1002/mnfr.201400914 PMID: 25641959

25. Cardoso AR, Kakimoto PA, Kowaltowski AJ. Diet-sensitive sources of reactive oxygen species in liver mitochondria: role of very long chain acyl-CoA dehydrogenases. PLoS One. 2013; 8: 1–13. https://doi.org/10.1371/journal.pone.0077088 PMID: 24116206

26. Spinazzi M, Casarin A, Pertegato V, Salviati L, Angelini C. Assessment of mitochondrial respiratory chain enzymatic activities on tissues and cultured cells. Nat Protoc. 2012; 7: 1235–1246. https://doi.org/10.1038/nprot.2012.058 PMID: 22653162

27. Herrero-Yraola A, Bakhit SMA, Franke P, Weise C, Schweiger M, Jorcke D, et al. Regulation of glutamate dehydrogenase by reversible ADP-ribosylation in mitochondria. EMBO J. 2001; 20: 2404–2412. https://doi.org/10.1093/emboj/20.10.2404 PMID: 11350929

28. Ihrig M, Dangler CA, Fox JG. Mice lacking inducible nitric oxide synthase develop spontaneous hypercholesterolaemia and aortic atheromas. Atherosclerosis. 2001; 156: 103–107. https://doi.org/10.1016/S0021-9150(00)00636-5 PMID: 11369002

29. Nozaki Y, Fujita K, Wada K, Yoneda M, Kessoku T, Shinohara Y, et al. Deficiency of iNOS-derived NO accelerates lipid accumulation-independent liver fibrosis in non-alcoholic steatohepatitis mouse model. BMC Gastroenterol. 2015; 15: 1–14. https://doi.org/10.1186/s12876-014-0226-6

30. Fujimoto M, Shimizu N, Kunii K, Martyn J, Ueki K, Kaneki M. A role for iNOS in fasting hyperglycemia and impaired insulin signaling in the liver of obese diabetic mice. Diabetes. 2005; 54: 1340–1348. https://doi.org/10.2337/diabetes.54.5.1340 PMID: 15855318

31. Lai M, Chandrasekera PC, Barnard ND. You are what you eat, or are you? The challenges of translating high-fat-fed rodents to human obesity and diabetes. Nutr Diabetes. 2014; 4: e135. https://doi.org/10.1038/nutd.2014.30 PMID: 25198237

32. Hariri N, Thibault L. High-fat diet-induced obesity in animal models. Nutr Res Rev. 2010; 23: 270–299. https://doi.org/10.1017/S0954422410000168 PMID: 20977819

33. Figueira TR, Barros MH, Camargo AA, Castilho RF, Ferreira JC, Kowaltowski A, et al. Mitochondria as a source of reactive oxygen and nitrogen species: from molecular mechanisms to human health. Antioxid Redox Signal. 2013; 18: 2029–2074. https://doi.org/10.1089/ars.2012.4729 PMID: 23244576

34. Weidinger A, Müllebner A, Paier-Pourani J, Banerjee A, Miller I, Lauterböck L, et al. Vicious inducible nitric oxide synthase-mitochondrial reactive oxygen species cycle accelerates inflammatory response and causes liver injury in rats. Antioxid Redox Signal. 2015; 22: 572–86. https://doi.org/10.1089/ars.2014.5996 PMID: 25365698

35. Mielke I. Animal fats and oils. In: Bockisch M, editor. Fats and Oils Handbook. Hamburg: Academic Press and AOCS Press; 1998. pp. 121–173. https://doi.org/10.1016/B978-0-9818936-0-0.50008–1

36. Kochhar SP. Minor and speciality oils. Vegetable Oils in Food Technology. Oxford, UK: Wiley-Blackwell; 2011. pp. 291–341. https://doi.org/10.1002/9781444339925.ch11

37. Wang T. Soybean oil. Vegetable Oils in Food Technology. Oxford, UK: Wiley-Blackwell; 2011. pp. 59–105. https://doi.org/10.1002/047167849X.bio041

38. Enos RT, Davis JM, Velázquez KT, McClellan JL, Day SD, Carnevale KA, et al. Influence of dietary saturated fat content on adiposity, macrophage behavior, inflammation, and metabolism: composition matters. J Lipid Res. 2013; 54: 152–163. https://doi.org/10.1194/jlr.M030700 PMID: 23103474

39. Buettner R, Schölmerich J, Bollheimer LC. High-fat diets: modeling the metabolic disorders of human obesity in rodents. Obesity (Silver Spring). 2007; 15: 798–808. https://doi.org/10.1038/oby.2007.608 PMID: 17426312

40. Ikemoto S, Takahashi M, Tsunoda N, Maruyama K, Itakura H, Ezaki O. High-fat diet-induced hyperglycemia and obesity in mice: Differential effects of dietary oils. Metabolism. 1996; 45: 1539–1546. https://doi.org/10.1016/S0026-0495(96)90185-7 PMID: 8969289

41. Kanuri BN, Kanshana JS, Rebello SC, Pathak P, Gupta AP, Gayen JR, et al. Altered glucose and lipid homeostasis in liver and adipose tissue pre-dispose inducible NOS knockout mice to insulin resistance. Sci Rep. 2017; 7: 41009. https://doi.org/10.1038/srep41009 PMID: 28106120

42. Petersen MC, Vatner DF, Shulman GI. Regulation of hepatic glucose metabolism in health and disease. Nat Rev Endocrinol. 2017; 13: 572–587. https://doi.org/10.1038/nrendo.2017.80 PMID: 28731034

43. Satapati S, Kucejova B, Duarte JAG, Fletcher JA, Reynolds L, Sunny NE, et al. Mitochondrial metabolism mediates oxidative stress and inflammation in fatty liver. J Clin Invest. 2015; 125: 1–16. https://doi.org/10.1172/JCI78652

44. Satapati S, Sunny NE, Kucejova B, Fu X, He TT, Méndez-Lucas A, et al. Elevated TCA cycle function in the pathology of diet-induced hepatic insulin resistance and fatty liver. J Lipid Res. 2012; 53: 1080–92. https://doi.org/10.1194/jlr.M023382 PMID: 22493093

45. Koliaki C, Roden M. Alterations of mitochondrial function and insulin sensitivity in human obesity and diabetes mellitus. Annu Rev Nutr. 2016; 1–31. https://doi.org/10.1146/annurev-nutr-071715-050854

46. Perry RJ, Camporez J-PPG, Kursawe R, Titchenell PM, Zhang D, Perry CJ, et al. Hepatic acetyl CoA links adipose tissue inflammation to hepatic insulin resistance and type 2 diabetes. Cell. 2015; 160: 745–758. https://doi.org/10.1016/j.cell.2015.01.012 PMID: 25662011

47. Franko A, Von Kleist-Retzow J, Neschen S, Wu M, Schommers P, Böse M, et al. Liver adapts mitochondrial function to insulin resistant and diabetic states in mice. J Hepatol. 2014; 60: 816–823. https://doi.org/10.1016/j.jhep.2013.11.020 PMID: 24291365

48. Martin B, Ji S, Maudsley S, Mattson MP, Poor I. "Control" laboratory rodents are metabolically morbid: Why it matters. 2010; 107: 6127–6133. https://doi.org/10.1073/pnas.0912955107

4. Results – Part 2: Lipid overload and its effects on mitochondrial form and function, and on cell redox signaling

In this Section, we aimed to evaluate the effects of fatty acid overload on mitochondrial morphology and hepatocyte function. Part of the work was conducted in collaboration with Professor Dr. Antonio Zorzano's Lab (Institute for Research in Biomedicine, Barcelona, Spain) during a one year "sandwich" internship. Part of these results were published as a pre-print in June 2020 (Kakimoto et al., 2020).

4.1. Background

High concentrations of nonesterified fatty acids in the plasma are a common feature in the metabolic syndrome, and reflect an incapacity to suppress lipolysis through insulin signaling or inadequate adipose tissue ability to store energetic surpluses (Feng et al., 2017; Hardy et al., 2016; Tchernof and Després, 2013). Palmitic acid, a sixteen-carbon saturated fatty acid (SFA), is the most abundant SFA in human blood (Feng et al., 2017; Quehenberger et al., 2010; Tomita et al., 2011). In excess, palmitate causes lipotoxicity, a disturbance that compromises cell or tissue function, promoted by lipid overload and/or lipid accumulation. In cell culture systems, palmitate overload can promote lipid accumulation, insulin resistance, endoplasmic reticulum (ER) and oxidative stress, as well as cell death (Alsabeeh et al., 2018; Ertunc and Hotamisligil, 2016; Ly et al., 2018), but the metabolic pathways sustaining changes induced by palmitate are still not clear.

Mitochondrial function is often suggested as a lipotoxicity target since they are central in metabolic control and lipid homeostasis, although mitochondria are flexible and can respond to environmental cues with profound changes in function and form (Chan, 2020; Sebastián et al., 2017). In addition to their roles related to ATP production and cell death, mitochondria act as important cell hubs regulating calcium signaling, supplying intermediates for lipid synthesis, and modulating the production and removal of oxidants such as superoxide radical anions.

Concomitantly, they sense nutrient availability and cooperate with metabolism-regulating pathways, including responses to insulin and its downstream effectors (del Campo et al., 2014; Cheng et al., 2010; Gordaliza-Alaguero et al., 2019; Wai and Langer, 2016; Zorzano et al., 2015).

Nutrient oversupply predominantly promotes mitochondrial fragmentation, while nutrient starvation is associated with elongation, and a more continuous network (Liesa and Shirihai, 2013; Wai and Langer, 2016; Zorzano et al., 2015). The bioenergetic output is that shortened mitochondria are usually thought to be less efficient in producing ATP than elongated ones (Schrepfer and Scorrano, 2016). Increased supply of fatty acids is an event in which the predominant form of the mitochondrial network is changed. Saturated fatty acid overload can promote mitochondrial fragmentation (Jheng et al., 2012; Kulkarni et al., 2016; Molina et al., 2009) or fusion (Jheng et al., 2012; Senyilmaz et al., 2015), depending on the acyl chain length and if unsaturated fatty acids are also present.

While most studies evaluated later timepoints of palmitate overload (> 12 hours), here we describe the early mitochondrial morphological and bioenergetic outcomes of lipotoxicity. Using real time measurements, we identified that mitochondrial oxygen consumption is not disturbed by palmitate overload over 6 hours, despite high mitochondrial fragmentation and cellular reductive imbalance. Interestingly, palmitate increased ATP synthesis through glycolysis after 1 hour, in a manner unrelated to the changes in morphology. We also found that the production of mitochondrial superoxide radicals/hydrogen peroxide by respiratory complex I may be associated with this metabolic rewiring promoted by palmitate.

4.2. Results

4.2.1. Palmitate promotes mitochondrial fragmentation and triglyceride accumulation

Palmitate overload promotes mitochondrial fragmentation in many cell types (Jheng et al., 2012; Kulkarni et al., 2016; Molina et al., 2009), but the relationship between these morphological changes and early functional bioenergetic consequences has not been

established. We observed that exposure to 0.2 mM palmitate for 6 h led to overt mitochondrial fragmentation in human hepatoma PLC/PRF/5 cells (**Fig 4.1 A** shows a typical image, quantified in **Fig 4.1 B**).

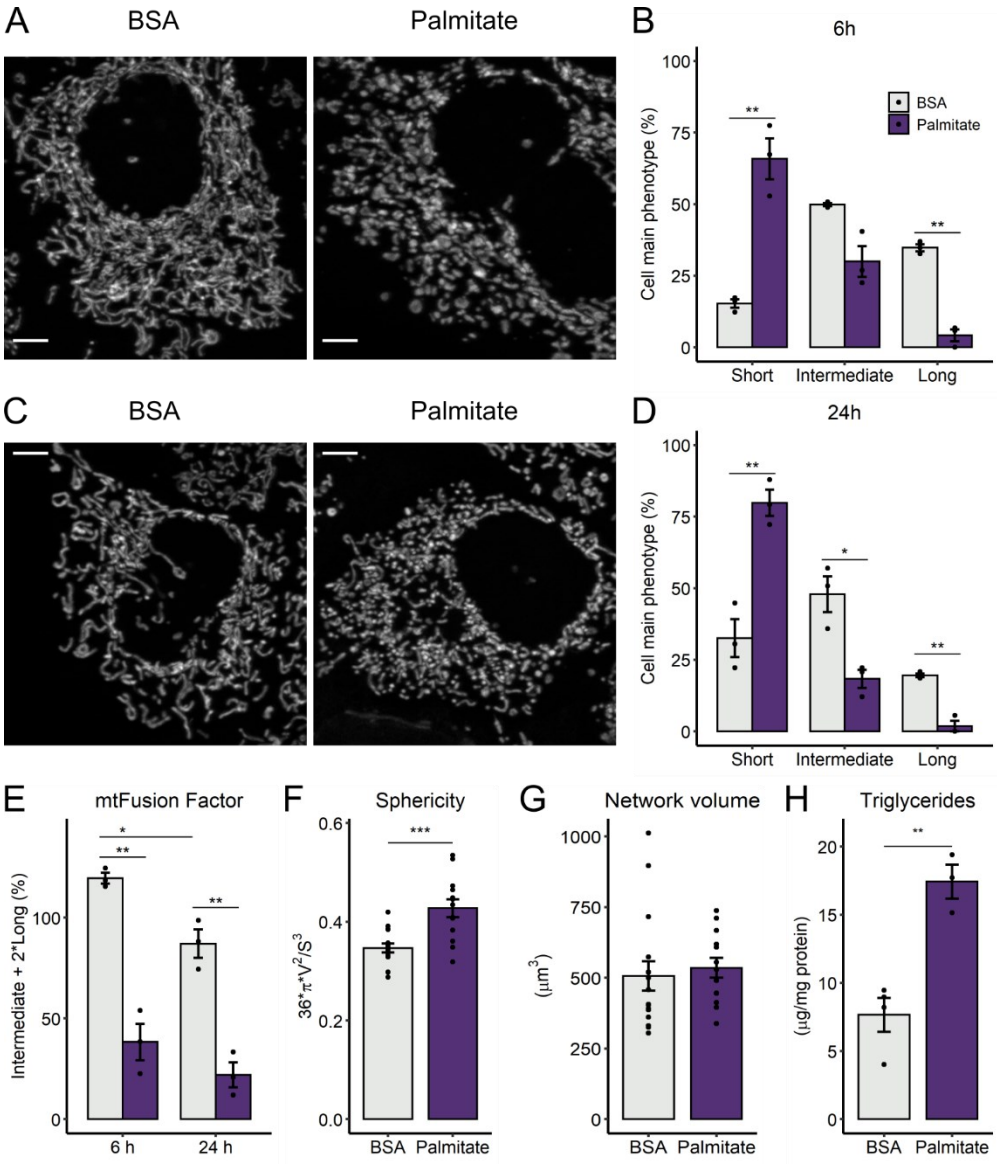

Figure 4.1: Palmitate overload promotes mitochondrial fragmentation and triglyceride accumulation - PLC/PRF/5 cells were incubated with palmitate/BSA (0.2 mM/ 0.25%) for 6 h or 24 h. Live mitochondrial morphology was evaluated by confocal microscopy in cells loaded with 0.4 µM TMRM at 6 h (A and B) or 24 h (C and D). Morphological parameters were measured as described in the Material and Methods section, in cell populations (B, D, E) or individual cells (F-G). Triglycerides were extracted and quantified after 6 h of palmitate incubation (H). * = $p < 0.05$, ** = $p < 0.01$, *** = $p < 0.001$ t-test (Panels B, D, F-H) or two-way ANOVA followed by Tukey's post-test (E). Data are mean + SD. Filled circles represent independent experiments. In F-G, filled circles represent individual cells obtained from 3 independent experiments. Scale bar = 5 µm.

Prolonged stimuli of 24 hours increased the fraction of short mitochondria (**Fig 4.1 C-D**). These morphological changes were confirmed by the quantified decrease of mitochondrial fusion factor (**Fig 4.1 E**) and by the automated quantification of the mitochondrial population in which individual sphericity is increased (**Fig 4.1 F**). Importantly, no changes were detected in total mitochondrial network volume (**Fig 4.1 G**). In parallel, we verified that 6 hours of palmitate treatment were enough to induce significant triglyceride accumulation (**Fig 4.1 H**). These results confirm the ability of palmitate overload to replicate mitochondrial fragmentation and lipid accumulation in PLC cells, validating it as a lipotoxicity model, with strong results detected as soon as 6 hours of incubation.

4.2.1. Palmitate induces glycolysis

Changes in the predominant shape of the mitochondrial network as a response to their microenvironment have been associated with modifications of mitochondrial bioenergetic capabilities, i.e., ATP production (Chan, 2020; Schrepfer and Scorrano, 2016). We followed real-time respiration of intact cells just after palmitate treatment, and up to 6 hours. Surprisingly, oxygen consumption rates (OCRs) of palmitate-treated cells were not significantly affected over time compared to the BSA controls (**Fig 4.2 A**). However, palmitate promoted a significant increase in extracellular acidification rates (ECARs; **Fig 4.2 B**).

Differences in ECARs can be related to lactate production, but also to changes in tricarboxylic acid cycle flux (due to CO_2), ATP turnover, or other acid-generating catabolic processes (Mookerjee et al., 2015). To evaluate the source of protons, we measured the secreted lactate in the supernatant and monitored ECARs in the presence of 2-deoxyglucose, an inhibitor of hexokinases. In palmitate-treated cells, accumulated lactate is significantly increased over time and, accordingly, 2-deoxyglucose blunted the ECAR increase (**Fig 4.2 C-E**) without changing OCR (**Fig 4.2 F**). Importantly, palmitate treatment very strongly increments the contribution of glycolysis in ATP production (**Fig 4.2 G**), while maintaining total ATP

production equal (**Fig 4.2 G**). Remarkably, PLC cells are not oxidizing palmitate, since etomoxir, an inhibitor of CPT1, has no effect on both OCR and ECAR (**Fig 4.3**).

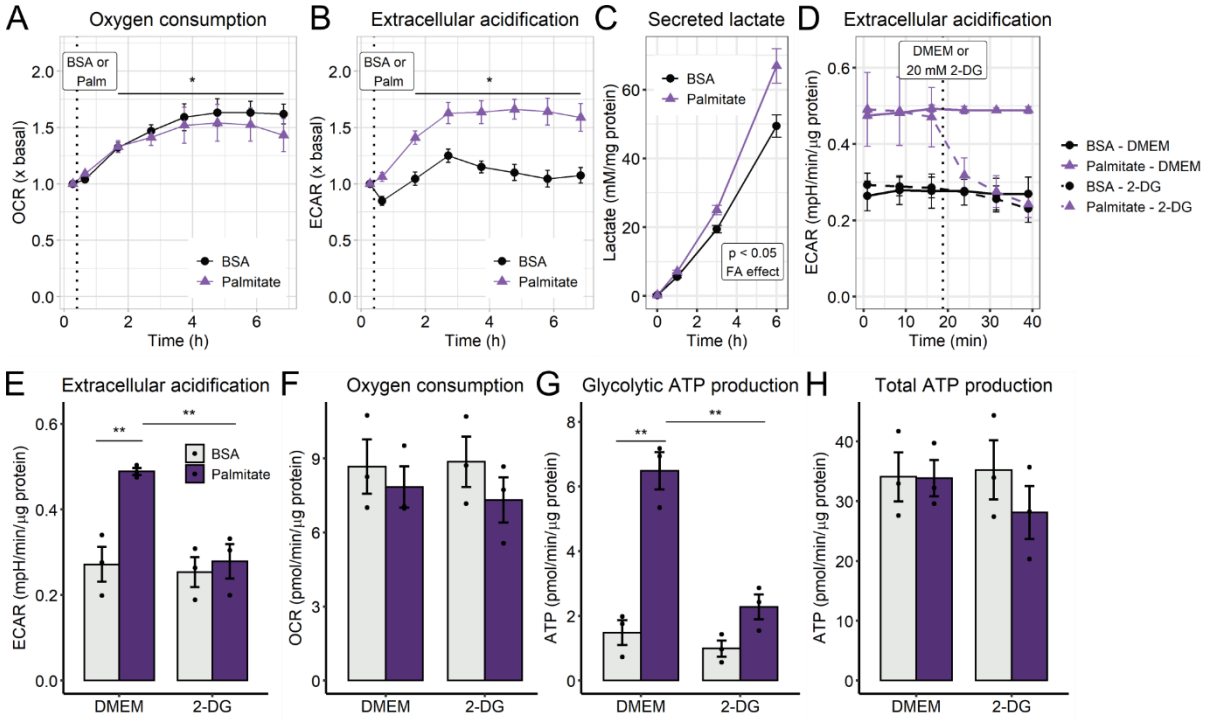

Figure 4.2: Palmitate overload increases glycolytic flux - Real-time OCRs and ECARs were measured in a Seahorse XFe24 analyzer over 6 h after 0.2 mM palmitate injection, indicated by the dotted line (A-B). Secreted lactate was measured in the supernatant over time (C). ECARs and OCRs were measured after 6 h palmitate incubation and modulated by 2-deoxyglucose (D-F). Glycolytic ATP and total ATP production were calculated as described in the Methods section (F-G). In A and B, * = $p < 0.05$ for time effect, two-way ANOVA repeated measurements. In D-G, ** = $p < 0.01$ two-way ANOVA followed by Tukey's post-test. OCR and ECAR plots are means + SEM. Bar plots are means + SD. Filled circles represent independent experiments.

Additionally, in another human hepatoma cell line, the HepG2 cells, Palmitate did not disturb OCR as well (**Fig 4.4 A, D-F**) and ECAR remained higher after palmitate, and was 2-DG sensitive, but without increasing lactate secretion (**Fig 4.4 B-C**). Interestingly, these cells are highly glycolytic, since about 50% of ATP come from glycolysis even in the BSA group (**Fig 4.4 G**). On the other hand, in AML12 cells, a mouse hepatocyte cell line, no differences were observed on ECAR over 2 hours, but rather an increasing OCR as a result of a higher proton-leak (**Fig 4.5 A-B, E**). These cells are non-tumor, highly oxidative, secrete lactate at lower levels than PLC cells independently of palmitate (**Fig 4.5 C**), and virtually 100% of their ATP comes from oxidative phosphorylation (**Fig 4.5 G**).

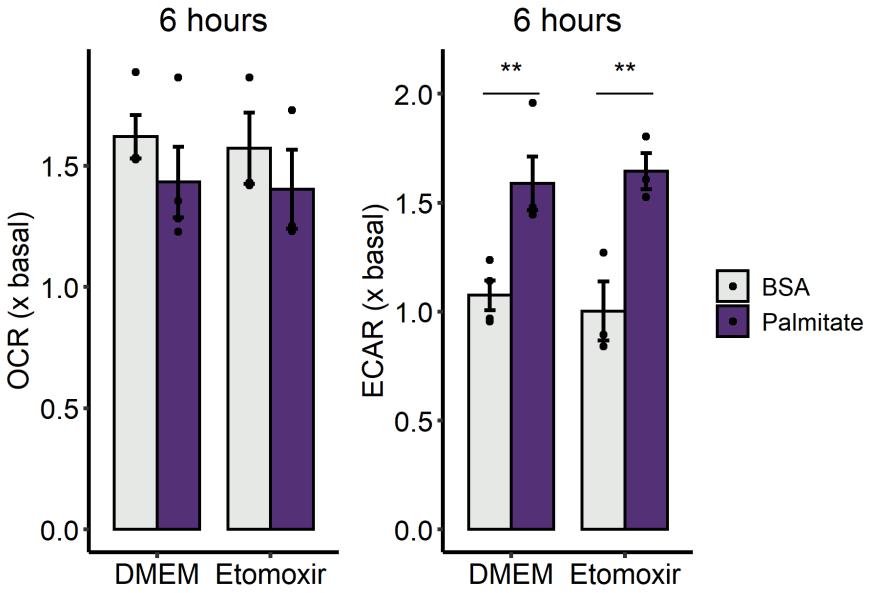

Figure 4.3: Blockage of LCFA entry to mitochondria does not affect glycolytic shift – Real-time OCRs and ECARs were measured in a Seahorse XFe24 analyzer over 6 h after 0.2 mM palmitate injection concomitantly to 0.5 µM etomoxir. ** = $p < 0.01$ vs BSA. Two-way ANOVA and Tukey's post-test. Bar plots are means + SD. Filled circles represent independent experiments. (n = 3-4)

HepG2 and PLC cells are cultivated in the same nutrient composition, i.e., DMEM 5.5 mM glucose, 4 mM glutamine, 1 mM pyruvate, while AML12 are in DMEM/F12, i.e., 17.5 mM glucose, 2.5 mM glutamine, 0.5 mM pyruvate. Discrepancies in cell lines from tumors are expected and suggest an effect specific for the conditions which PLC were adapted to. We followed the next experiments using PLC cells as an interesting and novel model of glycolytic modulation by palmitate. Increased respiration by palmitate in rodent cell lines, as seen in AML12, were recently described to be dependent on calcium signaling and glutamine anaplerosis (Egnatchik et al., 2019).

Up to now, we can conclude that increased mitochondrial fragmentation in PLC precedes any disruptions in mitochondrial oxygen consumption and overall ATP production upon palmitate exposure. Glycolytic flux is increased as soon as 1 h of palmitate treatment, meaning this metabolic switch is an early outcome of palmitate-induced lipotoxicity for these cells.

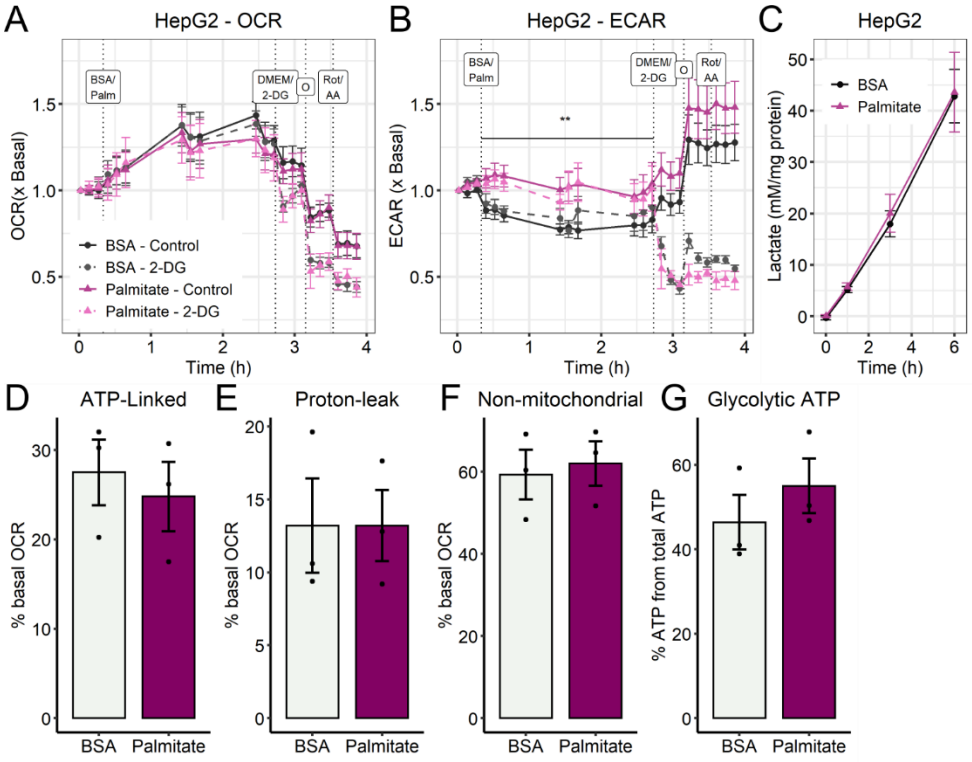

Figure 4.4: Palmitate overload does not increase glycolytic flux in HepG2 cells – Real-time OCRs and ECARs were measured in a Seahorse XFe24 analyzer over 2 h after 0.2 mM palmitate injection, indicated by the dotted line, and modulated by sequential additions of 2-deoxyglucose (20 mM), oligomycin (1 µM), rotenone (1 µM), and antimycin A (1 µM) (A-B, D-F). Secreted lactate was measured in the supernatant over 6 hours after palmitate/BSA treatment and normalized by total protein at the end of the experiment (C). Glycolytic ATP production rate was calculated as described in Material and Methods. ** = $p < 0.01$ for fatty acid effect, two-way ANOVA repeated measurements. OCR, ECAR and lactate plots are means + SEM. Bar plots are means + SD. Filled circles represent independent experiments. (n = 4-5)

4.2.1. Mitochondrial fragmentation and fuel dependency switch depending on substrate availability

We found it quite surprising that a fatty acid would induce such a significant increase in glycolytic ATP production, and decided to further characterize this effect by examining the role of different substrates present in culture media in this metabolic shift. Cells were treated with palmitate under glucose and/or glutamine deprivation for 6 hours to assess which media nutrients could be related to metabolic remodeling. Mitochondrial fragmentation was promoted only in full media, i.e., DMEM containing both glucose (Glc) and glutamine (Gln), (**Fig 4.6**).

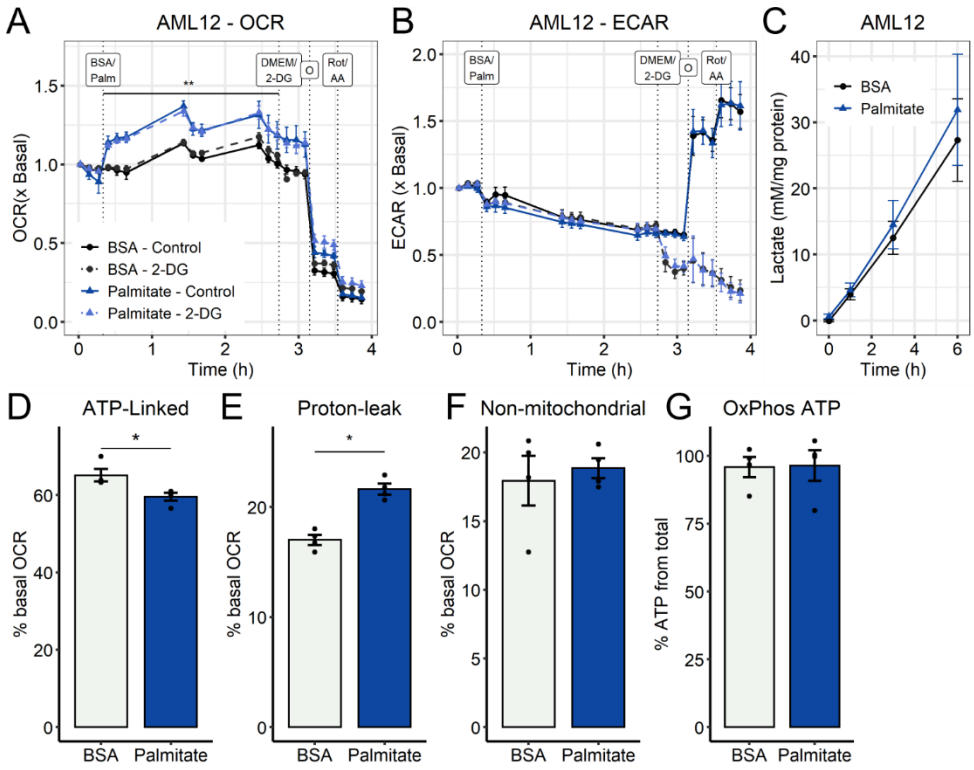

Figure 4.5: Palmitate overload increases oxygen consumption in AML12 cells – Real-time OCRs and ECARs were measured in a Seahorse XFe24 analyzer over 2 h after 0.2 mM palmitate injection, indicated by the dotted line, and modulated by sequential additions of 2-deoxyglucose (60 mM), oligomycin (1 µM), rotenone (1 µM), and antimycin A (1 µM) (A-B, D-F). Secreted lactate was measured in the supernatant over 6 hours after palmitate/BSA treatment and normalized by total protein at the end of the experiment (C). Oxidative phosphorylation ATP production rates were calculated as described in Material and Methods. ** = $p < 0.01$ for fatty acid effect, two-way ANOVA repeated measurements. OCR, ECAR and lactate plots are means + SEM. Bar plots are means + SD. Filled circles represent independent experiments. (n = 4-5)

Following glutamine deprivation, there was a significant decrease in mitochondrial OCRs (**Fig 4.7 A**), demonstrating the important role of this amino acid, which feeds into the TCA cycle and sustains mitochondrial ATP production when glucose is absent (Gln group). The presence of palmitate did not change total ATP production in any group, but glutamine deprivation (no additions and Glc groups) reduced it significantly (**Fig 4.7 C**). Mitochondrial fragmentation was not necessary for the activation of ATP synthesis from glycolysis, as this occurred both in the combined presence of glucose and glutamine, and with glucose alone (**Fig 4.7 B and D**). From these results, we can conclude that PLC cells have high flexibility for nutrient utilization. Additionally, palmitate does not impede ATP production, but promotes a

shift towards glycolysis only if glucose is available **(Fig 4.7 E),** suggesting that other carbon intermediates are not playing a significantly role in lactate production in this system.

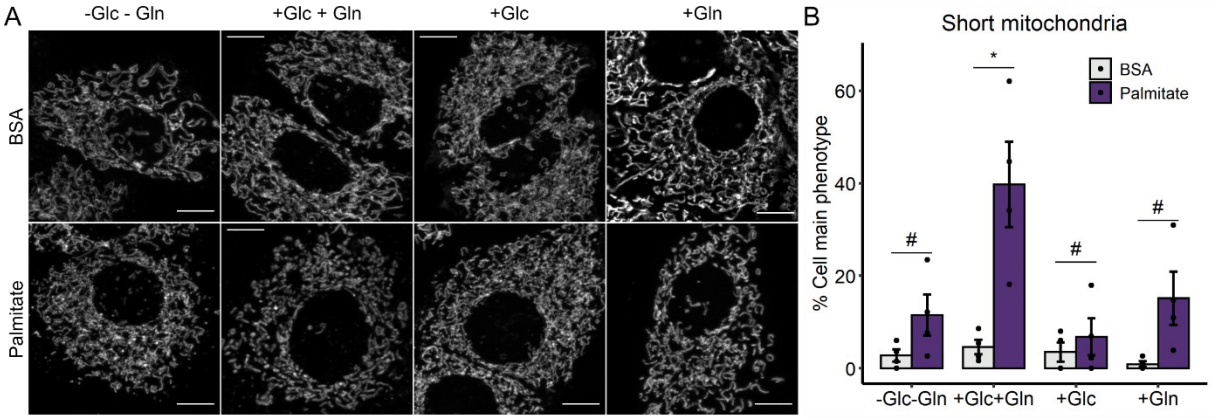

Figure 4.6: In absence of glucose and/or glutamine, palmitate does not promote mitochondrial network fragmentation - PLC/PRF/5 cells were incubated with palmitate/BSA (0.2 mM/ 0.25%) for 6 h in media without glucose nor glutamine (-Glc-Gln), or in the presence of glucose and glutamine (+Glc+Gln), or only glucose (+Glc), or only glutamine (+Gln). Live mitochondrial morphology was evaluated after 50 nM Mitotracker Deep Red loading by confocal microscopy at 6 h (A). Mitochondrial network morphology was classified as described in the Methods section (B). * = $p < 0.05$ vs respective BSA, # = $p < 0.05$ vs. +Glc+Gln group. Two-way ANOVA followed by Tukey's post-test. Bar plots are means + SD. Filled circles represent independent experiments. Scale bar = 10 μm.

4.2.1. NAD(P) redox state changes in palmitate-induced metabolic plasticity

Lipid overload is often associated with oxidative stress. The ability of a cell to handle oxidants is related to its NADPH pool, which is essential to maintain reduced glutathione and thioredoxin, involved in the main hydrogen peroxide-removing systems (Winterbourn, 2018). We measured NAD(P)H in cells by autofluorescence, using modulation by the electron transport chain inhibitors oligomycin or rotenone plus antimycin. The uncoupler CCCP was used to maximize reduction and oxidation, and thus estimate the total as well as oxidized and reduced pools (as described in the methods section). Surprisingly, by reducing the total pool of $NAD(P)^+$ (through the inhibition of electron transport chain complexes I and III simultaneously), we observed that palmitate treatment promotes a large increase in total NAD(P) (**Fig 4.8 A**). Furthermore, under basal conditions, NAD(P)H content is lower in palmitate versus BSA treated cells (**Fig 4.8 B**). We should note, however, that this assay cannot separate the different cell compartments, as mitochondrial modulation will also change NAD(P)H redox state in the cytosol, since the pools are connected by the reversible malate-

aspartate shuttle (Xiao and Loscalzo, 2019). Our results indicate that palmitate leads to redox imbalance in PLC cells.

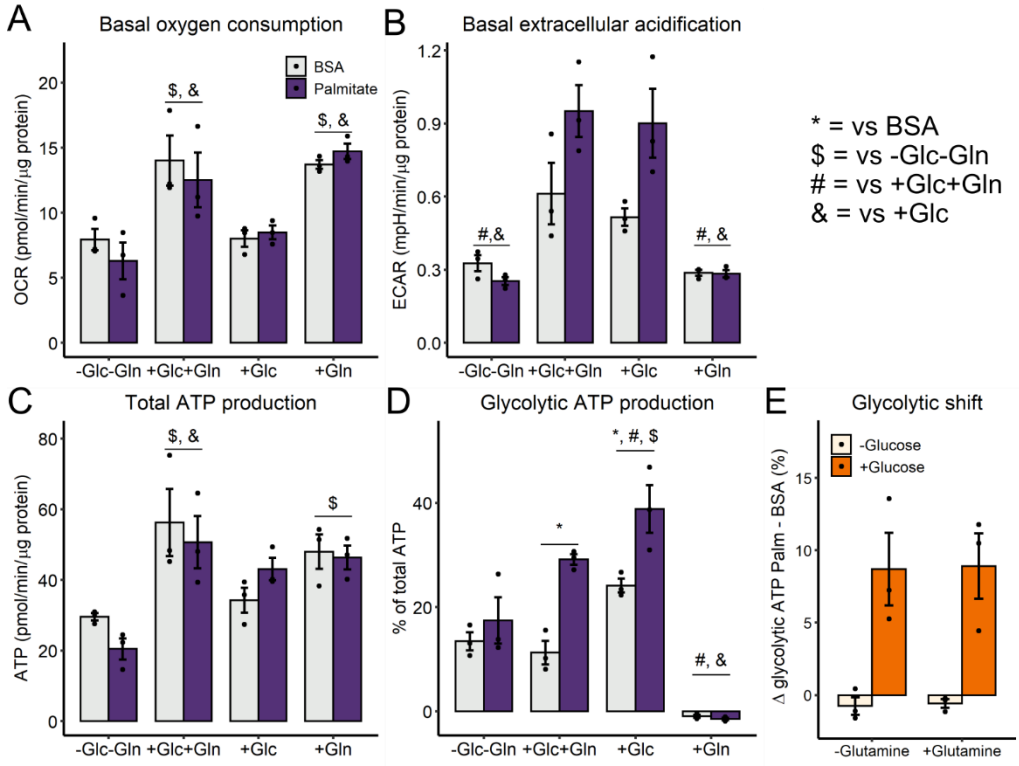

Figure 4.7: Palmitate metabolic shift requires glucose, but not glutamine - PLC/PRF/5 cells were incubated with palmitate/BSA (0.2 mM/ 0.25%) for 6 h in media without glucose nor glutamine (-Glc-Gln), or in the presence of glucose and glutamine (+Glc+Gln), or only glucose (+Glc), or only glutamine (+Gln). ECARs and OCRs were measured after 6 h (A-B). Total and glycolytic ATP production were calculated as described in the Methods section (C-D). In (E), delta glycolytic ATP production from values of B (palmitate – BSA). * = $p < 0.05$ vs respective BSA, # = $p < 0.05$ vs. +Glc+Gln group, $ = $p < 0.05$ vs. -Glc-Gln group, & = $p < 0.05$ vs. +Glc group. Two-way ANOVA followed by Tukey's post-test. Bar plots are means + SD. Filled circles represent independent experiments.

An important regulator of mitochondrial $NADP^+$/NADPH ratios is an enzyme located in the inner mitochondrial membrane, the nicotinamide nucleotide transhydrogenase (NNT), which promotes the reduction of $NADP^+$ by the oxidation of NADH, powered by the mitochondrial inner membrane potential ($\Delta\Psi$). The NNT is, consequently, a node that integrates energy production (NADH pool and $\Delta\Psi$) and the mitochondrial antioxidant system (recycling of glutathione and thioredoxin) (Rydström, 2006). Furthermore, NNT has been shown to be inhibited by long chain acyl-CoAs, with palmitoyl-CoA as the most specific inhibitor

(Rydström et al., 1971). Palmitate treatment did not change NNT protein content after 6 hours (**Fig 4.9 A-B**), although this does not exclude modulation of activity under these conditions.

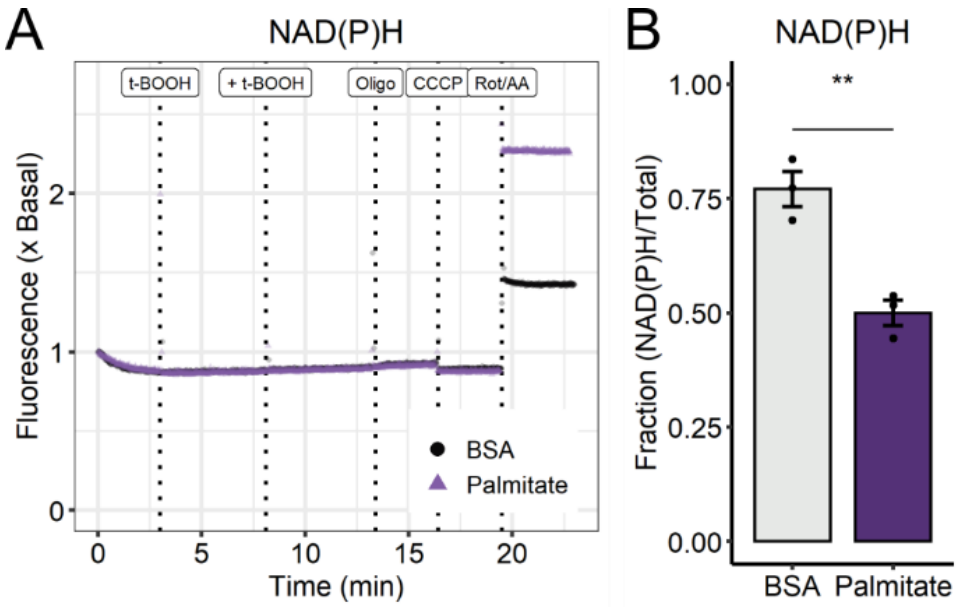

Figure 4.8: Palmitate promotes oxidative stress - PLC/PRF/5 cells were incubated with palmitate/BSA (0.2 mM/ 0.25%) for 6 h. NAD(P)H content was assessed in intact cells resuspended in DMEM media containing palmitate or BSA in the fluorimeter. Cells were challenged with two sequential additions of t-butyl hydroperoxide (0.5 mM), followed by oligomycin (1 µM), carbonyl cyanide 3-chlorophenylhydrazone (CCCP, 1 µM – to promote maximal oxidation), and rotenone (1 µM) plus antimycin A (1 µM), to promote maximal reduction. In (A) representative plot of 1 experiment. In (B), ratio of basal NAD(P)H and total NAD(P)H. ** = $p < 0.01$, Student's t-test. Bar plots are means + SD. Filled circles represent independent experiments.

Gameiro et al., 2013, described that NNT knockdown promotes a fuel switch from glutamine to glucose use by measuring their incorporation into TCA intermediates and lactate secretion (Gameiro et al., 2013). We speculated if palmitate-induced glycolytic activation could be related to NNT inhibition, and, thus, decreased NADPH content, and if NNT inhibition could exacerbate palmitate-induced glycolytic flux. To address this, we stably knocked down NNT using shRNA; the protein content was decreased to less than 50% of control levels (**Fig 4.9 C**). Both clones tended to decrease basal OCRs, independently of palmitate (**Fig 4.9 D**). Interestingly, the proton leak component of oxygen consumption is significantly reduced in the 28512 clone (i.e., NNT1, **Fig 4.9**), which is compatible with NNT function, that allows for proton re-entry into the matrix. The fraction of OCR associated to ATP production was decreased in the 28541 clone (i.e., NNT2), while its non-mitochondrial OCR was increased

(**Fig 4.9 E and G**). Furthermore, while there were no differences in total ATP production (**Fig 4.9 H**), ATP from glycolysis is significantly increased in NNT2 KD (**Fig 4.9 I**). This demonstrates that changing mitochondrial redox state either through palmitate treatment or NNT KD can promote glycolytic ATP production.

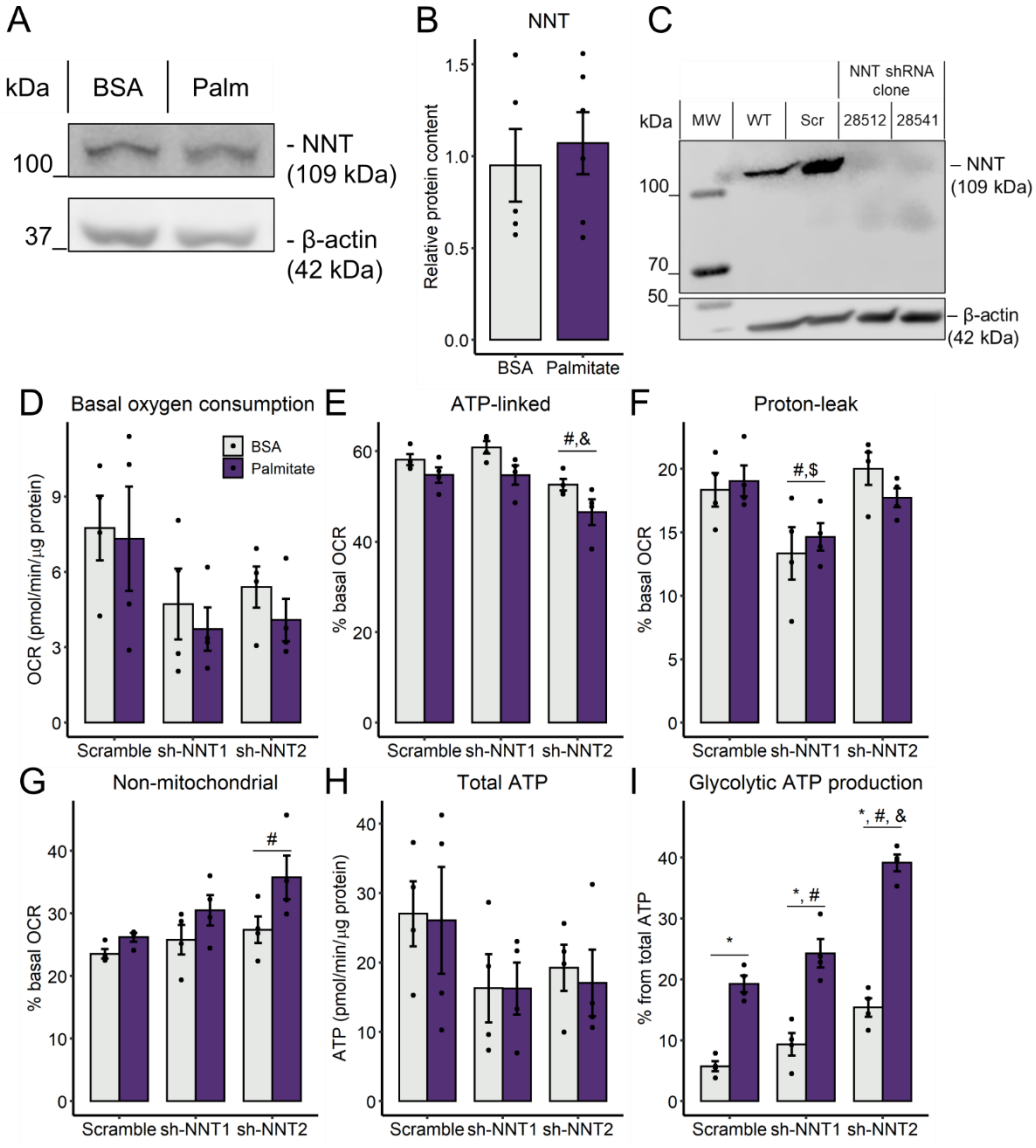

Figure 4.9: Nicotinamide nucleotide transhydrogenase knockdown exacerbates fuel switch - PLC/PRF/5 cells were incubated with palmitate/BSA (0.2 mM/ 0.25%) for 6 h. NNT protein content for WT cells (A-b), or puromycin-selected PLC cells for scramble or NNT knockdown (C). Real-time OCRs and ECARs were measured in a Seahorse XFe24 analyzer after 6 h palmitate treatment (D-I). ATP production was calculated as described in the Methods section. # = $p < 0.05$ vs. scramble; & = vs sh-NNT1, $ = vs sh-NNT2. Two-way ANOVA + Tukey´s post-test. Bar plots are mean + SD. Filled circles represent independent experiments.

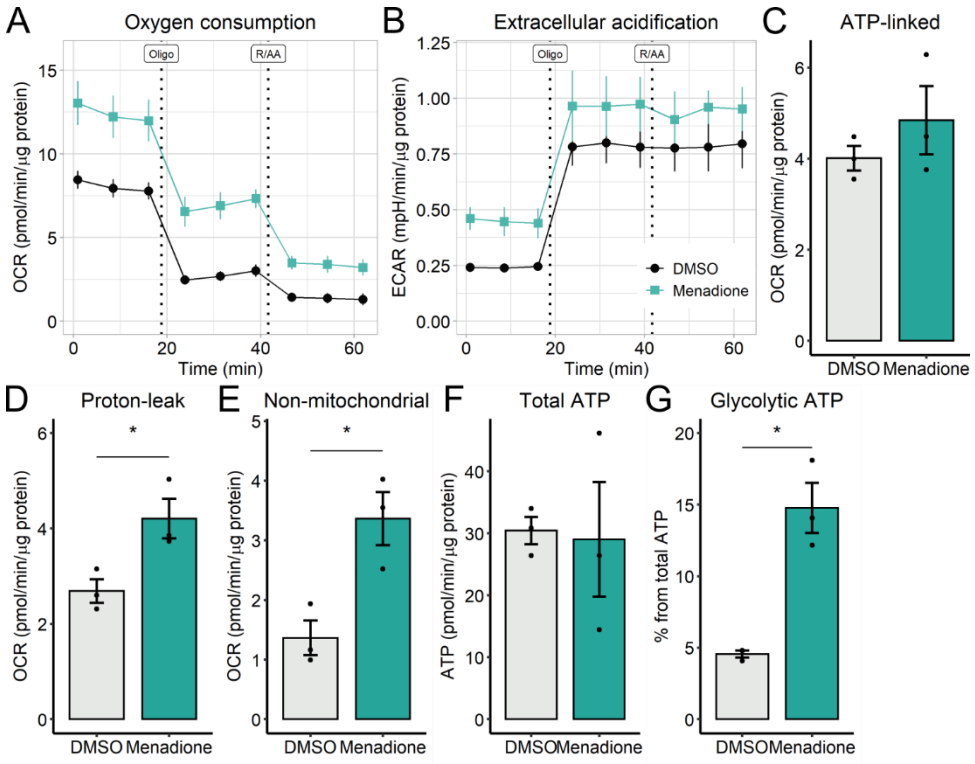

Figure 4.10: Menadione increased glycolytic flux - PLC/PRF/5 cells were incubated with 10 µM menadione for 6 hours. Vehicle is 0.1% DMSO. Real-time OCRs and ECARs were measured in a Seahorse XFe24 analyzer after 6 h. ATP production was calculated as described in the Methods section. * = $p < 0.05$ Student's t test. OCR and ECAR plots are mean + SEM. Bar plots are means + SD. Filled circles represent independent experiments.

4.2.2. Oxidative disturbances promote glycolysis

Based on the results seen up to now, we hypothesized that redox signals could play a decisive role in the upregulation of glycolytic ATP synthesis promoted by palmitate. We thus evaluated if the generation of oxidants could regulate glycolysis. To do so, we used the naphthoquinone analogue menadione, which increases superoxide formation and lowers NADPH levels (Smith et al., 1987). Menadione lead to increased OCRs as a consequence of enhanced proton leak and non-mitochondrial respiration (**Fig 4.10 A, D-E**), a result which differs from the effects of palmitate and NNT KD seen previously. Menadione also enhanced ECAR and glycolytic flow (**Fig 4.10 B and G**), without changing total ATP production (**Fig 4.10 F**). Interestingly, the contribution of glycolysis toward ATP production (**Fig 4.10 G**) was almost 3-fold higher with menadione than in the DMSO control, suggesting that 6 hours of

redox imbalance is enough to remodel cellular metabolism through glycolytic activation without compromising net ATP production.

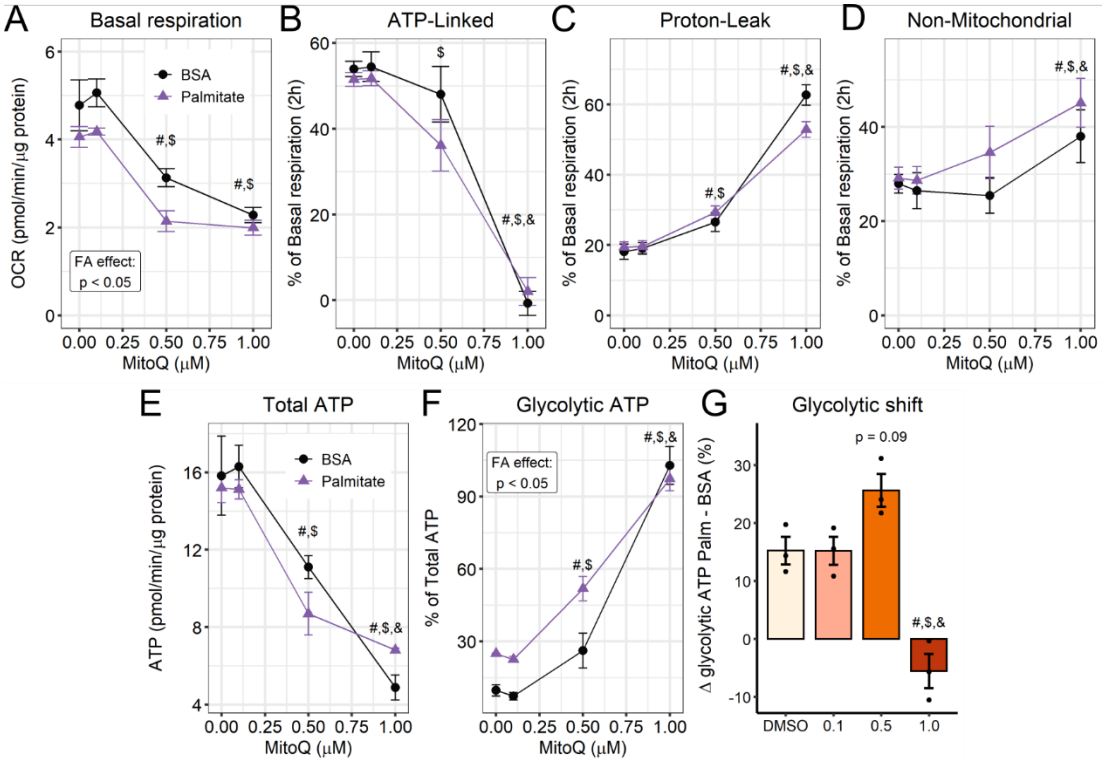

Figure 4.11: Mitoquinone increased glycolytic flux - PLC/PRF/5 cells were incubated with 0.1 µM mitoquinone followed by 2 hours of palmitate/BSA (0.2 mM/ 0.25%). Vehicle is 0.1% DMSO. Real-time OCRs and ECARs were measured in a Seahorse XFe24 analyzer. ATP production was calculated as described in the Methods section. Glycolytic shift was calculated as the difference between palmitate and BSA glycolytic ATP production (from data shown in figure F). # = $p < 0.05$ vs DMSO, $ = vs 0.1, & = vs 0.5. In A-F, Two-way ANOVA. In G, one-way ANOVA. Line plots are mean + SEM. Bar plots are means + SD. Filled circles represent independent experiments. (n = 3)

To evaluate the contribution of mitochondrially-generated oxidants toward palmitate-induced glycolysis, we pre-treated the cells with the antioxidant Mitoquinone (MitoQ) for 20 minutes and added palmitate, while following OCR and ECAR for up to 2 hours. MitoQ is targeted specifically to respiring mitochondria and cycles through the reduced and oxidized forms in the inner membrane, acting as a scavenger of leaked electrons. It cannot be oxidized by complex III but is recycled by complex II (Smith and Murphy, 2010). Surprisingly, MitoQ not only increased glycolytic ATP production but inhibited mitochondrial oxygen consumption (**Fig 4.11 A, F)**. The effects of MitoQ on ATP sources are unclear, as it acted similar to NNT KD by suppressing mitochondrial respiration and significantly reduced total ATP-production.

Nonetheless, the glycolytic shift promoted by palmitate was higher in the presence of 0.5 µM MitoQ (**Fig 4.11 G)**, suggesting an interaction between the two stimuli, while 1 µM MitoQ is already toxic to mitochondrial function.

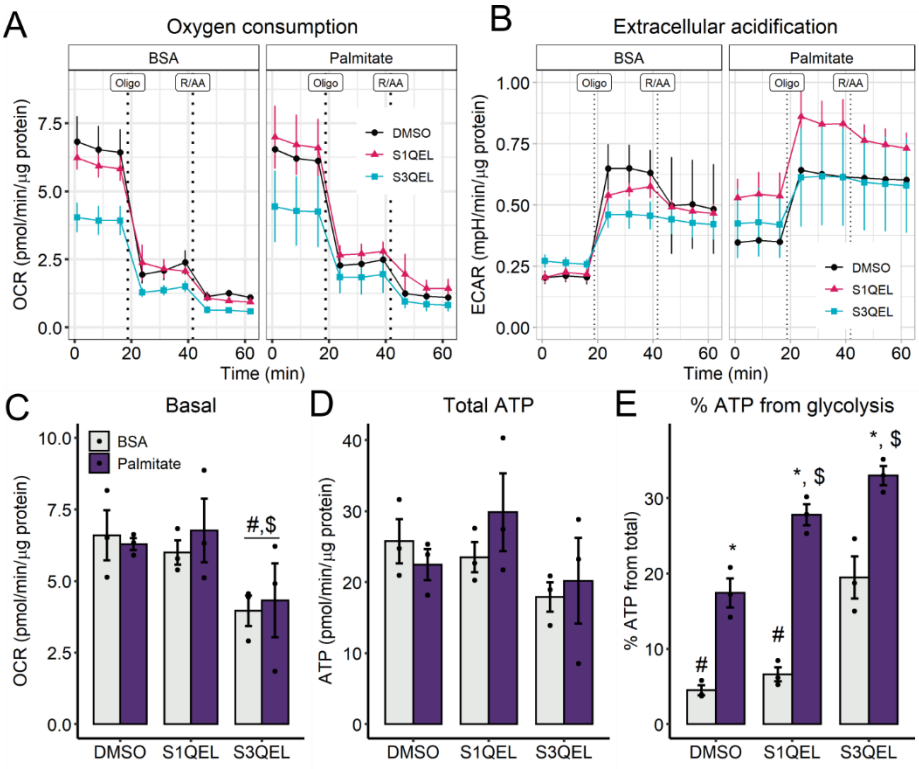

Figure 4.12: Inhibition of site I_Q hydrogen peroxide/superoxide production increased palmitate-induced glycolytic ATP rates - PLC/PRF/5 cells were incubated concomitantly with 10 µM S1QEL or S3QEL and palmitate/BSA (0.2 mM/ 0.25%) for 6 hours. Vehicle is 0.1% DMSO. Real-time OCRs and ECARs were measured in a Seahorse XFe24 analyzer. ATP production was calculated as described in the Methods section. * = $p < 0.05$ vs BSA, # = $p < 0.05$ vs DMSO, $ = vs S1QEL. Two-way ANOVA and Tukey's post-test. Line plots are mean + SEM. Bar plots are means + SD. Filled circles represent independent experiments. (n = 3)

To overcome the effects of antioxidants and pro-oxidants on mitochondrial respiration, we took advantage of suppressors of complex I and III site Q electron leak (S1QEL1.1 and S3QEL2, respectively). These are small molecules screened to block superoxide production from the electron transport chain without compromising electron flow to complex IV-bound oxygen (Brand et al., 2016; Orr et al., 2015). Despite this, in our cells, we observed that S3QEL, but not S1QEL (both at 10 µM), lowered oxygen consumption (**Fig 4.12 A, C**), but did not affect total ATP production (**Fig 4.12 D**). No significant effects were seen on ECARs either (**Fig 4.12 B**). Interestingly, both modulators exacerbated glycolysis in palmitate-treated cells,

and S3QEL also increased glycolytic flux in BSA controls (**Fig 4.12 E**). These results suggest that both I_Q and III_Q oxidant production sites provide signals that control cytoplasmic ATP production, and I_Q seems to be a site-sensitive to palmitate. Overall, these results demonstrate that palmitate and redox state are important determinants of glycolytic flux.

4.3. Discussion

Palmitate overload is well known to promote lipotoxicity in many cell types (Jheng et al., 2012; Kulkarni et al., 2016; Molina et al., 2009). Here, we aimed to understand the early metabolic effects of palmitate overload, and how these were related to mitochondrial morphological changes. We have previously found, in a BV2 microglial culture, that neither palmitate nor oleate overload for 24 hours promote changes in mitochondrial oxygen consumption. Additionally, significantly decreased glycolysis and distinct lipidic species accumulation was observed in this inflammatory cell line (Chausse et al., 2019).

Prior studies in hepatic cells (Bao et al., 2010; Egnatchik et al., 2014b; Geng et al., 2020b) suggested that palmitate promoted a late decrease in inner mitochondrial membrane potentials and increased oxygen consumption, secondary to calcium efflux from the ER and increased glutamine catabolism (Egnatchik et al., 2014b). We should note, however, that while mitochondrial function in intact cells is reliably evaluated by oxygen consumption rates (Brand and Nicholls, 2011), uncalibrated mitochondrial inner membrane potential estimates are much more artifact-prone (Gerencser et al., 2012), particularly when overt changes in morphology occur (Kowaltowski et al., 2002, 2019). Our experiments here show that, surprisingly, within 1 hour of incubation, palmitate can strongly increase glycolytic flux. An associated increase in glycolytic ATP production occurred, as soundly confirmed by 2-deoxyglucose inhibition of ECARs, but without disturbing mitochondrial oxygen consumption for up to 6 hours (**Fig 4.2**). Under these conditions, added palmitate was not oxidized, since etomoxir, a CPT1 inhibitor which prevents uptake of the fatty acid into mitochondria (Divakaruni et al., 2018), had no

effects on OCR or ECAR (**Fig 4.3**). However, cytosolic palmitate actions can rewire the TCA and promote differential use of carbon sources (Egnatchik et al., 2014b), which may explain our results.

At 6 hours under the same conditions of palmitate treatment, mitochondria are predominantly fragmented (**Fig 4.1**). However, our substrate availability studies showed that fragmentation and the increase in glycolytic ATP production are dissociated: while palmitate-induced mitochondrial fragmentation required the presence of both glutamine and glucose, palmitate-induced increases in ATP production from glycolysis required only glucose (**Fig 4.6**). Glutamine starvation was described recently as a strong pro-fusion signal (Cai et al., 2018), so we speculate that glutamine and/or glucose starvation are hierarchically stronger signals that favor elongation (Gomes et al., 2011), compared to palmitate-induced fragmentation. Carbon flux through glycerol-3-phosphate consumption may contribute toward the morphology-independent palmitate-induced increased glycolytic flux we observed. Indeed, glycerolipid synthesis has been recently shown to be increased by palmitate, resulting in diacylglycerol accumulation (Piccolis et al., 2019).

A possible node for the regulation of the metabolic switch promoted by palmitate is the interaction between adenosine monophosphate-activated protein kinase (AMPK) and CD36, which mediates palmitate entry into the cell. Palmitate interacts with CD36 and can palmitoylate it (Tao et al., 1996; Thorne et al., 2010; Zhao et al., 2018). This increases CD36 translocation to the plasma membrane and favors the formation of a complex with Fyn, Lyn and LKB1, preventing AMPK activation under chronic palmitate treatment conditions (Li et al., 2019a; Zhao et al., 2018). Acute binding to palmitate, on the other hand, may alleviate LKB1 inhibition, activating AMPK and lipophagy (Li et al., 2019a; Samovski and Abumrad, 2019; Samovski et al., 2015). Zhang and co-workers elegantly described the mild and early activation of AMPK upon glucose starvation before any changes in ATP levels, in a manner

regulated by aldolase activity (a glycolytic enzyme). AMPK is fully activated when AMP/ATP ratios start to rise in combination with glutamine deprivation (Zhang et al., 2017). Curiously, cells deprived of glucose do not activate glycolysis upon palmitate after 6 hours, indicating that PLC cells may be unable to provide carbons to form glycolytic intermediates, even when total ATP production is compromised (**Fig 4.6**). Interestingly, in more recent work, the group observed that AMPK is activated in a stratified manner in compartments, proportionally to the severity of nutrient stress (Zong et al., 2019).

Another clear metabolic effect of palmitate was an increase in total NAD(P) and a shift to a more oxidized redox state of the pyridine nucleotide pool. Palmitate was shown to activate NADPH oxidase production of superoxide in many cells, e.g., skeletal muscle, pancreatic islets, endothelial cells, and hepatocytes (Bettaieb et al., 2015; Lambertucci et al., 2008; Maloney Ezekiel et al., 2009; Morgan et al., 2007). Furthermore, the ability of palmitate to both decrease NNT (observed by McCambridge et al., 2019) content and inhibit it (Rydström et al., 1971) make NNT a notable redox control node, integrating redox state and substrate use during lipotoxicity in the mitochondria. Indeed, NNT is seminal in the control of NADPH content in the mitochondrial matrix, responsible for the maintenance of ~50% of the NADPH pool (Rydström, 2006). Since the discovery of a spontaneous NNT mutation in Jax C57BL/6J mice (Toye et al., 2005), NNT importance has been increasingly recognized. Mice lacking the functional enzyme are more sensitive to diet-induced metabolic diseases (Fisher-Wellman et al., 2016; Francisco et al., 2018; Navarro et al., 2017). In cell culture systems, NNT knockdown disrupts not only redox balance and bioenergetics (Yin et al., 2012), but also switches fuel preference from glutamine to glucose, by regulating the NADPH/$NADP^+$ ratios, increasing glucose incorporation into the TCA cycle, lactate secretion, and sensitivity to glucose deprivation (Gameiro et al., 2013).

Indeed, when we constructed NNT KD cells, we found that palmitate treatment combined with NNT2 KD increased the participation of glycolytic ATP in total production (**Fig 4.9**). However, we also observed decreased basal OCRs, mainly due to decreased ATP production from the electron transport chain, which is not seen with palmitate treatment alone, but could reflect the importance of NNT in mitochondrial functional maintenance. Increased non-mitochondrial oxygen consumption also suggests an enhanced activity of cellular oxidases and/or the production of reactive oxygen species in the knockdown cells. Given these effects, it is unclear if NNT KD can directly induce glycolysis in our model. Ward et al., 2020, showed that the NNT KD did not alter redox balance in several non-small cell lung cancer cell lines, but lowered mitochondrial respiratory capacity, and diminished the ability to oxidize palmitate (Ward et al., 2020). This suggests that the disruptive effects of NNT may be context-dependent.

Despite the ambiguous role of the NNT, the significant change in $NAD(P)^+$/NAD(P)H rations demonstrate that palmitate strongly impacts on redox state (**Fig 4.8**). Based on this, we investigated if glycolysis could be modulated by changes in oxidant production. Corroborating that, menadione increased glycolytic flux without disturbing total ATP production nor mitochondrial ATP-linked respiration (**Fig 4.10**). On the other hand, MitoQ severely impact mitochondrial function when at concentrations higher than 0.5 μM and has no effect below that (**Fig 4.11**). Notably, the glycolytic shift promoted by palmitate + 0.5 μM mitoQ was higher than in BSA, suggesting that the production of mitochondrial oxidants may play a role in the induction of glycolysis by palmitate.

Recently, Brand's lab generated important tools to investigate the role of electron transport chain reactive oxygen species production in cell biology (Brand et al., 2016; Orr et al., 2015). They found small molecules, S1QEL and S3QEL, that block, specifically, the production of superoxide/hydrogen peroxide without disturbing electron flow to oxygen, nor the production of oxidants at other sites. We took advantage of these molecules and identified

that palmitate-induced glycolysis is exacerbated by the inhibition of superoxide/hydrogen peroxide at site I_Q (**Fig 4.12**), a location within mitochondrial complex I that produces both superoxide and hydrogen peroxide toward the matrix. Site III_Q produces superoxide toward both the matrix and the intermembrane space. Curiously, S3QEL increased glycolysis in both BSA and palmitate groups. However, since OCRs were significantly inhibited by it, we cannot exclude that other effects may be associated with the increase. This respiratory inhibition was not observed with S1QEL, which nonetheless affected glycolytic ATP production (**Fig 4.12**). We can thus conclude that the production of oxidants in the I_Q site is associated with metabolic rewiring of glycolysis promoted by palmitate.

4.4. Conclusions

Our work uncovers important early bioenergetic effects promoted by palmitate overload in PLC cells. We found that palmitate relies on glutamine and glucose availability to promote mitochondrial fragmentation. However, mitochondrial ATP production is unperturbed by a high degree of mitochondrial network fragmentation and oxidative imbalance, while glycolysis is readily responsive to acute palmitate treatment, oxidative stress, and mitochondrial oxidant production. Interestingly, inhibition of superoxide/hydrogen peroxide production at complex I site IQ was sensitive to palmitate and activated glycolysis. This indicates a novel, fatty acid modulated, redox regulation of glycolytic ATP production.

4.5. Material and methods

4.5.1. Cell culture: maintenance

4.5.1.1. PLC/PRF/5 cells

PLC/PRR/5 cells, or human hepatoma derived "Alexander cells", were kindly gifted by Professor Antonio Zorzano (IRB Barcelona/Spain). Cells were maintained in Dulbecco's Modified Eagle Medium (DMEM) containing 5.5 mM glucose, 4 mM glutamine, 1 mM pyruvate, 25 mM Hepes, 1% penicillin/streptomycin, 10% fetal bovine serum (FBS), and kept in a humidified, 5% CO_2, and 37ºC incubator.

4.5.1.2. HepG2 cells

HepG2 cells (ATCC® HB-8065), human hepatoma derived, were maintained in DMEM containing 5.5 mM glucose, 4 mM glutamine, 1 mM pyruvate, 25 mM Hepes, 1% penicillin/streptomycin, 10% FBS, and kept in a humidified, 5% CO_2, and 37ºC incubator.

4.5.1.3. AML12 cells

AML12 cells (ATCC® CRL-2254), mouse hepatocyte derived, were maintained in DMEM containing 5.5 mM glucose, 4 mM glutamine, 1 mM pyruvate, 10 µg/mL insulin, 5.5 µg/mL transferrin, 6.7 pg/mL selenium, 25 mM Hepes, 1% penicillin/streptomycin, 10% FBS, and kept in a humidified, 5% CO_2, and 37ºC incubator.

4.5.1.4. Nicotinamide nucleotide transhydrogenase knockdown

NNT knockdown was performed on PLC/PRF/5 cells as described in Muñoz and Zorzano, 2015, with some modifications (Muñoz and Zorzano, 2015). Briefly, HEK293T cells were seeded on 10 cm plates in DMEM containing 25 mM glucose, 4 mM glutamine, 1 mM pyruvate, 25 mM Hepes, 10% FBS, and kept in a humidified, 5% CO_2, 37ºC incubator. Twenty-four hours later, cells were transfected for lentiviral production in media containing 5 µg of each lentiviral packing plasmid (pMD2.G and psPAX2, Addgene: #12259, #12260, respectively), 10 µg of the scramble pLKO.1 or the NNT constructs (named here 1 and 2, respectively, from Mission® shRNA: TRCN0000028512, TRCN0000028541), and PEI Max, then incubated for an additional 24 hours at 37ºC. The following day, media was replaced and cells were incubated at 33ºC for viral production. Twenty-four hours later, media was collected, filtered in a 0.45 µm filter, and mixed with 2.5 $\mu g.mL^{-1}$ of Polybrene for PLC/PRF/5 infection. A second infection was performed the following day. Puromycin-resistant cells were selected in complete DMEM supplemented with 2.5 $\mu g.mL^{-1}$ puromycin. After selection, cells were expanded and maintained in complete DMEM supplemented with 2.5 $\mu g.mL^{-1}$ puromycin.

4.5.2. Fatty acid conjugation to bovine serum albumin

Sodium palmitate was solubilized in MilliQ water by heating (70ºC) and conjugated to free fatty acid bovine serum albumin (BSA-FFA) at 37ºC. A stock solution (4 mM fatty acid in

5% albumin) was filtered (0.22 µm) and frozen under sterile conditions in the -20ºC freezer for later use.

4.5.3. Cell treatments: fatty acids and drugs

4.5.3.1. Fatty acids

Cells were plated in maintenance DMEM. After 24 hours, the cells were PBS-washed and the medium was replaced by DMEM (in the presence or absence of 5.5 mM glucose and 4 mM glutamine, as stated) supplemented with sodium palmitate conjugated to BSA-FFA to final concentration of 200 µM in 0.25% BSA-FFA. Control groups were incubated in 0.25% BSA-FFA.

4.5.3.2. Drugs

All the drugs, and the respective solvents, time of incubation, and concentrations are described in the following table:

Table 1: Drugs

Compound	Solvent	[] final (µM)	Source	Catalog number	Time
Menadione	DMSO	10	Sigma Aldrich	M5625	6 hours
Mitoquinone mesylate	DMSO	0.1, 0.5, 1	Medkoo	317102	2.5 hours
S1QEL1.1	DMSO	10	Sigma Aldrich	SML1948	6 hours
S3QEL2	DMSO	10	Sigma Aldrich	SML1554	6 hours

4.5.4. SDS Page and western blots

After incubation with fatty acids, cells were lysed in RIPA buffer and centrifuged (16000g, 30 minutes). The supernatant was collected, and protein quantification was performed using Pierce's BCA reagent and a BSA standard curve. Proteins were diluted in Laemli buffer containing 5% β-mercaptoethanol and heated for 5 minutes for denaturation. Proteins were separated in a denaturing polyacrylamide gel by electrophoresis and then transferred to a polyvinylidene difluoride (PVDF) membrane. After blocking with 5% defatted milk, the membranes were incubated (overnight, at 4ºC) with primary antibodies (anti-NNT cat. Abcam: ab110352; β-actin cat. Abcam ab8226). Membranes were then incubated with secondary antibodies conjugated to fluorescent (Licor®) anti-mouse. Semi-quantitative analyses were performed by densitometry in the ImageJ software.

4.5.5. Confocal microscopy

Within the final 30 minutes of incubation, Mitotracker Deep Red (50 nM, ThermoScientific ®) or methyl tetramethylrhodamine (TMRM 100 nM, ThermoScientific ®) were added to the cells (plated on 4-chamber CELLView, Greiner BioOne®) and incubated at 37ºC and 5% CO_2. Immediately after, live cells images were acquired using a Zeiss LSM 880 Elyra confocal microscope Airyscan, (temperature, humidity, and CO_2 control). The acquisition was made in 35 positions on the Z axis, to enable reconstruction in 3 dimensions, or in 7 positions on the Z axis and 9 XY blocks, in order to quantify the population.

4.5.6. Images analyses

The mitochondrial network was reconstructed in 3D with the aid of the macro MitoKondrY, developed by Dr. Sebastien Tosi (IRB Barcelona) for ImageJ. Briefly, the macro allows quantification in pixels of the volume and the length of the mitochondrial network. From that, objects that do not form branches are identified - i.e. not contained in the network - are filtered as "individuals" for further quantification of their volume, surface area, axis length, sphericity and aspect ratio (such as major axis / minor axis). The mitochondrial population evaluation took place after blind identification and sample randomization. The previous definition of cells containing a network was followed. Predominantly fragmented - classified as "short" - or predominantly elongated - called "long". The cells called "intermediate" present a network with some proportion of both the shortened and elongated phenotypes. Cells were classified and counted for later identification (Muñoz and Zorzano, 2015). Mitochondrial fusion factor (FF) is defined as (% intermediate cells + 2 *% elongated cells) (Senyilmaz-Tiebe et al., 2018).

4.5.7. Lactate production

After cell incubation on 24 plates, media was collected at times 0, 1, 3, and 6 hours, and the cells were PBS-washed, and frozen for protein quantification. The secreted lactate content was measured in the media by colorimetric assay, following the manufacturer's instructions

(LabTest®, Brazil). Protein was further harvested in RIPA buffer and quantified by BCA and BSA standard curve. Values were normalized by total cell protein content.

4.5.8. Triglyceride content

After incubation on P100 plates, cells were PBS-washed and scraped in 1 mL PBS. Eight-hundred microliters were centrifuged and 200 µL were kept for protein quantification. After centrifugation (5 min, 300 g), the lipids were extracted by Folch's method (adapted from Folch et al., 1957; Wang et al., 2017). Briefly, the pellets were resuspended in 1ml chloroform:methanol (2:1) and vigorously agitated for 1 hour. Two-hundred microliters of MilliQ water were added to the tube and vortexed. The organic phase was collected to a new tube and dried overnight in the fume hood. The pellet was resuspended in 200 µL chloroform and 2% Triton-X 100 and re-dried. The remaining pellet was resuspended in 50 µL MilliQ water and the triglyceride content was measured by a colorimetric assay, following the manufacturer's instructions (LabTest®, Brazil). Values were normalized by total cell protein content.

4.5.9. Oxygen consumption, extracellular acidification, and ATP production rates

4.5.9.1. Palmitate overload: time course of oxygen consumption extracellular acidification rates

Twenty-four hours after plating on XFe24 Seahorse plates (Agilent ®), cells were PBS-washed and incubated in DMEM containing 5.5 mM glucose, 4 mM glutamine, 1 mM pyruvate, 1% penicillin/streptomycin, and 5 mM Hepes. Medium did not contain bicarbonate nor FBS. Cells were kept for 30 minutes in humidified, 37 ºC incubator. After basal oxygen consumption and extracellular acidification rates were measured, sodium palmitate conjugated to FFA-BSA were injected to the wells to a final concentration of 200 µM/0.25% and control groups received 0.25% FFA-BSA. Etomoxir was injected in half of the plate to a final concentration of 0.5 µM. After injection, measurements were taken every hour up to 6 hours.

4.5.9.2. Palmitate overload: glycolysis modulation with 2-deoxyglucose

Twenty-four hours after plating on XFe24 Seahorse plates (Agilent®), cells were PBS-washed and incubated in DMEM containing 5.5 mM glucose, 4 mM glutamine, 1 mM pyruvate, 1% penicillin/streptomycin, 200 µM/0.25% palmitate/FFA BSA, 5 mM Hepes. Control groups received 0.25% FFA BSA. Media did not contain bicarbonate nor FBS. Cells were kept for 6 hours in a humidified 37ºC incubator. OCR and ECAR were measured under basal conditions and following the addition of 20 mM 2-deoxyglucose, 1 µM oligomycin (pre-titrated), 1 µM rotenone and 1 µM antimycin A. ATP production rates (glycolytic, mitochondrial, and total) were calculated from the ECAR, OCR, and proton exchange rate (PER = $ECAR*BF*Vol_{microchamber}*K_{vol}$), following the manufacturer's instructions. Briefly, mitochondrial-derived ATP is $(OCR_{basal} - OCR_{oligomycin})*P/O*2$. Glycolytic ATP is $PER_{Total} - (OCR_{basal} - OCR_{Rot/AA})*CCF$. Total ATP production is the sum of mitochondrial and glycolytic ATP. We used the manufacturer's standard values for K_{vol}, P/O (phosphate/oxygen ratio) and CCF (CO_2 contribution factor). BF (buffer factor) was previously measured as 3.13 $mM.pH^{-1}$.

For HepG2 and AML12 cells, after washing with PBS and changing to media without bicarbonate (DMEM and DMEM/F12 respectively), cells were kept for 30 minutes in a humidified 37ºC incubator. After basal oxygen consumption and extracellular acidification rates were measured, sodium palmitate conjugated to FFA-BSA were injected into the wells to a final concentration of 200 µM/0.25%. Control groups received 0.25% FFA-BSA. After injection measurements were taken every hour up to 2 hours, following the addition of 20 mM or 60 mM 2-deoxyglucose, 1 µM oligomycin (pre-titrated), 1 µM rotenone and 1 µM antimycin A. ATP production rates (glycolytic, mitochondrial, and total) were calculated from the ECAR, OCR, and PER considering the rates at 2 hours. Buffer factor for DMEM/F12 was previously measured as 2.46 $mM.pH^{-1}$.

4.5.9.3. Palmitate overload: glucose and/or glutamine starvation

Twenty-four hours after plating on XFe24 Seahorse plates (Agilent ®), cells were PBS-washed and incubated in DMEM containing, 1 mM pyruvate, 1% penicillin/streptomycin, 200 µM/0.25% palmitate/FFA-BSA, and 5 mM Hepes. Glucose at 5.5 mM and/or 4 mM glutamine was added as described. Control groups received 0.25% FFA-BSA. Media did not contain bicarbonate nor FBS. Cells were kept for 6 hours in humidified, 37ºC incubator. Oxygen consumption and extracellular acidification rates were measured under basal conditions, and after pre-titrated 1 µM oligomycin, followed by 1 µM rotenone and 1 µM antimycin A. ATP production rates were calculated following the manufacturer's instructions. Buffer factors were previously measured for every buffer (in $mM.pH^{-1}$): Glc+Gln = 3.13, Glc = 3.34 , Gln = 3.13 , No-additions = 3.6.

4.5.9.4. Palmitate overload: oxidant production modulation

Twenty-four hours after plating on XFe24 Seahorse plates (Agilent®), PLC WT or scramble, sh-NNT1, and sh-NNT2 cells were PBS-washed and incubated in DMEM containing 5.5 mM glucose, 4 mM glutamine, 1 mM pyruvate, 1% penicillin/streptomycin, 200 µM/0.25% palmitate/FFA BSA and 5 mM Hepes. Wild type cells were concomitantly incubated with 10 µM S1QEL 1.1, S3QEL 2, or menadione. Control groups received 0.25% FFA BSA and/or 0.1% DMSO as vehicle. Media did not contain bicarbonate nor FBS. Cells were kept for 6 hours in a humidified 37ºC incubator. Oxygen consumption and extracellular acidification rates were measured under basal conditions, and after the addition of 1 µM oligomycin, followed by 1 µM rotenone and 1 µM antimycin A. ATP production rates were calculated as described in the manufacturer's instructions.

For MitoQ titration, after washing with PBS and changing to media without bicarbonate (DMEM and DMEM/F12 respectively), cells were kept for 30 minutes in a humidified 37ºC incubator. After basal oxygen consumption and extracellular acidification rates were measured, mitoquinone was injected into the wells to a final concentration of 0.1, 0.5, and 1.0 µM and

OCR and ECAR were immediately acquired, following sodium palmitate conjugated to FFA-BSA injection to a final concentration of 200 µM/0.25%. Control groups received 0.25% FFA-BSA. Every hour, measurements were taken up to 2 hours, following the addition of 1 µM oligomycin (pre-titrated), 1 µM rotenone and 1 µM antimycin A. ATP production rates (glycolytic, mitochondrial, and total) were calculated from the ECAR, OCR, and PER considering the rates at 2 hours.

4.5.9.5. Protein normalization

After every run, the media was removed, and the cells were frozen. Post-thawing, cells were disrupted by RIPA buffer and vigorous agitation. Protein quantification was performed using Pierce's BCA reagent and a BSA standard curve.

4.5.10. NAD(P)H fluorescence

After 6h in 200 µM/0.25% palmitate or 0.25% BSA, cells plated on P100 plates were PBS-washed and tripsinized. Cells were resuspended in DMEM with 5.5. mM glucose, 4 mM glutamine, 1 mM pyruvate, and 5 mM Hepes, and counted. Half million cells per milliliter were incubated in DMEM containing 200 µM/0.25% palmitate. NAD(P)H fluorescence (excitation 366 nm, emission 450 nm) was followed in a Hitachi ® F4500 fluorimeter with magnetic stirring. Cells were challenged with sequential additions of: tert-butyl hydroperoxide (0.5 mM), oligomycin (1 µM), carbonyl cyanide 3-chlorophenylhydrazone (CCCP, 1 µM), and rotenone (1 µM) and antimycin A (1 µM).

4.5.11. Statistics

The analysis was conducted using Microsoft Excel, RStudio, or JASP. Outliers were removed by Grubb’s test (alpha = 0.05). The groups mean were compared by Student's t test or Analysis of Variance (ANOVA) followed by Tukey’s post-test, according to the experimental design. Levels of significance were considered at $p < 0.05$.

4.5.12. Materials

Culture media, supplements, TMRM, and MitoTracker Deep Red were purchased from Thermo Scientific, except DMEM no glucose (cat. D5030), from Sigma Aldrich. Oligomycin, CCCP, rotenone, and antimycin A were from Santa Cruz Biotechnology. All the other reagents were purchased from Sigma-Aldrich unless stated differently.

5. Conclusions

This thesis's main objective was to integrate nutritional, hormonal, and inflammatory stimuli in the bioenergetic and redox signaling of hepatic steatosis models. In the first part, we promoted obesity with a high-fat diet for 2, 4, and 8 weeks. Despite animals gaining fat mass and being resistant to insulin, liver mitochondrial function was not affected by the HFD, and, surprisingly, nor by the combination of HFD plus KO. We propose that hepatic mitochondrial function is resistant to fat overload and insensitive to inflammatory nitric oxide. Additionally, we observed that systemic insulin resistance and glucose intolerance does not require hepatic mitochondrial dysfunction to settle. In the second part, using an in vitro steatosis model, we observed that fatty acid overload sharply increased glucose usage for ATP production in the cytoplasm of PLC cells, mediated by hydrogen peroxide/superoxide in the I_Q site of mitochondrial respiratory complex I. Remarkably, cells can sustain the same mitochondrial respiration and ATP production even under oxidative stress and extensive mitochondrial fragmentation. In summary, we described that the hepatic mitochondrial function is resilient to lipidic overload. Its notorious dysfunction in fatty liver is probably not causative, but rather a downstream target of toxicity.

6. References

Adeva-Andany, M.M., Carneiro-Freire, N., Seco-Filgueira, M., Fernández-Fernández, C., and Mouriño-Bayolo, D. (2019). Mitochondrial β-oxidation of saturated fatty acids in humans. Mitochondrion *46*, 73–90.

Alsabeeh, N., Chausse, B., Kakimoto, P.A., Kowaltowski, A.J., and Shirihai, O. (2018). Cell culture models of fatty acid overload: Problems and solutions. Biochim. Biophys. Acta BBA - Mol. Cell Biol. Lipids *1863*, 143–151.

Anhê, F.F., Varin, T.V., Le Barz, M., Desjardins, Y., Levy, E., Roy, D., and Marette, A. (2015). Gut microbiota dysbiosis in obesity-linked metabolic diseases and prebiotic potential of polyphenol-rich extracts. Curr. Obes. Rep. *4*, 389–400.

Anstee, Q.M., Darlay, R., Cockell, S., Meroni, M., Govaere, O., Tiniakos, D., Burt, A.D., Bedossa, P., Palmer, J., Liu, Y.-L., et al. (2020). Genome-wide association study of non-alcoholic fatty liver and steatohepatitis in a histologically characterised cohort☆. J. Hepatol. *0*.

Arruda, A.P., Pers, B.M., Parlakgül, G., Güney, E., Inouye, K., and Hotamisligil, G.S. (2014). Chronic enrichment of hepatic endoplasmic reticulum-mitochondria contact leads to mitochondrial dysfunction in obesity. Nat. Med. *20*, 1427–35.

Bao, J., Scott, I., Lu, Z., Pang, L., Dimond, C.C., Gius, D., and Sack, M.N. (2010). SIRT3 is regulated by nutrient excess and modulates hepatic susceptibility to lipotoxicity. Free Radic. Biol. Med. *49*, 1230–1237.

Barnett, S.D., and Buxton, I.L.O. (2017). The role of S-nitrosoglutathione reductase (GSNOR) in human disease and therapy. Crit. Rev. Biochem. Mol. Biol. *52*, 340–354.

Bettaieb, A., Jiang, J.X., Sasaki, Y., Chao, T.-I., Kiss, Z., Chen, X., Tian, J., Katsuyama, M., Yabe-Nishimura, C., Xi, Y., et al. (2015). Hepatocyte Nicotinamide Adenine Dinucleotide Phosphate Reduced Oxidase 4 Regulates Stress Signaling, Fibrosis, and Insulin Sensitivity During Development of Steatohepatitis in Mice. Gastroenterology *149*, 468-480.e10.

Betz, C., Stracka, D., Prescianotto-Baschong, C., Frieden, M., Demaurex, N., and Hall, M.N. (2013). mTOR complex 2-Akt signaling at mitochondria- associated endoplasmic reticulum membranes (MAM) regulates mitochondrial physiology. Proc. Natl. Acad. Sci. U. S. A. *110*, 12526.

Blüher, M. (2019). Obesity: global epidemiology and pathogenesis. Nat. Rev. Endocrinol. *15*, 288–298.

Boland, M.L., Oró, D., Tølbøl, K.S., Thrane, S.T., Nielsen, J.C., Cohen, T.S., Tabor, D.E., Fernandes, F., Tovchigrechko, A., Veidal, S.S., et al. (2019). Towards a standard diet-induced and biopsy-confirmed mouse model of non-alcoholic steatohepatitis: Impact of dietary fat source. World J. Gastroenterol. *25*, 4904–4920.

Boursier, J., Mueller, O., Barret, M., Machado, M., Fizanne, L., Araujo-Perez, F., Guy, C.D., Seed, P.C., Rawls, J.F., David, L.A., et al. (2016). The severity of nonalcoholic fatty liver disease is associated with gut dysbiosis and shift in the metabolic function of the gut microbiota. Hepatology *63*, 764–775.

Boutari, C., and Mantzoros, C.S. (2020). Adiponectin and leptin in the diagnosis and therapy of NAFLD. Metab. - Clin. Exp. *103,* 154028.

Brand, M.D. (2016). Mitochondrial generation of superoxide and hydrogen peroxide as the source of mitochondrial redox signaling. Free Radic. Biol. Med. *100*, 14–31.

Brand, M.D., and Nicholls, D.G. (2011). Assessing mitochondrial dysfunction in cells. Biochem. J. *435*, 297–312.

Brand, M.D., Gonçalves, R.L.S., Orr, A.L., Vargas, L., Gerencser, A.A., Borch Jensen, M., Wang, Y.T., Melov, S., Turk, C.N., Matzen, J.T., et al. (2016). Suppressors of superoxide-H2O2 production at site IQ of mitochondrial complex I protect against stem cell hyperplasia and ischemia-reperfusion injury. Cell Metab. *24*, 582–592.

Brasil, Ministério da Saúde (2020). Vigitel Brasil 2019: vigilância de fatores de risco e proteção para doenças crônicas por inquérito telefônico: estimativas sobre frequência e distribuição sociodemográfica de fatores de risco e proteção para doenças crônicas nas capitais dos 26 estados brasileiros e no Distrito Federal em 2019 (Brasília: Delano de Aquino Silva).

Cai, W.-F., Zhang, C., Wu, Y.-Q., Zhuang, G., Ye, Z., Zhang, C.-S., and Lin, S.-C. (2018). Glutaminase GLS1 senses glutamine availability in a non-enzymatic manner triggering mitochondrial fusion. Cell Res. *28*, 865–867.

del Campo, A., Parra, V., Vásquez-Trincado, C., Gutiérrez, T., Morales, P.E., López-Crisosto, C., Bravo-Sagua, R., Navarro-Marquez, M.F., Verdejo, H.E., Contreras-Ferrat, A., et al. (2014). Mitochondrial fragmentation impairs insulin-dependent glucose uptake by modulating Akt activity through mitochondrial Ca2+ uptake. AJP Endocrinol. Metab. *306*, E1–E13.

Cardoso, A.R., Kakimoto, P.A.H.B., and Kowaltowski, A.J. (2013). Diet-sensitive sources of reactive oxygen species in liver mitochondria: role of very long chain acyl-CoA dehydrogenases. PLoS ONE *8*, e77088.

Chan, D.C. (2020). Mitochondrial dynamics and its involvement in disease. Annu. Rev. Pathol. Mech. Dis. *15*, 235–259.

Charbonneau, A., and Marette, A. (2010). Inducible nitric oxide synthase induction underlies lipid-induced hepatic insulin resistance in mice: potential role of tyrosine nitration of insulin signaling proteins. Diabetes *59*, 861–871.

Chausse, B., Kakimoto, P.A., Caldeira-da-Silva, C.C., Chaves-Filho, A.B., Yoshinaga, M.Y., da Silva, R.P., Miyamoto, S., and Kowaltowski, A.J. (2019). Distinct metabolic patterns during microglial remodeling by oleate and palmitate. Biosci. Rep. *39*.

Cheng, Z., Tseng, Y., and White, M.F. (2010). Insulin signaling meets mitochondria in metabolism. Trends Endocrinol. Metab. *21*, 589–598.

Cunningham, R.P., Sheldon, R.D., and Rector, R.S. (2020). The emerging role of hepatocellular enos in non-alcoholic fatty liver disease development. Front. Physiol. *11*, 767.

Di Ciaula, A., Baj, J., Garruti, G., Celano, G., De Angelis, M., Wang, H.H., Di Palo, D.M., Bonfrate, L., Wang, D.Q.-H., and Portincasa, P. (2020). Liver steatosis, gut-liver axis,

microbiome and environmental factors. A never-ending bidirectional cross-talk. J. Clin. Med. *9*, 2648.

Divakaruni, A.S., Hsieh, W.Y., Minarrieta, L., Duong, T.N., Kim, K.K.O., Desousa, B.R., Andreyev, A.Y., Bowman, C.E., Caradonna, K., Dranka, B.P., et al. (2018). Etomoxir inhibits macrophage polarization by disrupting CoA homeostasis. Cell Metab. *28*, 490-503.e7.

Doulias, P.-T., Tenopoulou, M., Greene, J.L., Raju, K., and Ischiropoulos, H. (2013). Nitric oxide regulates mitochondrial fatty acid metabolism through reversible protein S-nitrosylation. Sci. Signal. *6*, rs1.

Eaton, S. (2002). Control of mitochondrial β-oxidation flux. Prog. Lipid Res. *41*, 197–239.

Egnatchik, R.A., Leamy, A.K., Noguchi, Y., Shiota, M., and Young, J.D. (2014a). Palmitate-induced activation of mitochondrial metabolism promotes oxidative stress and apoptosis in H4IIEC3 rat hepatocytes. Metabolism *63*, 283–295.

Egnatchik, R.A., Leamy, A.K., Jacobson, D.A., Shiota, M., and Young, J.D. (2014b). ER calcium release promotes mitochondrial dysfunction and hepatic cell lipotoxicity in response to palmitate overload. Mol. Metab. *3*, 544–553.

Egnatchik, R.A., Leamy, A.K., Sacco, S.A., Cheah, Y.E., Shiota, M., and Young, J.D. (2019). Glutamate–oxaloacetate transaminase activity promotes palmitate lipotoxicity in rat hepatocytes by enhancing anaplerosis and citric acid cycle flux. J. Biol. Chem. *294*, 3081–3090.

Enos, R.T., Davis, J.M., Velázquez, K.T., McClellan, J.L., Day, S.D., Carnevale, K.A., and Murphy, E.A. (2013). Influence of dietary saturated fat content on adiposity, macrophage behavior, inflammation, and metabolism: composition matters. J. Lipid Res. *54*, 152–163.

Enos, R.T., Velázquez, K.T., and Murphy, E.A. (2014). Insight into the impact of dietary saturated fat on tissue-specific cellular processes underlying obesity-related diseases. J. Nutr. Biochem. *25*, 600–612.

Ertunc, M.E., and Hotamisligil, G.S. (2016). Lipid signaling and lipotoxicity in metaflammation: indications for metabolic disease pathogenesis and treatment. J. Lipid Res. *57*, 2099–2114.

Feng, R., Luo, C., Li, C., Du, S., Okekunle, A.P., Li, Y., Chen, Y., Zi, T., and Niu, Y. (2017). Free fatty acids profile among lean, overweight and obese non-alcoholic fatty liver disease patients: a case – control study. Lipids Health Dis. *16*, 165.

Figueira, T.R., Barros, M.H., Camargo, A.A., Castilho, R.F., Ferreira, J.C., Kowaltowski, A.J., Sluse, F.E., Souza-Pinto, N.C., and Vercesi, A.E. (2013). Mitochondria as a source of reactive oxygen and nitrogen species: from molecular mechanisms to human health. Antioxid Redox Signal *18*, 2029–2074.

Filadi, R., Pendin, Di., and Pizzo, P. (2018). Mitofusin 2: From functions to disease. Cell Death Dis. *9*.

Fisher-Wellman, K.H., Ryan, T.E., Smith, C.D., Gilliam, L.A.A., Lin, C.-T., Reese, L.R., Torres, M.J., and Neufer, P.D. (2016). A direct comparison of metabolic responses to high-fat diet in C57BL/6J and C57BL/6NJ mice. Diabetes *65*, 3249–3261.

Fletcher, J.A., Deja, S., Satapati, S., Fu, X., Burgess, S.C., and Browning, J.D. (2019). Impaired ketogenesis and increased acetyl-CoA oxidation promote hyperglycemia in human fatty liver. JCI Insight *5,* e127737.

Folch, J., Lees, M., and Stanley, G.H.S. (1957). A simple method for the isolation and purification of total lipides from animal tissues. J. Biol. Chem. *226*, 497–509.

Francisco, A., Ronchi, J.A., Navarro, C.D.C., Figueira, T.R., and Castilho, R.F. (2018). Nicotinamide nucleotide transhydrogenase is required for brain mitochondrial redox balance under hampered energy substrate metabolism and high-fat diet. J. Neurochem. *147*, 663–677.

Friedman, S.L., Neuschwander-Tetri, B.A., Rinella, M., and Sanyal, A.J. (2018). Mechanisms of NAFLD development and therapeutic strategies. Nat. Med. *24*, 908.

Fujimoto, M., Shimizu, N., Kunii, K., Martyn, J.A.J., Ueki, K., and Kaneki, M. (2005). A role for iNOS in fasting hyperglycemia and impaired insulin signaling in the liver of obese diabetic mice. Diabetes *54*, 1340–1348.

Gameiro, P.A., Laviolette, L.A., Kelleher, J.K., Iliopoulos, O., and Stephanopoulos, G. (2013). Cofactor balance by nicotinamide nucleotide transhydrogenase (NNT) coordinates reductive carboxylation and glucose catabolism in the tricarboxylic acid (TCA) cycle. J. Biol. Chem. *288*, 12967–12977.

Ganesh-Kumar, K., Zhang, J., Gao, S., Rossi, J., McGuinness, O.P., Halem, H.H., Culler, M.D., Mynatt, R.L., and Butler, A.A. (2012). Adropin deficiency is associated with increased adiposity and insulin resistance. Obesity *20*, 1394–1402.

Geng, L., Lam, K.S.L., and Xu, A. (2020a). The therapeutic potential of FGF21 in metabolic diseases: from bench to clinic. Nat. Rev. Endocrinol. 1–14.

Geng, Y., Hernández Villanueva, A., Oun, A., Buist-Homan, M., Blokzijl, H., Faber, K.N., Dolga, A., and Moshage, H. (2020b). Protective effect of metformin against palmitate-induced hepatic cell death. Biochim. Biophys. Acta BBA - Mol. Basis Dis. *1866*, 165621.

Gerencser, A.A., Chinopoulos, C., Birket, M.J., Jastroch, M., Vitelli, C., Nicholls, D.G., and Brand, M.D. (2012). Quantitative measurement of mitochondrial membrane potential in cultured cells: Calcium-induced de- and hyperpolarization of neuronal mitochondria. J. Physiol. *590*, 2845–2871.

Ghisla, S., and Thorpe, C. (2004). Acyl-CoA dehydrogenases. Eur. J. Biochem. *271*, 494–508.

Godoy-Matos, A.F., Silva Júnior, W.S., and Valerio, C.M. (2020). NAFLD as a continuum: from obesity to metabolic syndrome and diabetes. Diabetol. Metab. Syndr. *12*, 60.

Gomes, L.C., Benedetto, G.D., and Scorrano, L. (2011). During autophagy mitochondria elongate, are spared from degradation and sustain cell viability. Nat. Cell Biol. *13*, 589–598.

Gordaliza-Alaguero, I., Cantó, C., and Zorzano, A. (2019). Metabolic implications of organelle–mitochondria communication. EMBO Rep. *20*, e47928.

Hansen, H.H., Ægidius, H.M., Oró, D., Evers, S.S., Heebøll, S., Eriksen, P.L., Thomsen, K.L., Bengtsson, A., Veidal, S.S., Feigh, M., et al. (2020). Human translatability of the GAN diet-induced obese mouse model of non-alcoholic steatohepatitis. BMC Gastroenterol. *20*, 210.

Hardy, T., Oakley, F., Anstee, Q.M., and Day, C.P. (2016). Nonalcoholic fatty liver disease: pathogenesis and disease spectrum. Annu. Rev. Pathol. Mech. Dis. *11*, 451–496.

Hernández-Alvarez, M.I., Sebastián, D., Vives, S., Ivanova, S., Bartoccioni, P., Kakimoto, P., Plana, N., Veiga, S.R., Hernández, V., Vasconcelos, N., et al. (2019). Deficient endoplasmic reticulum-mitochondrial phosphatidylserine transfer causes liver disease. Cell *177*, 881-895.e17.

Hickok, J.R., Sahni, S., Shen, H., Arvind, A., Antoniou, C., Fung, L.W.M., and Thomas, D.D. (2011). Dinitrosyliron complexes are the most abundant nitric oxide-derived cellular adduct: biological parameters of assembly and disappearance. Free Radic. Biol. Med. *51*, 1558–1566.

Hill, B.G., Benavides, G.A., Lancaster, J.R., Ballinger, S., Dell'Italia, L., Zhang, J., and Darley-Usmar, V.M. (2012). Integration of cellular bioenergetics with mitochondrial quality control and autophagy. Biol. Chem. *393*, 1485–1512.

Hodson, L., and Gunn, P.J. (2019). The regulation of hepatic fatty acid synthesis and partitioning: the effect of nutritional state. Nat. Rev. Endocrinol. *15*, 689–700.

Jheng, H.-F., Tsai, P.-J., Guo, S.-M., Kuo, L.-H., Chang, C.-S., Su, I.-J., Chang, C.-R., and Tsai, Y.-S. (2012). Mitochondrial fission contributes to mitochondrial dysfunction and insulin resistance in skeletal muscle. Mol. Cell. Biol. *32*, 309–319.

Kakimoto, P.A., and Kowaltowski, A.J. (2016). Effects of high fat diets on rodent liver bioenergetics and oxidative imbalance. Redox Biol. *8*, 216–225.

Kakimoto, P., Zorzano, A., and Kowaltowski, A.J. (2020). Increased glycolysis is an early outcome of palmitate-mediated lipotoxicity. BioRxiv 2020.06.10.144808.

Kakimoto, P.A., Chausse, B., Caldeira da Silva, C.C., Donato Júnior, J., and Kowaltowski, A.J. (2019). Resilient hepatic mitochondrial function and lack of iNOS dependence in diet-induced insulin resistance. PLOS ONE *14*, e0211733.

Kakimoto, P.A.H.B., Tamaki, F.K., Cardoso, A.R., Marana, S.R., and Kowaltowski, A.J. (2015). H2O2 release from the very long chain acyl-CoA dehydrogenase. Redox Biol. *4*, 375–380.

Keenan, S.N., Meex, R.C., Lo, J.C.Y., Ryan, A., Nie, S., Montgomery, M.K., and Watt, M.J. (2019). Perilipin 5 deletion in hepatocytes remodels lipid metabolism and causes hepatic insulin resistance in mice. Diabetes *68*, 543–555.

Kleiner, D.E., Brunt, E.M., Natta, M.V., Behling, C., Contos, M.J., Cummings, O.W., Ferrell, L.D., Liu, Y.-C., Torbenson, M.S., Unalp-Arida, A., et al. (2005). Design and validation of a histological scoring system for nonalcoholic fatty liver disease. Hepatology *41*, 1313–1321.

Koliaki, C., Szendroedi, J., Kaul, K., Jelenik, T., Nowotny, P., Jankowiak, F., Herder, C., Carstensen, M., Krausch, M., Knoefel, W.T., et al. (2015). Adaptation of hepatic mitochondrial

function in humans with non-alcoholic fatty liver is lost in steatohepatitis. Cell Metab. *21*, 739–746.

Kowaltowski, A.J., Cosso, R.G., Campos, C.B., and Fiskum, G. (2002). Effect of Bcl-2 overexpression on mitochondrial structure and function. J. Biol. Chem. *277*, 42802–42807.

Kowaltowski, A.J., Menezes-Filho, S.L., Assali, E.A., Gonçalves, I.G., Cabral-Costa, J.V., Abreu, P., Miller, N., Nolasco, P., Laurindo, F.R.M., Bruni-Cardoso, A., et al. (2019). Mitochondrial morphology regulates organellar Ca2+ uptake and changes cellular Ca2+ homeostasis. FASEB J. *33*, 13176–13188.

Krahmer, N., Najafi, B., Schueder, F., Quagliarini, F., Steger, M., Seitz, S., Kasper, R., Salinas, F., Cox, J., Uhlenhaut, N.H., et al. (2018). Organellar proteomics and phospho-proteomics reveal subcellular reorganization in diet-induced hepatic steatosis. Dev. Cell *47*, 205-221.e7.

Kubota, N., Kubota, T., Kajiwara, E., Iwamura, T., Kumagai, H., Watanabe, T., Inoue, M., Takamoto, I., Sasako, T., Kumagai, K., et al. (2016). Differential hepatic distribution of insulin receptor substrates causes selective insulin resistance in diabetes and obesity. Nat. Commun. *7*, 12977.

Kulkarni, S.S., Joffraud, M., Boutant, M., Ratajczak, J., Gao, A.W., Maclachlan, C., Hernandez-Alvarez, M.I., Raymond, F., Metairon, S., Descombes, P., et al. (2016). Mfn1 deficiency in the liver protects against diet-induced insulin resistance and enhances the hypoglycemic effect of metformin. Diabetes. *65*, 3552–3560.

Lambertucci, R.H., Hirabara, S.M., Silveira, L. dos R., Levada-Pires, A.C., Curi, R., and Pithon-Curi, T.C. (2008). Palmitate increases superoxide production through mitochondrial electron transport chain and NADPH oxidase activity in skeletal muscle cells. J. Cell. Physiol. *216*, 796–804.

Li, Y., Yang, P., Zhao, L., Chen, Y., Zhang, X., Zeng, S., Wei, L., Varghese, Z., Moorhead, J.F., Chen, Y., et al. (2019a). CD36 plays a negative role in the regulation of lipophagy in hepatocytes through an AMPK-dependent pathway. J. Lipid Res. *60*, 844–855.

Li, Y.-J., Cao, Y.-L., Feng, J.-X., Qi, Y., Meng, S., Yang, J.-F., Zhong, Y.-T., Kang, S., Chen, X., Lan, L., et al. (2019b). Structural insights of human mitofusin-2 into mitochondrial fusion and CMT2A onset. Nat. Commun. *10*, 4914.

Liesa, M., and Shirihai, O.S. (2013). Mitochondrial dynamics in the regulation of nutrient utilization and energy expenditure. Cell Metab. *17*, 491–506.

Liu, Z., Patil, I.Y., Jiang, T., Sancheti, H., Walsh, J.P., Stiles, B.L., Yin, F., and Cadenas, E. (2015). High-fat diet induces hepatic insulin resistance and impairment of synaptic plasticity. PLOS ONE *10*, e0128274.

Loomba, R., and Adams, L.A. (2019). The 20% rule of NASH progression: the natural history of advanced fibrosis and cirrhosis caused by NASH. Hepatology *70*, 1885–1888.

Loomis, A.K., Kabadi, S., Preiss, D., Hyde, C., Bonato, V., St. Louis, M., Desai, J., Gill, J.M.R., Welsh, P., Waterworth, D., et al. (2016). Body mass index and risk of nonalcoholic fatty liver disease: two electronic health record prospective studies. J. Clin. Endocrinol. Metab. *101*, 945–952.

Ly, L.D., Xu, S., Choi, S.-K., Ha, C.-M., Thoudam, T., Cha, S.-K., Wiederkehr, A., Wollheim, C.B., Lee, I.-K., and Park, K.-S. (2018). Oxidative stress and calcium dysregulation by palmitate in type 2 diabetes. Exp. Mol. Med. *49*, e291.

Lyu, K., Zhang, Y., Zhang, D., Kahn, M., ter Horst, K.W., Rodrigues, M.R.S., Gaspar, R.C., Hirabara, S.M., Luukkonen, P.K., Lee, S., et al. (2020). A membrane-bound diacylglycerol species induces PKCε-mediated hepatic insulin resistance. Cell Metab. *32,* 654–664.e5.

Majumdar, A., and Tsochatzis, E.A. (2020). Changing trends of liver transplantation and mortality from non-alcoholic fatty liver disease. Metabolism. *111s,* 154291.

Maloney Ezekiel, Sweet Ian R., Hockenbery David M., Pham Matilda, Rizzo Norma O., Tateya Sanshiro, Handa Priya, Schwartz Michael W., and Kim Francis (2009). Activation of NF-κB by Palmitate in Endothelial Cells. Arterioscler. Thromb. Vasc. Biol. *29*, 1370–1375.

Maslak, E., Zabielski, P., Kochan, K., Kus, K., Jasztal, A., Sitek, B., Proniewski, B., Wojcik, T., Gula, K., Kij, A., et al. (2015). The liver-selective NO donor, V-PYRRO/NO, protects against liver steatosis and improves postprandial glucose tolerance in mice fed high fat diet. Biochem. Pharmacol. *93*, 389–400.

Mason, R.R., Mokhtar, R., Matzaris, M., Selathurai, A., Kowalski, G.M., Mokbel, N., Meikle, P.J., Bruce, C.R., and Watt, M.J. (2014). PLIN5 deletion remodels intracellular lipid composition and causes insulin resistance in muscle. Mol. Metab. *3*, 652–663.

Masuda, M., Miyazaki-Anzai, S., Keenan, A.L., Okamura, K., Kendrick, J., Chonchol, M., Offermanns, S., Ntambi, J.M., Kuro-o, M., and Miyazaki, M. (2015). Saturated phosphatidic acids mediate saturated fatty acid–induced vascular calcification and lipotoxicity. J. Clin. Invest. *125*, 4544–4558.

McCambridge, G., Agrawal, M., Keady, A., Kern, P.A., Hasturk, H., Nikolajczyk, B.S., and Bharath, L.P. (2019). Saturated fatty acid activates T cell inflammation through a nicotinamide nucleotide transhydrogenase (NNT)-dependent mechanism. Biomolecules *9*, 79.

McNaughton, L., Puttagunta, L., Martinez-Cuesta, M.A., Kneteman, N., Mayers, I., Moqbel, R., Hamid, Q., and Radomski, M.W. (2002). Distribution of nitric oxide synthase in normal and cirrhotic human liver. Proc. Natl. Acad. Sci. U. S. A. *99*, 17161–17166.

Meex, R.C.R., and Watt, M.J. (2017). Hepatokines: linking nonalcoholic fatty liver disease and insulin resistance. Nat. Rev. Endocrinol. *13*, 509–520.

Meex, R.C., Hoy, A.J., Morris, A., Brown, R.D., Lo, J.C.Y., Burke, M., Goode, R.J.A., Kingwell, B.A., Kraakman, M.J., Febbraio, M.A., et al. (2015). Fetuin B is a secreted hepatocyte factor linking steatosis to impaired glucose metabolism. Cell Metab. *22*, 1078–1089.

Molina, A.J.A., Wikstrom, J.D., Stiles, L., Las, G., Mohamed, H., Elorza, A., Walzer, G., Twig, G., Katz, S., Corkey, B.E., et al. (2009). Mitochondrial networking protects β-cells from nutrient-induced apoptosis. Diabetes *58*, 2303–2315.

Monetti, M., Levin, M.C., Watt, M.J., Sajan, M.P., Marmor, S., Hubbard, B.K., Stevens, R.D., Bain, J.R., Newgard, C.B., Farese, R.V., et al. (2007). Dissociation of hepatic steatosis and insulin resistance in mice overexpressing DGAT in the liver. Cell Metab. *6*, 69–78.

Mookerjee, S.A., Goncalves, R.L.S., Gerencser, A.A., Nicholls, D.G., and Brand, M.D. (2015). The contributions of respiration and glycolysis to extracellular acid production. Biochim. Biophys. Acta BBA - Bioenerg. *1847*, 171–181.

Mookerjee, S.A., Gerencser, A.A., Nicholls, D.G., and Brand, M.D. (2017). Quantifying intracellular rates of glycolytic and oxidative ATP production and consumption using extracellular flux measurements. J. Biol. Chem. *292*, 7189–7207.

Morgan, D., Oliveira-Emilio, H.R., Keane, D., Hirata, A.E., Santos da Rocha, M., Bordin, S., Curi, R., Newsholme, P., and Carpinelli, A.R. (2007). Glucose, palmitate and pro-inflammatory cytokines modulate production and activity of a phagocyte-like NADPH oxidase in rat pancreatic islets and a clonal beta cell line. Diabetologia *50*, 359–369.

Muñoz, J.P., and Zorzano, A. (2015). Analysis of mitochondrial morphology and function under conditions of mitofusin 2 deficiency. In Mitochondrial Medicine: Volume II, Manipulating Mitochondrial Function, V. Weissig, and M. Edeas, eds. (New York, NY: Springer New York), pp. 307–320.

Navarro, C.D.C., Figueira, T.R., Francisco, A., Dal'Bó, G.A., Ronchi, J.A., Rovani, J.C., Escanhoela, C.A.F., Oliveira, H.C.F., Castilho, R.F., and Vercesi, A.E. (2017). Redox imbalance due to the loss of mitochondrial NAD(P)-transhydrogenase markedly aggravates high fat diet-induced fatty liver disease in mice. Free Radic. Biol. Med. *113*, 190–202.

Nicholson, A., Reifsnyder, P.C., Malcolm, R.D., Lucas, C.A., MacGregor, G.R., Zhang, W., and Leiter, E.H. (2010). Diet-induced obesity in two C57BL/6 substrains with intact or mutant nicotinamide nucleotide transhydrogenase (Nnt) gene. Obesity *18*, 1902–1905.

Nozaki, Y., Fujita, K., Wada, K., Yoneda, M., Kessoku, T., Shinohara, Y., Imajo, K., Ogawa, Y., Nakamuta, M., Saito, S., et al. (2015a). Deficiency of iNOS-derived NO accelerates lipid accumulation-independent liver fibrosis in non-alcoholic steatohepatitis mouse model. BMC Gastroenterol. *15*, 42.

Nozaki, Y., Fujita, K., Wada, K., Yoneda, M., Shinohara, Y., Imajo, K., Ogawa, Y., Kessoku, T., Nakamuta, M., Saito, S., et al. (2015b). Deficiency of eNOS exacerbates early-stage NAFLD pathogenesis by changing the fat distribution. BMC Gastroenterol. *15*, 177.

Olzmann, J.A., and Carvalho, P. (2018). Dynamics and functions of lipid droplets. Nat. Rev. Mol. Cell Biol. *20*, 137–155.

O'Neill, S., and O'Driscoll, L. (2015). Metabolic syndrome: A closer look at the growing epidemic and its associated pathologies. Obes. Rev. *16*, 1–12.

Orr, A.L., Vargas, L., Turk, C.N., Baaten, J.E., Matzen, J.T., Dardov, V.J., Attle, S.J., Li, J., Quackenbush, D.C., Goncalves, R.L.S., et al. (2015). Suppressors of superoxide production from mitochondrial complex III. Nat. Chem. Biol. *11*, 834–836.

Pal, D., Dasgupta, S., Kundu, R., Maitra, S., Das, G., Mukhopadhyay, S., Ray, S., Majumdar, S.S., and Bhattacharya, S. (2012). Fetuin-A acts as an endogenous ligand of TLR4 to promote lipid-induced insulin resistance. Nat. Med. *18*, 1279–1285.

Parthasarathy, G., Revelo, X., and Malhi, H. (2020). Pathogenesis of nonalcoholic steatohepatitis: An overview. Hepatol. Commun. *4*, 478.

Parto, P., and Lavie, C.J. (2017). Obesity and cardiovascular diseases. Curr. Probl. Cardiol. *42*, 376–394.

Peng, K.-Y., Watt, M.J., Rensen, S., Greve, J.W., Huynh, K., Jayawardana, K.S., Meikle, P.J., and Meex, R.C.R. (2018). Mitochondrial dysfunction-related lipid changes occur in nonalcoholic fatty liver disease progression. J. Lipid Res. *59*, 1977–1986.

Perreault, M., and Marette, A. (2001). Targeted disruption of inducible nitric oxide synthase protects against obesity-linked insulin resistance in muscle. Nat. Med. *7*, 1138–1143.

Petersen, M.C., Madiraju, A.K., Gassaway, B.M., Marcel, M., Nasiri, A.R., Butrico, G., Marcucci, M.J., Zhang, D., Abulizi, A., Zhang, X., et al. (2016). Insulin receptor Thr 1160 phosphorylation mediates lipid-induced hepatic insulin resistance. J Clin Invest *126*, 1–11.

Petersen, M.C., Vatner, D.F., and Shulman, G.I. (2017). Regulation of hepatic glucose metabolism in health and disease. Nat. Rev. Endocrinol. *13*, 572–587.

Piccolis, M., Bond, L.M., Kampmann, M., Pulimeno, P., Chitraju, C., Jayson, C.B.K., Vaites, L.P., Boland, S., Lai, Z.W., Gabriel, K.R., et al. (2019). Probing the global cellular responses to lipotoxicity caused by saturated fatty acids. Mol. Cell *74*, 32-44.e8.

Priest, C., and Tontonoz, P. (2019). Inter-organ cross-talk in metabolic syndrome. Nat. Metab. *1*, 1177–1188.

Qian, Q., Zhang, Z., Orwig, A., Chen, S., Ding, W.-X., Xu, Y., Kunz, R.C., Lind, N.R.L., Stamler, J.S., and Yang, L. (2018). S-Nitrosoglutathione reductase dysfunction contributes to obesity-associated hepatic insulin resistance via regulating autophagy. Diabetes *67*, 193–207.

Qian, Q., Zhang, Z., Li, M., Savage, K., Cheng, D., Rauckhorst, A.J., Ankrum, J.A., Taylor, E.B., Ding, W., Xiao, Y., et al. (2019). Hepatic lysosomal iNOS activity impairs autophagy in obesity. Cell. Mol. Gastroenterol. Hepatol. *8*, 95–110.

Quehenberger, O., Armando, A.M., Brown, A.H., Milne, S.B., Myers, D.S., Merrill, A.H., Bandyopadhyay, S., Jones, K.N., Kelly, S., Shaner, R.L., et al. (2010). Lipidomics reveals a remarkable diversity of lipids in human plasma. J. Lipid Res. *51*, 3299–3305.

Rambold, A.S., Kostelecky, B., Elia, N., and Lippincott-Schwartz, J. (2011). Tubular network formation protects mitochondria from autophagosomal degradation during nutrient starvation. Proc. Natl. Acad. Sci. *108*, 10190–10195.

Rambold, A.S., Cohen, S., and Lippincott-Schwartz, J. (2015). Fatty acid trafficking in starved cells: Regulation by lipid droplet lipolysis, autophagy, and mitochondrial fusion dynamics. Dev. Cell *32*, 678–692.

Reddy, J.K., and Hashimoto, T. (2001). Peroxisomal β-oxidation and peroxisome proliferator–activated receptor α: an adaptive metabolic system. Annu. Rev. Nutr. *21*, 193–230.

Resh, M.D. (2016). Fatty acylation of proteins: The long and the short of it. Prog. Lipid Res. *63*, 120–131.

Rodrigues, J.V., and Gomes, C.M. (2012). Mechanism of superoxide and hydrogen peroxide generation by human electron-transfer flavoprotein and pathological variants. Free Radic. Biol. Med. *53*, 12–19.

Ronchi, J.A., Figueira, T.R., Ravagnani, F.G., Oliveira, H.C.F., Vercesi, A.E., and Castilho, R.F. (2013). A spontaneous mutation in the nicotinamide nucleotide transhydrogenase gene of C57BL/6J mice results in mitochondrial redox abnormalities. Free Radic. Biol. Med. *63*, 446–456.

Ronchi, J.A., Francisco, A., Passos, L.A.C., Figueira, T.R., and Castilho, R.F. (2016). The contribution of nicotinamide nucleotide transhydrogenase to peroxide detoxification is dependent on the respiratory state and counterbalanced by other sources of NADPH in liver mitochondria. J. Biol. Chem. *291*, 20173–20187.

Rydström, J. (2006). Mitochondrial NADPH, transhydrogenase and disease. Biochim. Biophys. Acta BBA - Bioenerg. *1757*, 721–726.

Rydström, J., Panov, A.V., Paradies, G., and Ernster, L. (1971). Inhibition of mitochondrial nicotinamide nucleotide transhydrogenase by CoA-thioesters of long-chain fatty acids. Biochem. Biophys. Res. Commun. *45*, 1389–1397.

Samovski, D., and Abumrad, N.A. (2019). Regulation of lipophagy in NAFLD by cellular metabolism and CD36. J. Lipid Res. *60*, 755–757.

Samovski, D., Sun, J., Pietka, T., Gross, R.W., Eckel, R.H., Su, X., Stahl, P.D., and Abumrad, N.A. (2015). Regulation of AMPK activation by CD36 links fatty acid uptake to β-Oxidation. Diabetes *64*, 353–359.

Santoleri, D., and Titchenell, P.M. (2019). Resolving the paradox of hepatic insulin resistance. Cell. Mol. Gastroenterol. Hepatol. *7*, 447–456.

Schrepfer, E., and Scorrano, L. (2016). Mitofusins, from mitochondria to metabolism. Mol. Cell *61*, 683–694.

Sebastián, D., Hernández-Alvarez, M.I., Segalés, J., Sorianello, E., Muñoz, J.P., Sala, D., Waget, A., Liesa, M., Paz, J.C., Gopalacharyulu, P., et al. (2012). Mitofusin 2 (Mfn2) links mitochondrial and endoplasmic reticulum function with insulin signaling and is essential for normal glucose homeostasis. Proc. Natl. Acad. Sci. U. S. A. *109*, 5523–8.

Sebastián, D., Palacín, M., and Zorzano, A. (2017). Mitochondrial dynamics: coupling mitochondrial fitness with healthy aging. Trends Mol. Med. *23*, 201–215.

Seebacher, F., Zeigerer, A., Kory, N., and Krahmer, N. (2020). Hepatic lipid droplet homeostasis and fatty liver disease. Semin. Cell Dev. Biol.

Senyilmaz, D., Virtue, S., Xu, X., Tan, C.Y., Griffin, J.L., Miller, A.K., Vidal-Puig, A., and Teleman, A.A. (2015). Regulation of mitochondrial morphology and function by stearoylation of TFR1. Nature *525*, 124–128.

Senyilmaz-Tiebe, D., Pfaff, D.H., Virtue, S., Schwarz, K.V., Fleming, T., Altamura, S., Muckenthaler, M.U., Okun, J.G., Vidal-Puig, A., Nawroth, P., et al. (2018). Dietary stearic acid regulates mitochondria in vivo in humans. Nat. Commun. *9*.

Sheldon, R.D., Meers, G.M., Morris, E.M., Linden, M.A., Cunningham, R.P., Ibdah, J.A., Thyfault, J.P., Laughlin, M.H., and Rector, R.S. (2019). eNOS deletion impairs mitochondrial quality control and exacerbates Western diet-induced NASH. Am. J. Physiol.-Endocrinol. Metab. *317*, E605–E616.

Shinozaki, S., Choi, C.S., Shimizu, N., Yamada, M., Kim, M., Zhang, T., Dong, H.H., Kim, Y.-B., and Kaneki, M. (2011). Liver-specific inducible nitric-oxide synthase expression is sufficient to cause hepatic insulin resistance and mild hyperglycemia in mice. J. Biol. Chem. *286*, 34959–34975.

Silva, M.V.F., Loures, C. de M.G., Alves, L.C.V., de Souza, L.C., Borges, K.B.G., and Carvalho, M. das G. (2019). Alzheimer's disease: risk factors and potentially protective measures. J. Biomed. Sci. *26*, 33.

Smith, R.A.J., and Murphy, M.P. (2010). Animal and human studies with the mitochondria-targeted antioxidant MitoQ. Ann. N. Y. Acad. Sci. *1201*, 96–103.

Smith, P.F., Alberts, D.W., and Rush, G.F. (1987). Menadione-induced oxidative stress in hepatocytes isolated from fed and fasted rats: The role of NADPH-regenerating pathways. Toxicol. Appl. Pharmacol. *89*, 190–201.

Soto-Cámara, R., González-Bernal, J.J., González-Santos, J., Aguilar-Parra, J.M., Trigueros, R., and López-Liria, R. (2020). Age-related risk factors at the first stroke event. J. Clin. Med. *9*, 2233.

Spinelli, J.B., and Haigis, M.C. (2018). The multifaceted contributions of mitochondria to cellular metabolism. Nat. Cell Biol. *20*, 745–754.

Sutti, S., and Albano, E. (2020). Adaptive immunity: an emerging player in the progression of NAFLD. Nat. Rev. Gastroenterol. Hepatol. *17*, 81–92.

Tao, N., Wagner, S.J., and Lublin, D.M. (1996). CD36 is Palmitoylated on both N- and C-terminal cytoplasmic tails. J. Biol. Chem. *271*, 22315–22320.

Tchernof, A., and Després, J.-P. (2013). Pathophysiology of human visceral obesity: an update. Physiol. Rev. *93*, 359–404.

Thorne, R.F., Ralston, K.J., de Bock, C.E., Mhaidat, N.M., Zhang, X.D., Boyd, A.W., and Burns, G.F. (2010). Palmitoylation of CD36/FAT regulates the rate of its post-transcriptional processing in the endoplasmic reticulum. Biochim. Biophys. Acta BBA - Mol. Cell Res. *1803*, 1298–1307.

Tilg, H., and Moschen, A.R. (2010). Evolution of inflammation in nonalcoholic fatty liver disease: The multiple parallel hits hypothesis. Hepatology *52*, 1836–1846.

Tilg, H., Adolph, T.E., and Moschen, A.R. (2020). Multiple parallel hits hypothesis in NAFLD – revisited after a decade. Hepatology *n/a*.

Toledo, J.C., and Augusto, O. (2012). Connecting the chemical and biological properties of nitric oxide. Chem. Res. Toxicol. *25*, 975–989.

Tomita, K., Teratani, T., Yokoyama, H., Suzuki, T., Irie, R., Ebinuma, H., Saito, H., Hokari, R., Miura, S., and Hibi, T. (2011). Plasma free myristic acid proportion is a predictor of nonalcoholic steatohepatitis. Dig. Dis. Sci. *56*, 3045–3052.

Tomiyama, A.J. (2019). Stress and obesity. Annu. Rev. Psychol. *70*, 703–718.

Toye, A.A., Lippiat, J.D., Proks, P., Shimomura, K., Bentley, L., Hugill, A., Mijat, V., Goldsworthy, M., Moir, L., Haynes, A., et al. (2005). A genetic and physiological study of impaired glucose homeostasis control in C57BL/6J mice. Diabetologia *48*, 675–686.

Tsuchida, T., and Friedman, S.L. (2017). Mechanisms of hepatic stellate cell activation. Nat. Rev. Gastroenterol. Hepatol. *14*, 397–411.

Tubbs, E., Theurey, P., Vial, G., Bendridi, N., Bravard, A., Chauvin, M.-A., Ji-Cao, J., Zoulim, F., Bartosch, B., Ovize, M., et al. (2014). Mitochondria-associated endoplasmic reticulum membrane (MAM) integrity is required for insulin signaling and is implicated in hepatic insulin resistance. Diabetes *63*, 3279–3294.

Wai, T., and Langer, T. (2016). Mitochondrial dynamics and metabolic regulation. Trends Endocrinol. Metab. *27*, 105–117.

Wang, C., Zhao, Y., Gao, X., Li, L., Yuan, Y., Liu, F., Zhang, L., Wu, J., Hu, P., Zhang, X., et al. (2015). Perilipin 5 improves hepatic lipotoxicity by inhibiting lipolysis. Hepatology *61*, 870–882.

Wang, L., Zhou, J., Yan, S., Lei, G., Lee, C.-H., and Yin, X.-M. (2017). Ethanol-triggered lipophagy requires SQSTM1 in AML12 hepatic cells. Sci. Rep. *7*, 12307.

Ward, N.P., Kang, Y.P., Falzone, A., Boyle, T.A., and DeNicola, G.M. (2020). Nicotinamide nucleotide transhydrogenase regulates mitochondrial metabolism in NSCLC through maintenance of Fe-S protein function. J. Exp. Med. *217*.

Winterbourn, C.C. (2018). Biological production, detection, and fate of hydrogen peroxide. Antioxid. Redox Signal. *29*, 541–551.

World Health Organization (2020). Obesity and overweight.

Xiao, W., and Loscalzo, J. (2019). Metabolic responses to reductive stress. Antioxid. Redox Signal.

Yamaguchi, K., Yang, L., McCall, S., Huang, J., Yu, X.X., Pandey, S.K., Bhanot, S., Monia, B.P., Li, Y.-X., and Diehl, A.M. (2007). Inhibiting triglyceride synthesis improves hepatic steatosis but exacerbates liver damage and fibrosis in obese mice with nonalcoholic steatohepatitis. Hepatology *45*, 1366–1374.

Yin, F., Sancheti, H., and Cadenas, E. (2012). Silencing of nicotinamide nucleotide transhydrogenase impairs cellular redox homeostasis and energy metabolism in PC12 cells. Biochim. Biophys. Acta BBA - Bioenerg. *1817*, 401–409.

Younossi, Z.M., Koenig, A.B., Abdelatif, D., Fazel, Y., Henry, L., and Wymer, M. (2016). Global epidemiology of nonalcoholic fatty liver disease—Meta-analytic assessment of prevalence, incidence, and outcomes. Hepatology *64*, 73–84.

Zhang, C.-S., Hawley, S.A., Zong, Y., Li, M., Wang, Z., Gray, A., Ma, T., Cui, J., Feng, J.W., Zhu, M., et al. (2017). Fructose-1,6-bisphosphate and aldolase mediate glucose sensing by AMPK. Nature *548*, 112–116.

Zhang, Y., Jiang, L., Hu, W., Zheng, Q., and Xiang, W. (2011). Mitochondrial dysfunction during in vitro hepatocyte steatosis is reversed by omega-3 fatty acid–induced up-regulation of mitofusin 2. Metabolism *60*, 767–775.

Zhang, Y., Bharathi, S.S., Beck, M.E., and Goetzman, E.S. (2019). The fatty acid oxidation enzyme long-chain acyl-CoA dehydrogenase can be a source of mitochondrial hydrogen peroxide. Redox Biol. *26*, 101253.

Zhao, L., Zhang, C., Luo, X., Wang, P., Zhou, W., Zhong, S., Xie, Y., Jiang, Y., Yang, P., Tang, R., et al. (2018). CD36 palmitoylation disrupts free fatty acid metabolism and promotes tissue inflammation in non-alcoholic steatohepatitis. J. Hepatol. *69*, 705–717.

Zong, Y., Zhang, C.C.-S., Li, M., Wang, W., Wang, Z., Hawley, S.A., Ma, T., Feng, J.-W., Tian, X., Qi, Q., et al. (2019). Hierarchical activation of compartmentalized pools of AMPK depends on severity of nutrient or energy stress. Cell Res.

Zorzano, A., Hernández-Alvarez, M.I., Sebastián, D., and Muñoz, J.P. (2015). Mitofusin 2 as a driver that controls energy metabolism and insulin signaling. Antioxid. Redox Signal. *22*, 1020–1031.

7. Annexes

7.1. Curriculum summary

Name: Kakimoto, Pâmela A. H. B.
Birthplace: São Paulo/SP – Brazil
Birthdate: 12/02/1991

7.1.1. Education

- **26th February 2016 - current (expected defense in January 2021): Biological Sciences (Biochemistry), Ph.D.**
  Instituto de Química, Universidade de São Paulo, Brazil
  Thesis: Bioenergetic and redox signaling in hepatic steatosis models: Integrative analysis of nutritional, hormonal, and inflammatory stimuli (Advisor: Alicia J. Kowaltowski, MD, Ph.D.)
- **8th February 2010 – 13th January 2016: Diploma in Pharmacy-Biochemistry, B.Sc.**
  Faculdade de Ciências Farmacêuticas, Universidade de São Paulo, Brazil
  Undergrad thesis: Effects of high fat diets on rodent liver bioenergetics and oxidative imbalance (Advisor: Alicia J. Kowaltowski, MD, Ph.D.)

7.1.2. Professional experience

- **26th February 2016 - current: Ph.D. Student**
  Instituto de Química, Universidade de São Paulo, Brazil
  Energy Metabolism Lab – Advisor: Alicia J. Kowaltowski, MD, Ph.D.
- **7th September 2018 – 29th August 2019: Visiting Student**
  Instituto for Research in Biomedicine, Barcelona, Spain
  Complex Metabolic Diseases and Mitochondria Lab – Supervisor: Antonio Zorzano, Ph.D.
  Project: Mitochondrial dynamics and insulin signaling of hepatic cells upon lipid overload.
- **16th April 2012 – 16th January 2016: Undergrad Student**
  Instituto de Química, Universidade de São Paulo, Brazil
  Energy Metabolism Lab – Advisor: Alicia J. Kowaltowski, MD, Ph.D.
  Project: Hepatic mitochondrial oxidant production characterization of steatotic mice.
- **8th July 2015 – 4th November 2015: Visiting Student**
  Université Laval, Québec, Canada
  Supervisor: Andre Marette, Ph.D.
  Project: Oxidant production and insulin signaling of hepatic cells upon lipid overload and inflammatory stimuli.

7.1.3. Publications

(reverse chronological order)

1. Cerqueira, F. M.; von Stockum, S.; Giacomello, M.; Goliand, I.; **Kakimoto, P.**; Marchesan, E.; De Stefani, D.; Kowaltowski, A. J.; Ziviani, E.; Shirihai, O. S. (2020) A New Target for an Old DUB: UCH-L1 Regulates Mitofusin-2 Levels, Altering Mitochondrial Morphology, Function and Calcium Uptake. Redox Biol. 101676. https://doi.org/10.1016/j.redox.2020.101676
2. Chausse, B.; **Kakimoto, P. A.**; Kann, O. (2020) Microglia and Lipids: How Metabolism Controls Brain Innate Immunity. Semin. Cell Dev. Biol. https://doi.org/10.1016/j.semcdb.2020.08.001

3. Hernández-Alvarez, M.I., Sebastián, D., Vives, S., Ivanova, S., Bartoccioni, P., **Kakimoto, P.,** Plana, N., Veiga, S.R., Hernández, V., Vasconcelos, N., Peddinti, G., Adrover, A., Jové, M., Pamplona, R., Gordaliza-Alaguero, I., Calvo, E., Cabré, N., Castro, R., Kuzmanic, A., Boutant, M., Sala, D., Hyotylainen, T., Orešič, M., Fort, J., Errasti-Murugarren, E., Rodrígues, C.M.P., Orozco, M., Joven, J., Cantó, C., Palacin, M., Fernández-Veledo, S., Vendrell, J., Zorzano, A. (2019) Deficient endoplasmic reticulum-mitochondrial phosphatidylserine transfer causes liver disease. Cell 177, 881-895.e17. https://doi.org/10.1016/j.cell.2019.04.010
4. **Kakimoto, P.A.[#],** Chausse, B., Caldeira da Silva, C.C., Donato Júnior, J., Kowaltowski, A.J. (2019). Resilient hepatic mitochondrial function and lack of iNOS dependence in diet-induced insulin resistance. PLOS ONE 14, e0211733. https://doi.org/10.1371/journal.pone.0211733
   [#] corresponding author
5. Chausse, B., **Kakimoto, P.A.,** Caldeira-da-Silva, C.C., Chaves-Filho, A.B., Yoshinaga, M.Y., da Silva, R.P., Miyamoto, S., Kowaltowski, A.J. (2019) Distinct metabolic patterns during microglial remodeling by oleate and palmitate. Biosci. Rep. 39. https://doi.org/10.1042/BSR20190072
6. Alsabeeh, N., Chausse, B., **Kakimoto, P.A.*,** Kowaltowski, A.J., Shirihai, O. (2018) Cell culture models of fatty acid overload: Problems and solutions. Biochim. Biophys. Acta BBA - Mol. Cell Biol. Lipids 1863, 143–151. https://doi.org/10.1016/j.bbalip.2017.11.006
   *shared first authorship
7. Amigo, I., da Cunha, F.M., Forni, M.F., Garcia-Neto, W., **Kakimoto, P.A.*,** Luevano-Martinez, L.A., Macedo, F., Menezes-Filho, S.L., Peloggia, J., Kowaltowski, A.J. (2016) Mitochondrial form, function and signalling in aging. Biochem. J. 473, 3421–3449. https://doi.org/10.1042/BCJ20160451
   *shared first authorship
8. **Kakimoto, P.A.,** Kowaltowski, A.J. (2016) Effects of high fat diets on rodent liver bioenergetics and oxidative imbalance. Redox Biol. 8, 216–225. https://doi.org/10.1016/j.redox.2016.01.009
9. **Kakimoto, P.A.**, Tamaki, F.K., Cardoso, A.R., Marana, S.R., Kowaltowski, A.J. (2015) H2O2 release from the very long chain acyl-CoA dehydrogenase. Redox Biol. 4, 375–380. https://doi.org/10.1016/j.redox.2015.02.003
10. Cardoso, A.R., **Kakimoto, P.A.**, Kowaltowski, A.J. (2013) Diet-sensitive sources of reactive oxygen species in liver mitochondria: role of very long chain acyl-CoA dehydrogenases. PLOS ONE 8, e77088. https://doi.org/10.1371/journal.pone.0077088

7.1.4. Pre-print

1. **Kakimoto, P.A.[#]**, Zorzano, A., Kowaltowski, A.J. (2020) Increased glycolysis is an early outcome of palmitate-mediated lipotoxicity. bioRxiv. https://doi.org/10.1101/2020.06.10.144808.
   [#] corresponding author

7.1.5. Funding and awards

(reverse chronological order)

- **2018-2019:** Research scholarship ("Sandwich" Ph.D. internship)
  Coordenação de Aperfeiçoamento de Pessoal de Nível Superior (Brazil)
- **2018:** Travel award
  SBBq - Conesul, Sociedade Brasileira de Bioquímica e Biologia Molecular.

- **2016-2021:** Research scholarship (Ph.D.)
  Fundação de Amparo à Pesquisa do Estado de São Paulo (Brazil)
- **2015:** Research scholarship for internship abroad
  Fundação de Amparo à Pesquisa do Estado de São Paulo (Brazil)
- **2014:** Travel award (declined)
  Young Scientist Program, 23rd IUBMB and 44th SBBq.
- **2013-2015**: Research scholarship (undergrad)
  Fundação de Amparo à Pesquisa do Estado de São Paulo (Brazil)

7.1.6. International events and congresses, and talks

(reverse chronological order)

- **2020:** Biochemistry Seminars – *Instituto de Química/ Universidade de São Paulo (São Paulo* – Brazil) – Invited speaker.
- **2020:** Redoxoma Seminars – Research Center of Redox Processes in Biomedicine *(São Paulo* – Brazil) – Invited speaker.
- **2018:** SBBq: 47th *Reunião Anual da Sociedade Brasileira de Bioquímica e Biologia Molecular* (*Santa Catarina* – Brazil) – Selected for oral presentation.
- **2018:** International Symposium of Refinement and Reproducibility in Animal Experiments (*São Paulo* – Brazil). Invited speaker.
- **2017:** SBBq: 46th *Reunião Anual da Sociedade Brasileira de Bioquímica e Biologia Molecular* (*São Paulo*– Brazil) – Poster presentation.
- **2017:** Gordon Research Conference on Oxidative Stress & Disease (Barga – Italy) – Poster presentation.
- **2017:** 10th Mitomeeting (*Minas Gerais* – Brazil) – Oral presentation.
- **2016**: 3rd Prof. Eric A. Newsholme Research Symposium (*São Paulo* – Brazil) – Poster presentation.
- **2014**: 8th Mitomeeting (*Minas Gerais* – Brazil) – Oral presentation.
- **2014**: Antioxidants and redox process in health – Bilateral Meeting Brazil – Japan (*São Paulo* – Brazil). Poster presentation.

7.1.7. Supervising and teaching activities

I co-supervised one undergrad student (Chen Minzhen, B.Sc. Pharmacy-Biochemistry) in 2017-2018. I worked as a teacher's aide for undergrad Biochemistry classes for two terms (for veterinarian and biomedical sciences students at the *Instituto de Química da USP*, March-December 2016).